TAILORING THE THERMOELECTRIC BEHAVIOR OF ELECTRICALLY CONDUCTIVE POLYMER COMPOSITES

A Dissertation

by

GREGORY PATRICK MORIARTY

Submitted to the Office of Graduate Studies of
Texas A&M University
in partial fulfillment of the requirements for the degree of

DOCTOR OF PHILOSOPHY

Chair of Committee,	Jaime C. Grunlan
Committee Members,	Raymundo Arroyave
	Karl T. Hartwig
	Choongho Yu
Intercollegiate Faculty Chair,	Ibrahim Karaman

August 2013

Major Subject: Materials Science and Engineering

ABSTRACT

Numerous alternative energy sources are being researched for sustainable energy applications, but their overall benefit is still too costly for them to be considered viable. Commonly produced temperature gradients created by the environment, or are man-made, can be converted into useful energy by using thermoelectric materials. Inorganic semiconductors are the most commonly used thermoelectric materials, but have raised concerns due to toxicity issues, rarity of heavy elements used, and high fabrication temperatures. These concerns have led research efforts into electrically conductive polymer composites prepared in ambient conditions from aqueous solutions. By combining polymer latex with carbon nanotubes (CNT), electrical conductivity can resemble metals while thermal conductivity remains similar to polymers. Using different CNT stabilizers for these fully organic composites can tailor the thermoelectric properties and harvest thermal gradients from previously inconceivable places (e.g., body heat converted into a voltage).

A semiconducting CNT stabilizer, *meso*-tetra(4-carboxyphenyl) porphine (TCPP), was used to investigate the influence stabilizers have on composite thermoelectric properties. As TCPP was compared to a similar system containing an insulating stabilizer, sodium deoxycholate (DOC), the multi-walled carbon nanotube (MWNT)-filled composites showed a 5x increase in the Seebeck coefficient (*S*). TCPP did not have a distinct effect on the electrical conductivity (σ), demonstrating the tailorability of *S* with this molecule.

An intrinsically conductive polymer, poly(3,4-ethylenedioxythiophene) :poly(styrene sulfonate) (PEDOT:PSS), was used to stabilize highly conductive double-walled carbon nanotubes (DWNT) and demonstrate the promise of fully organic composites as thermoelectric materials. This combination of CNT and stabilizer produced metallic electrical conductivity (200,000 S m^{-1}) and power factors ($S^2\sigma$) within an order of magnitude of commonly used semiconductors (~400 μW m^{-1} K^{-2}). Electrical conductivity was doubled by stabilizing single-walled carbon nanotubes (SWNT) with PEDOT:PSS in a thin film without the insulating polymer latex.

To further demonstrate the tailorability of polymer composites, a dual stabilizer approach using semiconducting and intrinsically conductive stabilizers was used. This approach effectively provided the high electrical conductivity from PEDOT:PSS and the enhanced Seebeck coefficients of TCPP. By using multiple stabilizers for CNTs within the same composite, power factors among the highest reported for fully organic composites are achieved (~500 μW m^{-1} K^{-2}). These water-based, flexible composites are becoming real competition as their conversion efficiencies, when normalized by density, are similar to commonly used semiconductors.

DEDICATION

To my family, whose unconditional love provided strength to persevere,

To my brother, who always stood by my side offering words of encouragement,

To my parents, who continually give the best gift a son can receive, they believe in me.

ACKNOWLEDGEMENTS

There are many people that I would like to thank that have helped with the completion of this dissertation. My advisor, Prof. Jaime Grunlan, has been a true mentor to me through my years at Texas A&M. His words and advice have been a guide throughout graduate school and directed me to strive for the highest level of research. Most of all, he has taught me to maintain integrity in all facets of life. I would also like to thank my committee members, Prof. Raymundo Arroyave, Prof. Karl T. Hartwig, and Prof. Choongho Yu for their much appreciated interest in my work and serving on my committee.

Special thanks goes to my undergraduate assistants, Jamie Wheeler, Katherine Sun, Henry Harrity, Kenneth Briggs, and Robert Piper, who graciously offered their time and energy to help with my research. This body of work would not be possible without their hard work and dedication. I would also like to acknowledge my current and past colleagues for all the intellectual discussions and candid conversations throughout the years: Dr. Krishna Etika, Dr. Yu-Chin Li, Kyungwho Choi, Amanda Cain, Bart Stevens, David Hagen, Ping Tzeng, Fangming Xiang, and Kevin Holder. I would like to sincerely thank Dr. Morgan Priolo and Dr. Galina Laufer for always being available to help when needed, inviting me into their lives, and providing much appreciated friendship and laughter.

Finally, I would like to thank my family for all of their love and support during all the highs and lows throughout my life. Their ability to always focus on the positives has truly been an inspiration. I would not be where I am today without their words of

motivation, guidance, and encouragement. With that said, I am eternally in debt to my Lord and Savior, Jesus Christ, who has blessed me with a great family and strong supporting cast of friends. All the glory goes to Him, as He has made all of this possible with his infinite wisdom and mercy. "This is my command — be strong and courageous! Do not be afraid or discouraged. For the LORD your God is with you wherever you go," – Joshua 1:9.

NOMENCLATURE

ASTM	American Society for Testing and Materials
BMR	Basal Metabolic Rate
CB	Carbon Black
CNT	Carbon Nanotube
CPVC	Critical Pigment Volume Concentration
DMA	Dynamic Mechanical Analyzer
DOC	Sodium Deoxycholate
DSC	Differential Scanning Calorimeter
DWNT	Double-Walled Carbon Nanotube
ICP	Intrinsically Conductive Polymer
MWNT	Multi-Walled Carbon Nanotube
PEDOT	Poly(3,4-ethylenedioxythiophene)
PF	Power Factor ($S^2\sigma$)
PSS	Poly(styrene sulfonate)
PTC	Percolation Threshold Concentration
PVAc	Poly(vinyl acetate)
SEM	Scanning Electron Microscopy
SWNT	Single-Walled Carbon Nanotube
TCPP	*meso*-Tetra(4-carboxyphenyl) Porphine
T_g	Glass Transition Temperature

TABLE OF CONTENTS

Page

LIST OF FIGURES

FIGURE Page

FIGURE Page

FIGURE Page

FIGURE Page

FIGURE Page

LIST OF TABLES

TABLE Page

CHAPTER I

INTRODUCTION

1.1 Background

Renewable energy technologies are receiving significant attention as the United States works to supply sufficient amounts of energy for a progressively rising demand. In 2009, it was estimated that 27,700 terawatt hours (TWh) were generated for various energy services from traditional fossil fuels and alternative energy sources (e.g., solar, nuclear, hydro, etc.).[1] The majority of this energy was produced from fossil fuel-based thermal power plants operating at ~30% efficiency. These plants discard large amounts of heat into the environment through large cooling towers or nearby water sources. Excessive waste heat was also generated by the consumption of petroleum in inefficient combustion engines that dominate the transportation industry.[1,2] This has been a major issue for many other countries, as over 60% of energy produced is never fully utilized for its desired purpose.[1,3]

Alternative energy sources are continually being researched and implemented to provide sustainable energy, but most are still too costly to be entirely viable (close to $1 per watt).[4] Temperature gradients, however, are commonly produced by the environment (e.g., solar or geothermal energy) and by most power consuming/producing devices. Although these gradients are generally too small for conventional systems to adequately harvest energy from, thermoelectric materials have the ability to successfully convert these modest temperature gradients into useful electricity.[5-7] To effectively

harness this energy, an electrical current is created from the waste heat's temperature gradient via diffusion of charge carriers (e.g., electrons or holes) through the material from the hot side to the cold, or vice versa (i.e., the Seebeck effect described in Section 2.1.1).[8-11] Traditional thermoelectric materials have garnered significant research due to their simple structure, high power density, and total lack of noise pollution that would be produced from moving parts.[6,12-18] These attributes make thermoelectric modules useful for a broad range of applications where waste heat recovery devices could be applied to existing technology to make energy consumption more efficient (e.g., cars, household appliances, the human body, etc.).[19-21]

Existing thermoelectric materials typically generate a greater amount of electricity at elevated temperatures (> 500 K).[5] This, in conjunction with many other factors, has limited the widespread use of commercially available thermoelectric devices for lower temperature applications.[21] A conceivable niche application would be to harvest the heat dissipated by the human body, which would involve temperatures near ambient conditions.[19] The basal metabolic rate (BMR), which relates to the energy required to sustain vital organs, correlates body composition (e.g., weight, height, age, and gender) and total heat produced when the body is at complete rest.[22-23] This means that the average American male body (weight = 91.8 kg, height = 176.3 cm, and age = 45 yrs)[24] dissipates 87 W of power simply by sustaining itself throughout the day. Harvesting a portion of this energy could charge the batteries of small electronic devices (e.g., cell phones) simply by embedding a thermoelectric device into an article of

clothing. Within the thermoelectric community, flexible, light-weight materials are needed to make these niche applications possible.

Fully-organic, electrically conductive composites are an exciting new class of thermoelectric materials. Polymer-based materials are interesting because of their intrinsically low thermal conductivity (≤ 0.4 W m^{-1} K^{-1}),[25-27] inherently low density,[25] relatively simple processing techniques,[28-29] and desirable mechanical properties (e.g., flexibility).[25,30-31] Electrically conductive composites are typically prepared by either melt blending[32-36] or solution processing.[37-44] These randomly dispersed composites require a high concentration of filler to achieve reasonable conductivity[45-48] and this can drastically diminish desirable mechanical properties. A segregated network, composed of conductive nanoparticles in a polymer emulsion (or latex), allows conductive composites to be prepared from aqueous mixtures in ambient conditions with relatively low concentrations of filler.[49-59] Upon drying (Figure 1.1), the larger suspended polymer particles (~0.1 – 1 μm in diameter)[60] force the smaller conductive nanoparticles (e.g., carbon black (CB), carbon nanotubes (CNT), inorganic particles, etc.)[61-64] into the interstitial positions between them. This excluded volume effect can improve electrical conductivity and produce a flexible composite after the polymer particles coalesce. Utilizing this segregated network approach with highly conductive fillers brings electrical conductivity into degenerate-semiconductor or metallic regimes.[65-68]

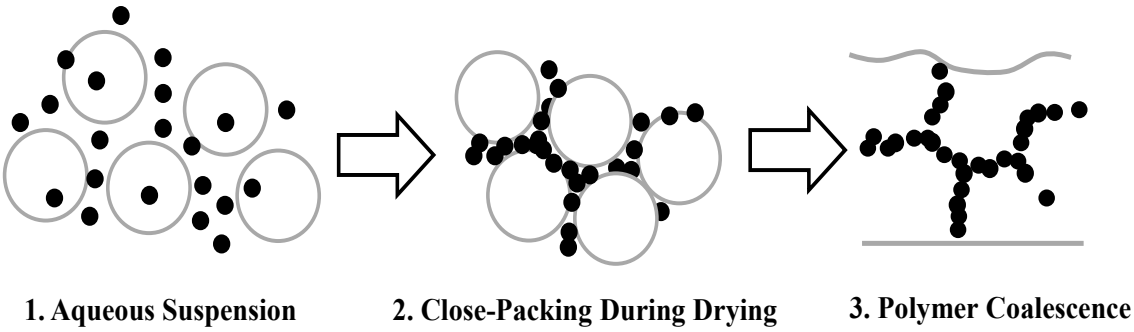

Figure 1.1. Schematic illustration of the formation of a carbon black-filled (black circles) segregated network, where the polymer particles (white circles) assume a close-packed configuration as water evaporates out of the system and ultimately coalesce into a coherent film.

1.2 Objectives and Dissertation Outline

Polymer nanocomposites, prepared with a poly(vinyl acetate) (PVAc) emulsion and various CNTs, are the model composite constituents used throughout this dissertation because the thermoelectric properties can be easily influenced while sustaining the mechanical properties of the polymer matrix. By using different stabilizers for CNTs, thermoelectric properties are tailored by manipulating the junctions between each nanotube. The objective of this research is to develop fully organic, flexible composites that rival traditional thermoelectric materials in energy conversion efficiency. These novel composites are created by employing the segregated network approach, using water-based processing and drying under ambient (or near ambient) conditions. The ultimate goal of this work is to effectively show a useful energy being created with a temperature gradient applied to polymer composites.

Chapter II provides a brief literature review of thermoelectricity, inorganic thermoelectrics, and electrically conductive organic materials. The thermoelectric effect and its mechanisms of charge carrier diffusion are first presented, followed by the behavior of traditional inorganic thermoelectric materials that have been thoroughly researched over the past several decades. The second part of this review covers the basics of electrically conductive composites, with emphasis on utilizing the segregated network approach to create organic thermoelectrics.

Chapter III explores the use of a semiconducting or insulating stabilizer, and the influence each has on the Seebeck coefficient of CNT-filled composites. PVAc copolymer latex-based composites were prepared with multi-walled carbon nanotubes (MWNT), stabilized with sodium deoxycholate (DOC) or *meso*-tetra(4-carboxyphenyl) porphine (TCPP). The segregated network microstructures of these systems were confirmed using scanning electron microscopy (SEM). Through-thickness thermal conductivity was examined using a homemade steady-state setup (in accordance with ASTM D5470).[7] The percolation thresholds were evaluated with a four-point probe that measured the sheet resistance, which was then converted to electrical conductivity. The effect of the stabilizer on the Seebeck coefficient was investigated using a home-built, shielded four-point probe apparatus.[7] These same composite characterization techniques were used in all subsequent chapters. TCPP was found to enhance the Seebeck coefficient of these composites, providing an opportunity for greater thermoelectric efficiency.

Chapter IV describes the effect an intrinsically conductive stabilizer, poly(3,4-ethylenedioxythiophene):poly(styrene sulfonate) (PEDOT:PSS), has on the thermoelectric properties of double-walled carbon nanotube (DWNT)-filled composites. Composites with filler concentrations of up to 40 wt% DWNT (in a PVAc emulsion) were prepared at a 1:1 DWNT:(PEDOT:PSS) dry weight ratio. A demonstration of the thermoelectric behavior of these organic materials was shown with thermal gradients close to ambient. Composites with electrical conductivity of 200,000 S m^{-1}, and a power factor of ~400 μW m^{-1} K^{-2}, were achieved in this study.

Chapter V investigates a dual stabilizer approach used to manipulate the numerous CNT junctions in an effort to increase both electrical conductivity (σ) and Seebeck coefficient (S). Composites were created with varying weight concentrations of MWNT:(PEDOT:PSS):TCPP to systematically examine the effect on the thermoelectric properties. 1:1:0.25 DWNT:(PEDOT:PSS):TCPP were also prepared to test the universality of this approach and to observe the effect of DWNT on the thermoelectric properties. This chapter will provide an understanding of how using multiple stabilizers for CNTs within the same composite can be used to achieve among the highest power factors ($PF = S^2\sigma$) reported for fully organic materials (~500 μW m^{-1} K^{-2}).

Chapter VI explores the use of organic thin film nanocomposites for their thermoelectric behavior and superior electrical properties. These thin films were prepared by liquid-phase exfoliation and did not require the use of an insulating polymer matrix. The single-walled carbon nanotube (SWNT) concentration was increased from 10 to 95 wt%, with the remaining concentration in each thin film being PEDOT:PSS.

Through-thickness thermal conductivity for these thin films was measured with a Nanoflash LFA 447 in accordance with ASTM E1461-07. Thin films achieved among the highest electrical conductivity values reported for a fully organic material (~400,000 S m^{-1}) and a modest $S^2\sigma$ (140 μW m^{-1} K^{-2}).

Chapter VII provides some conclusions and direction for future research. This dissertation investigates using different types of carbon nanotube stabilizers (insulating, semiconducting, and/or intrinsically conductive) to tailor the thermoelectric properties of polymer-based composites. To further improve the thermoelectric behavior of these organic composites, PEDOT:PSS can be doped with other solvents or combining smaller anions (e.g., iron (III) *tris*-p-toluenesulphonate (Tos)) with PEDOT to help increase its electrical properties. Finally, high efficiency thin films could be prepared using liquid-phase exfoliation and a combination of DWNT, PEDOT:PSS, and TCPP.

CHAPTER II

LITERATURE REVIEW

2.1 Introduction

Over the past 20 years, there has been growing interest in the progression of thermoelectric materials to make existing devices more efficient.[21] The recent interest into this special class of material is due to the unique ability to scavenge waste heat and convert it into useful energy. This behavior, which is known as the Seebeck effect, was first discovered in 1821 by the German physicist, Thomas Johann Seebeck.[10,69-73] The inverse of this effect, known as the Peltier effect, was later discovered in 1834 by Jean Charles Peltier when he made a current flow through a junction composed of two dissimilar materials, resulting in a temperature gradient.[74] The combination of these two behaviors, in addition to the Thomson effect (absorption/production of heat when current flows in a material with a temperature gradient),[21] constitutes the overall definition of thermoelectricity. For the purposes of this dissertation, the Seebeck effect will be the primary focus as it relates to the harvesting of waste heat.

2.1.1 Seebeck Effect

The Seebeck effect, the basic principle for thermocouples, can be defined as a voltage generated as a temperature gradient is applied to any isolated electrically conductive material.[10] Charge carriers, either electrons or holes, in select materials (e.g., metals, semiconductors, or insulators) have the ability to carry electrical and

thermal energy. As the carriers are thermally excited from the valence band to the conduction band, they are free to move similarly to gas molecules and diffuse through the material from the hot side to the cold, or vice versa.[5] This constant diffusion creates an electrical potential as charge build up occurs from the mobile carriers leaving behind their oppositely charged, immobile nuclei. Charge carriers will continue to diffuse along this temperature gradient until an equilibrium between electrostatic repulsion, due to built-up charge, and chemical potential for diffusion is reached.[5,9] To quantize this phenomenon, the Seebeck coefficient is generally used.

The Seebeck coefficient (*S*, also known as thermopower) of a material can be defined as the magnitude of an induced thermoelectric field (ΔV) from an established temperature gradient (ΔT), when there is no net flow of current ($S = \Delta V/\Delta T$).[25,75] This quantity is a measure of the tendency, or ability, of charge carriers to diffuse with an applied temperature gradient.[75] The sign of the Seebeck coefficient represents the potential of the cold side with respect to the hot. For an n-type semiconductor, electrons will diffuse from the hot side to the cold creating a more negative potential, resulting in a negative Seebeck coefficient. The opposite is true for a p-type semiconductor whose charge carriers are holes, which are defined as empty electron states near the top of an otherwise filled valence band and behave as positively charged particles.[25] A more rigorous analysis to quantify the Seebeck coefficient would involve determining the asymmetry in the density of states near the Fermi level (ε_f) (e.g., larger asymmetry will lead to a higher electronic density of states above ε_f and higher *S*).[21] This movement of charge carriers is manipulated in a standard thermoelectric device to generate electricity

from thermal gradients, where n- and p-type semiconductors are connected electrically in series and thermally in parallel (**Figure 2.1**).[76] This leg-type configuration is typical for energy generation as it minimizes any parasitic losses that may occur due to electrical resistance within the series. To calculate how efficient thermoelectric materials are at converting waste heat into electricity, several material properties must be taken into consideration.

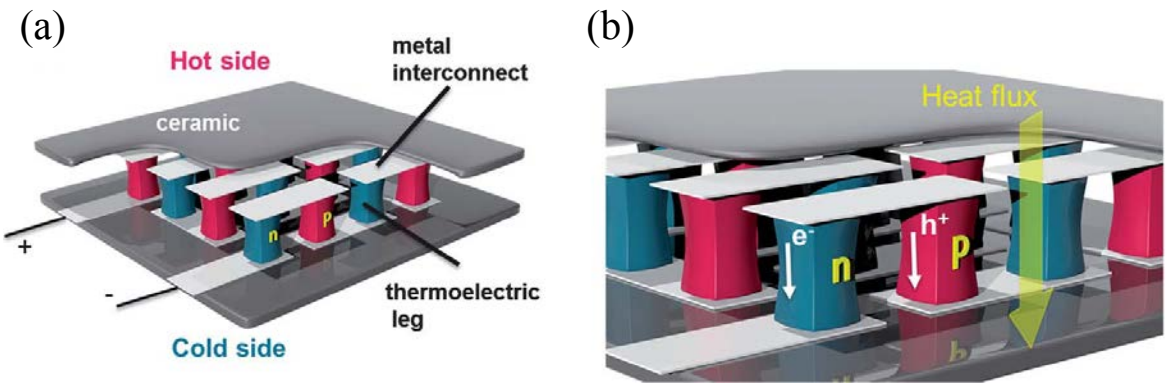

Figure 2.1. A schematic representing a commonly used configuration for standard thermoelectric energy generators that incorporates alternating n- and p-type legs (a). As the legs are connected electrically in series and thermally in parallel, respective charge carriers diffuse in the direction of the heat flux (b), creating an electrical current that can harnessed.[76]

In order to compare the efficiency of harvesting electricity from temperature gradients for different materials, the thermoelectric figure of merit (ZT) is traditionally used. This dimensionless quantity is defined as:

$$ZT = \left(\frac{S^2\sigma}{k}\right)T \qquad (2.1)$$

where S (in V K^{-1}) is the thermopower, σ (in S m^{-1}) is the electrical conductivity, k (in W m^{-1} K^{-1}) is the thermal conductivity, and T (in K) is the absolute measurement temperature.[10] On a microscopic level, ZT describes the coupling behavior between electrical charge and thermal energy transport by carriers within a material.[77] A ZT of 1, which corresponds to ~8% of the Carnot efficiency,[78] is the universal goal for a material to be considered thermoelectrically efficient.[18] It is interesting to note that a thermoelectric material having a ZT of 4 would correspond to ~30% of the Carnot efficiency, which is equal to that of a home refrigerator.[28] Due to thermal conductivity being the least variable among these properties, the power factor ($PF = S^2\sigma$) is also commonly reported in literature and is a simpler measure of conversion efficiency.[5] For many of the inorganic materials used in thermoelectric devices, the transport properties are highly correlated to each other, making it difficult to achieve highly efficient materials.

2.1.2 Thermoelectric Properties of Inorganic Semiconductors

Inorganic materials have been predominately used throughout the thermoelectric community because they possess the best combination of transport properties. **Figure 2.2**a shows the correlation between these properties. Electrical and thermal conductivities increase with carrier concentration, while the Seebeck coefficient largely decreases. Insulators have relatively high Seebeck coefficients and low thermal conductivity, but are not feasible thermoelectrics due to their low electrical conductivity. Metals are also not feasible for waste heat conversion as they have among the lowest

Seebeck coefficients. This is due to the large electronic contribution to the thermal conductivity (Figure 2.2b) and the Fermi level being pushed further into the conduction band (i.e., density of states is more symmetric).[79] The Wiedemann-Franz law, which is the ratio of the electronic contribution of the thermal conductivity to the electrical conductivity,[25] makes it difficult to attain high ZT in conventional metals.[5,18] As a result, the most efficient thermoelectric materials are typically inorganic semiconductors and their alloys. These materials generally produce the highest ZT because they provide the best compromise in transport properties (Figure 2.2a).

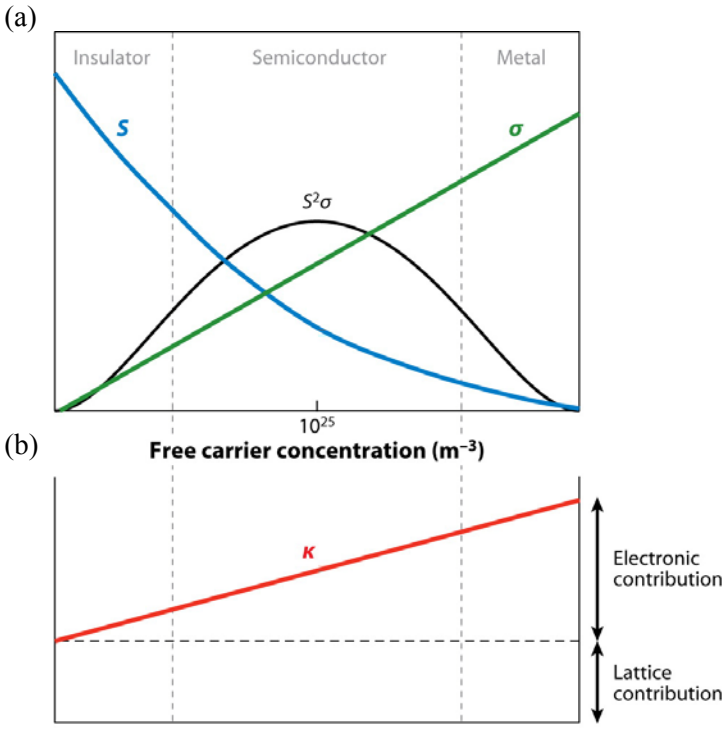

Figure 2.2. Seebeck coefficient, electrical conductivity, power factor (a), and the thermal conductivity (b), as a function of the number of free carriers for monolithic materials.[21]

Bulk inorganic semiconductors have been studied heavily thus far due to the tailorability of their transport properties.[80] When certain elements are alloyed together (e.g., bismuth [Bi], tellurium [Te], or lead [Pb]), carrier concentrations can be increased to electrical conductivity similar to metals. The alloying of these high atomic weight elements also decreases the lattice thermal conductivity, as the transport of phonons is disrupted, resulting in many of the commercially available thermoelectric materials.[11,80] Nanocrystalline Bi_2Te_3, which is a traditional thermoelectric material for cooling applications, achieves a ZT ~ 1 at room temperature ($S^2\sigma \sim 2{,}000\ \mu W\ m^{-1}\ K^{-2}$).[15] As a commonly used material for energy generation, single crystal PbTe achieves a room temperature ZT ~ 0.1 ($S^2\sigma \sim 500\ \mu W\ m^{-1}\ K^{-2}$).[82-83] The efficiencies of these bulk semiconductors is still too low for them to be viably used in more ubiquitous applications. To further optimize alloyed semiconductors with metallic conductivity, dopants can be added to maximize the electronic density of states above the Fermi level (i.e., increase the Seebeck coefficient).[84] Even with significant developments in recent years, it remains difficult to favorably change one property without diminishing another. To overcome this challenge, research into synthesizing new complex crystal structures and nanostructuring current semiconductors are investigated.

The ability to nanostructure materials using lower dimensional inclusions has led to significant increases in ZT that are not possible with monolithic materials.[80,85] The fabrication of these nanostructures can be done by using superlattices (2D), nanowires (1D), and/or quantum dots (0D) to form thin film materials. **Figure 2.3** summarizes the recent advances in ZT for both n- and p-type thermoelectrics as a function of both year

and temperature.[12-14,86-97] Since the discovery of Bi_2Te_3 in the 1950s,[86-87] there has not been significant improvement in this field until the past 10 years. Many of these nanostructured materials have achieved high ZT values ($ZT \geq 1$) by quantum confinement of carrier transport. This creates sharp features that increase the asymmetry in the electronic density of states and lead to the tunability of the thermoelectric properties through doping.[98] Many of these materials still have difficulties achieving high ZT at room temperature and are not feasible for commercial applications because they are prepared by atomic layer deposition (slow, expensive, and difficult to scale to large quantities).[80]

Simpler processes to fabricate large quantities of high ZT bulk nanocomposites from low dimensional materials have recently been investigated (e.g., hot pressing or matrix encapsulation).[80] Many of these inorganic nanocomposites have been found to have similar efficiencies as the nanostructured materials, resulting from the reduced lattice thermal conductivity associated with the high density of interfaces between the differing components.[99] Despite this progress, these inorganic alloys still contain rare elements with large densities,[12-14] require high processing temperatures for fabrication,[15-16] are mechanically brittle, and suffer from toxicity issues.[100] Many of these factors have played a role in limiting the widespread use of thermoelectrics in everyday applications, where thermal gradients could be converted into useful energy. A relatively new way to decouple the thermoelectric transport properties, using environmentally-friendly alternatives to traditional semiconductors, is to tailor electrically conductive polymer composites.

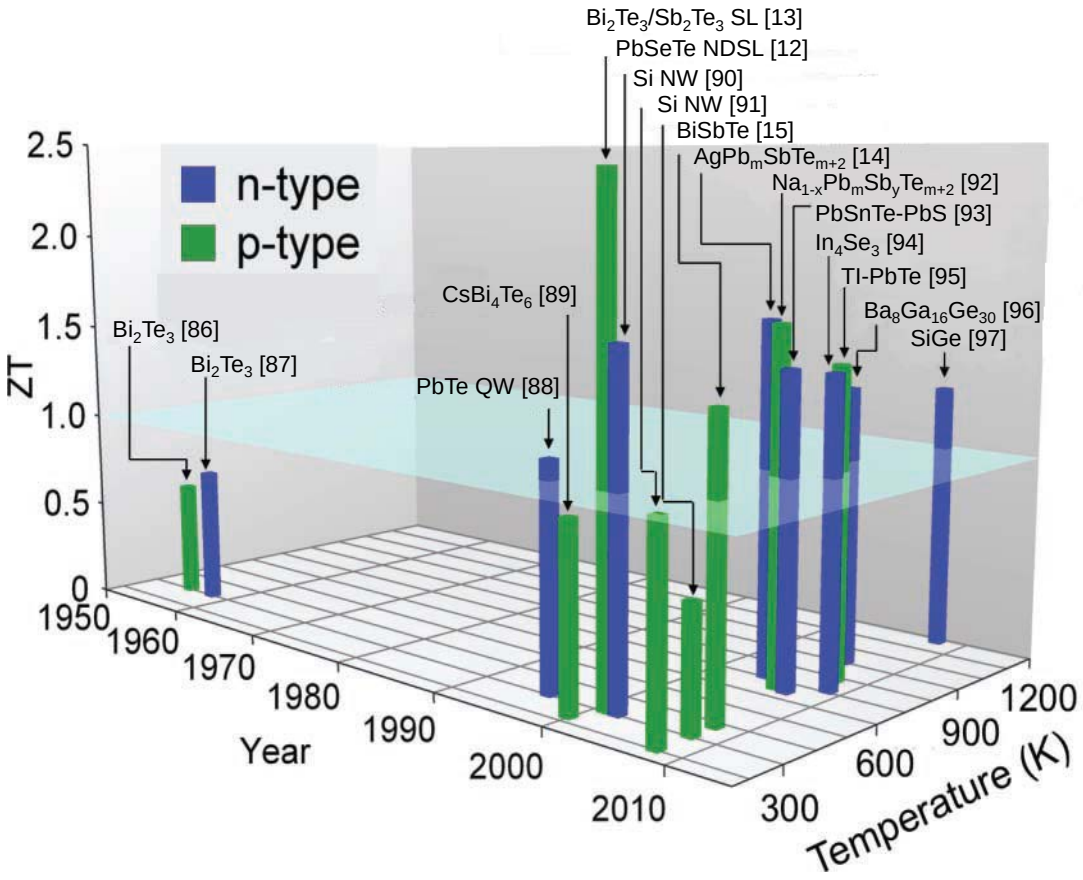

Figure 2.3. Recent thermoelectric efficiency milestones for inorganics as a function of both year and temperature. A light blue line is added at ZT = 1 to signify the importance of achieving efficiencies greater than this.[18]

2.2 Electrically Conductive Polymer Composites

As electrically conductive fillers are added to an insulating polymer matrix, the desired properties associated with the composite's ingredients are combined. Light weight, flexibility, and toughness are a few of the mechanical properties maintained by polymer composites as the electrical conductivity increases with filler concentration. These materials have been used for many different applications ranging from thermal resistors,[101-102] electromagnetic interference shielding,[103-104] sensors (chemical,

temperature, and pressure),[105-110] and thermoelectrics.[7,65,67] Electrically conductive composites can be prepared by either randomly dispersing the filler (e.g., melt blending[32-33,111] or solution processing[37-38]) or by manipulating the filler organization (e.g., immiscible polymer blends[44,50] or a particulate polymer matrix (emulsion)[29-30,45,53-54]). Randomly-dispersed composites generally require a significant amount of filler in order to achieve a reasonable conductivity. This increased filler loading results in an increase in the composite brittleness due the porosity developed by filler aggregates.[45-46] Using polymers with exclusionary microstructures (i.e., segregated network composites) can resolve this issue by reducing the amount of filler needed to achieve reasonable conductivity, while maintaining the mechanical integrity of the composite.[112-114]

2.2.1 Percolation Theory and Models

The ability to add electrically conductive filler to an insulating matrix has led to a broad range of applications where these organic composites can be used. The electrical conductivity can be significantly increased when a critical filler concentration, called the percolation threshold concentration (PTC),[115-116] is reached. **Figure 2.4** shows a schematic of the electrical conductivity behavior of polymer composites as a function of conductive filler concentration. Below the PTC (i.e., insulating zone), no interconnection between the filler particles occurs and electronic behavior is dominated by the insulating nature of the polymer (i.e., electrical conductivity in the range of 10^{-12} to 10^{-18} S cm^{-1}).[117] As the filler concentration reaches the PTC, which is defined as the

amount of filler needed to create one conductive pathway through the composite, a transition from insulator to a conductor occurs. In this percolation zone, there are many different mechanisms of conduction (e.g., capacitance, tunneling, hopping, or ballistic) depending on the temperature, frequency, electric field strength, and type of filler.[118-120] With filler concentrations beyond the PTC, more conductive pathways are created through the microstructure and the composite enters the conduction zone. There have been many theoretical models proposed to understand and predict the PTC of a composite with differing matrices and conductive fillers.

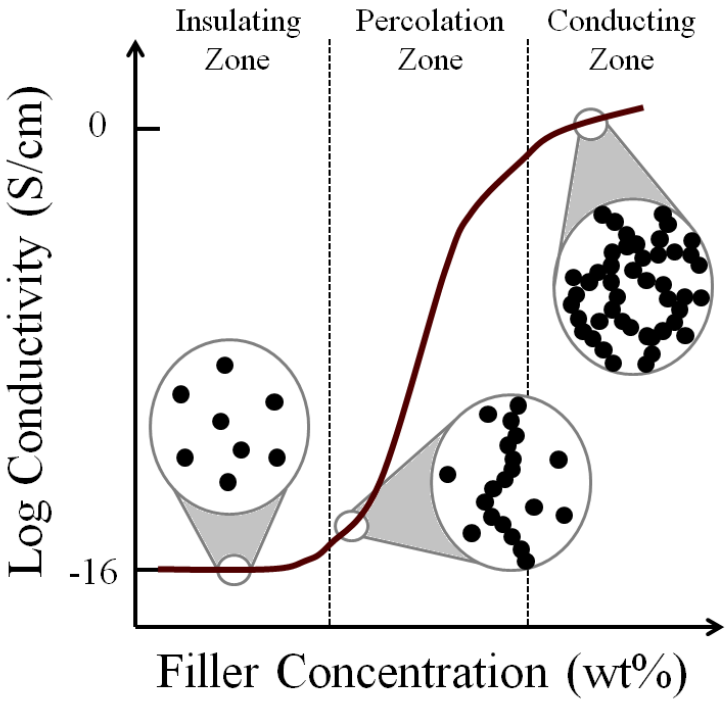

Figure 2.4. Schematic of composite electrical conductivity, as a function of filler concentration, as it transitions from insulating to conducting. The cartoon images (gray outlined circles) highlight the composite microstructure as the filler concentration is increased (small black circles).

The most common percolation theory used for polymer composites was formalized in 1973 by Kirkpatrick in an effort to predict the conductivity above the PTC.[121] This theory states that composite electrical conductivity generally obeys the empirical percolation power law:

$$\sigma = \sigma_0 \left(V - V_c\right)^s \qquad (2.2)$$

where σ_0 is a proportionality constant related to the intrinsic conductivity of the filler, V is the volume fraction of conductive filler, V_c is the critical volume fraction of filler associated with the percolation threshold (PTC), and s is the power law exponent (typically 1.6 – 2.0 for three-dimensional cases).[122] It is worth noting that this percolation theory predicts a PTC of approximately 15 vol% filler when there is no interaction between the matrix and randomly dispersed spherical filler.[47] Equation 2.2 has been shown to accurately fit experimental results involving many different types of fillers (metal particles,[123] CB,[29,118] CNT,[67-68] intrinsically conductive polymers,[124] etc.) in an insulating matrix.

Another percolation model, formulated by Janzen, considered the relationship between the percolation threshold (V_c) and the average number of contacts between filler particles:[125]

$$V_c = [1 + (C/x)\rho v]^{-1} \qquad (2.3)$$

where C is the coordination number in a specific lattice, x is the mean number of contacts between nearest neighbors (NN), ρ is the density of the filler particles, and v is the specific void space of randomly packed filler. To obtain accurate predictions of CB-filled rubber, the matrix was assumed to form a simple cubic lattice (NN = 6).[125-126]

This model concluded that the PTC is dependent on the average number of contacts between conductive filler within a lattice.[125]

Malliaris and Turner considered the relationship between the insulating:conducting particle size ratio and the percolation threshold. For a compacted mixture of polymer and conductive particles, the percolation threshold should decrease as the ratio of polymer to conductive particle size increases according to:[59]

$$V_c = 50A\left[1 + B\left(\frac{R_p}{R_m}\right)\right]^{-1} \quad (2.4)$$

where A is a constant related to the distribution of conductive particles (e.g., A = 0.33 for hexagonal, 0.5 for square, and 0.67 for triangular), B is a constant related to the packing of the conductive particles (e.g., B = 0.2775 for hexagonal), R_p is the radius of the polymer particle, and R_m is the radius of the conductive particle. An assumption was made that the surfaces of the polymer particles are uniformly covered by the conductive fillers.[59] Other models have explained the percolation behavior within conducting composites by taking numerous factors into consideration,[127-131] but there is not a model that can accurately capture all of the key parameters. Kirkpatrick's percolation model will be the primary focus of this dissertation as it has been used to successfully analyze the behavior of segregated network composites.

2.2.2 Segregated Network Composites

First coined by Kusy in 1977 while using electrically conductive mixtures of polymer and metal powders,[49] segregated network composites have been extensively

studied in recent years.[49-59] Kusy defined this new microstructure as the dispersion of metallic particles restricted by the presence of much larger polymeric domains.[49] The metallic fillers used in early studies have become less useful, primarily due to stabilization and oxidation issues (i.e., insulating layers created on their surfaces) during processing.[132-133] Carbon-based fillers (e.g., CB, CNT, graphene, etc.) have been rigorously investigated and are now more commonly used.[7,54,65-68,118]

Segregated network composites, when compared to randomly dispersed composites, can reduce the percolation threshold and help retain the desired mechanical behavior of the polymer matrix. Polymer matrices with exclusionary microstructures can restrict the volume in which conductive filler can reside, resulting in the formation of an electrically conductive network at low concentrations (**Figure 2.5**a). This behavior is fundamentally different from randomly dispersed composites, which allow the filler to freely organize in a homogeneous network as the solution (melt) dries (cools). Solvated polymer chains within these solutions or melts have the liquid-like ability to envelop the conductive filler, which disrupts a conductive network from forming at low concentrations by blocking direct filler-filler contacts (Figure 2.5b).[54] The increased amount of filler required to reach the PTC will simultaneously increase the viscosity of the mixture during processing and the porosity within the microstructure as the polymer chains cannot envelop every filler (i.e., creation of microvoids that degrade mechanical properties as they act as zero modulus filler).[48,54]

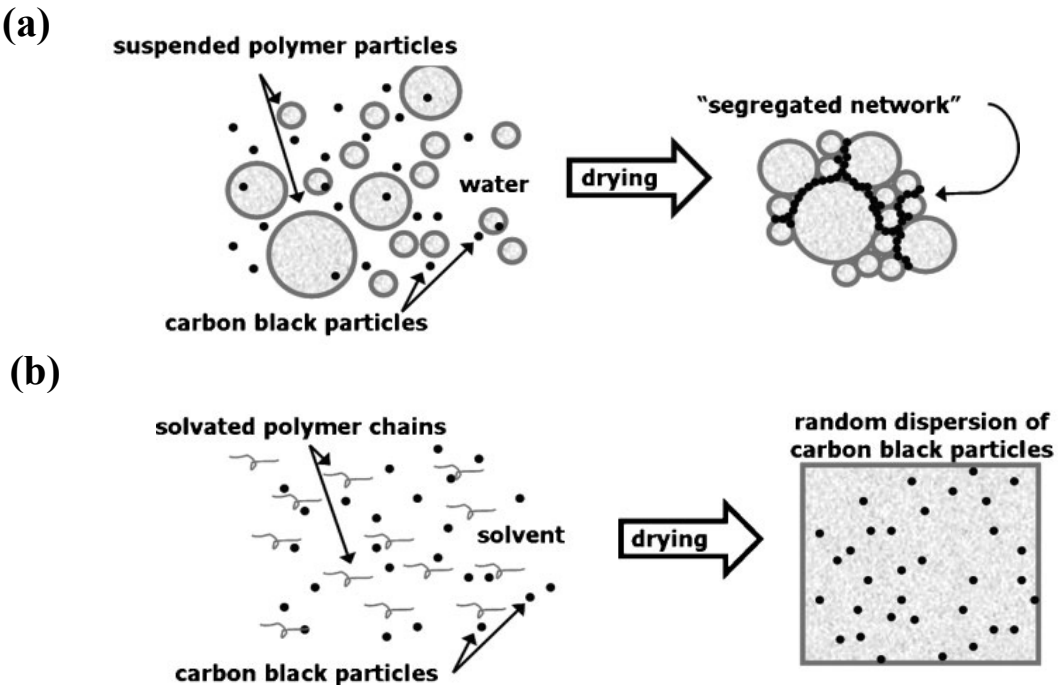

Figure 2.5. Schematics of the development of composite microstructures for carbon black-filled composites using an exclusionary aqueous polymer (segregated network) (a) and a polymer dissolved in solvent (solution) (b).[54]

The electrical conductivity behavior for CB-filled solution-based and emulsion-based composites using PVAc as the matrix were directly compared in **Figure 2.6**.[54] Nearly an order of magnitude reduction in the PTC was observed when solution-based PVAc was replaced by the emulsion (i.e., suspended microscopic solid polymer particles in water).[51] Electrical conductivity for the emulsion-based system was also increased at every CB concentration in comparison to the solution, which can be attributed to the solvated polymer chains enveloping the filler (Figure 2.6b), while the emulsion particles forced the CB into more direct filler-filler contact (Figure 2.6c). Percolation thresholds of 0.1 – 27 vol% filler for melt-processed (polypropylene (PP),[112,134-138] polyethylene

(PE),[32,129,139-145] etc.) and ≥ 0.1 vol% CB for solution-processed (epoxy,[38,146-154] PVAc,[54] etc.) are typical and limit their use in thermoelectric applications as high concentrations of filler are needed to reach high conductivity. Altering the properties of the matrix and using different highly conductive fillers are several ways to further reduce the PTC of polymer composites and improve conductivity, but segregated networks are the focus of the present dissertation.

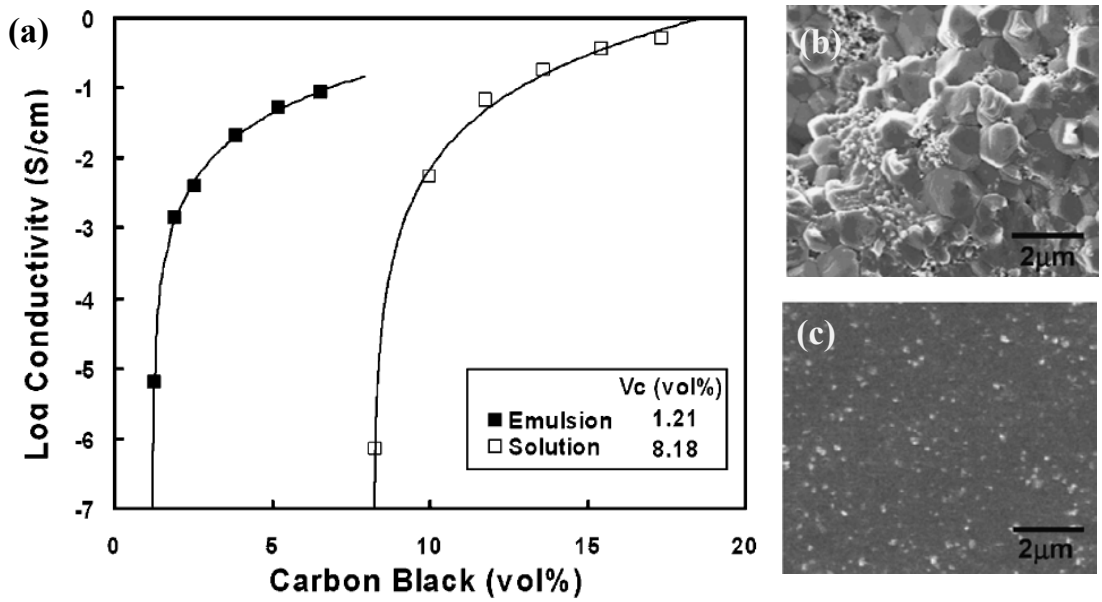

Figure 2.6. Electrical conductivity of PVAc emulsion- and solution-based composites as a function of carbon black concentration (a). The percolation power law is fitted to the experimental data as solid black lines. Freeze-fractured cross-sectional SEM images showing 5.2 vol% CB in PVAc/CB emulsion-based (b) and solution-based (c) composite microstructure (adapted from [54]).

Immisicible polymer blends and emulsion-based composites have been used to create highly conductive polymer composites with their exclusionary microstructures. Blends reduce the PTC ($\leq$ 1 vol%)[155-164] and segregate conductive filler by causing it to either occupy the interstitial space between the different polymer domains or by the filler's preference to be in one polymer domain relative to the other.[41-44] Emulsion-based segregated networks have been used to create electrically conductive polymer composites with antimony-doped tin oxide,[52,62] CB,[30,53-54] and more recently, CNT.[7,55-58,68] Electrical conductivities of these filled emulsions can achieve values greater than 1,000 S cm^{-1}[65] and percolation thresholds below 0.1 vol%.[58,65,165-176] The low percolation thresholds are a direct result of the polymer particles restricting the location of the filler and assuming a close-packed configuration as water evaporates, ultimately coalescing into a coherent film if the minimum film formation temperature of the polymer is exceeded (Figure 2.5a).[51] The high electrical conductivity of these networks, in contrast to randomly dispersed composites, can be attributed to the lack of filler enveloped by solid polymer particles, which discourages electron transport at higher filler loadings due to a decrease in direct filler-filler contacts.[30,54,68]

With CNTs as the electrically conductive filler, emulsion-based composites can achieve conductivities in the degenerate-semiconductor to metallic regimes.[65] There are two primary types of CNTs that exhibit electrical conductivity in the range of 100,000 – 20,000,000 S m^{-1}.[177-179] Single-walled carbon nanotubes (SWNT) (**Figure 2.7**a) consist of a single sheet of graphene rolled up to form a ~1 nm diameter cylinder and can be up to centimeters in length.[63,180-182] The electronic properties of SWNT can

range from semiconducting to metallic, which depends on the chirality (i.e., helicity created by rolling of the graphene).[183-185] Metallic SWNT (Figure 2.7c) have the armchair orientation (0 eV band gap), while semiconducting tubes (Figure 2.7d) have the zig-zag (band gap between 0.18 – 1.8 eV).[184-185] MWNT (Figure 2.7b) can be micrometers in length, have diameters between 2 – 100 nm, and consist of multiple concentric cylinders each separated by ~0.35 nm.[186-187] MWNT can act as either small band gap semi-conductors or metals depending on the chirality of each concentric tube. DWNT are the simplest MWNT with inner tube diameters between 1.0 – 2.0 nm, outer tube diameters between 1.6 – 3.0 nm, and interlayer distance between 0.33 – 0.41 nm.[188-192] The two concentric tubes in DWNT are believed to electrically act as independent SWNT, which provides enhanced electrical conductivity after stabilization.[188-192]

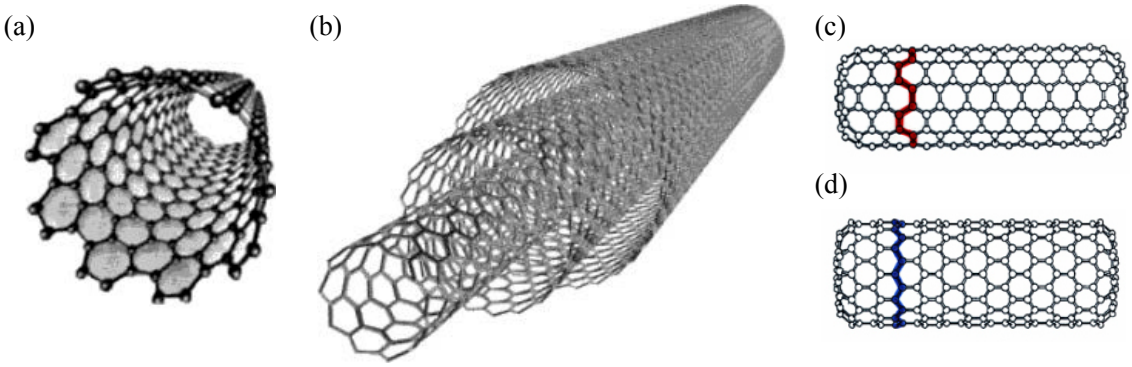

Figure 2.7. Structural representation of single-walled (a) and multi-walled (b) carbon nanotubes,[193] with either armchair (c) or zig-zag chirality (d).[192]

Several other ways to modify the conductive behavior of emulsion-based composites involve using different stabilizing agents for CNTs and manipulating the polymer matrix. In order to make emulsion-based composites containing CNTs, stabilizing agents are required to overcome their hydrophobic and highly entangled nature. Strong Van der Waals interactions prevent CNTs from completely dispersing and/or exfoliating in water.[194-195] Several different types of stabilizers, each having a unique influence on the electron transport across junctions, have successfully been used including surfactants,[196-199] polymers,[200-203] and inorganic nanoparticles.[204-205] Intrinsically conductive polymer stabilizers, in particular, can dramatically increase composite electrical conductivity by creating less resistive junctions.[7,65,206] The conductivity can also be increased, with a reduction in the PTC, by manipulating the polymer modulus,[30] emulsion particle size,[29] and drying temperature.[30,65] By increasing the modulus of the polymer, by increasing glass transition temperature (T_g), the emulsion particles maintain their shape during coalescence and more effectively force the filler particles into the interstitial space between them.[30,206] An increase in the emulsion particle size also reduces the PTC (Eq. 4) by further restricting the volume in which filler can reside.[29] At filler loadings well above the PTC ($\geq$ 20 vol%), baking the composite at an elevated temperature helps tighten the network by reducing the porosity and resulting in more intimate filler contacts.[65] Electrical conductivity is an important property needed for a material to be thermoelectric, but segregated network composites also have the ability to decouple this property from the Seebeck coefficient.

2.2.3 Thermoelectric Polymer Composites

Intrinsically conductive polymers (ICPs) and electrically conductive polymer composites provide the opportunity to combine the thermoelectric behavior of inorganic semiconductors with the flexibility, low density, low temperature processing, and rational tuning of energy levels relative to typical polymers.[207] ICPs that have been studied for their thermoelectric behavior include polyacetylene,[208-210] polyaniline,[211-214] poly(3,4ethylenedioxythiophene) (PEDOT),[215-220] and polypyrrole (**Figure 2.8**).[76, 221] Doping of ICPs, using either oxidizing or reducing agents, can transition their electronic properties from semiconducting to metallic by controlling the number of charge carriers on the conjugated backbone.[222-224] Increased control of the oxidization (p-type doping), or reduction (n-type doping), to further tailor their thermoelectric properties can be accomplished by using electrochemical polymerization or by electrochemically doping.[76,225] Seebeck coefficients can vary from ~10 – 1,000 $\mu V\ K^{-1}$,[208-216,225-226] but exhibit similar S – σ coupling to that observed for inorganic thermoelectrics.[226] Polyacetylene (PA) was one of the earliest doped ICPs studied and was found to have an $S^2\sigma$ ~400 $\mu W\ m^{-1}\ K^{-2}$ due to its high electrical conductivity,[210] but this polymer is very unstable in air.[76,208-2010,228-229] PANI, doped with hydrochloric acid (HCl), showed typical thermoelectric behavior for ICPs, with a power factor of ~12 $\mu W\ m^{-1}\ K^{-2}$.[214] More recent efforts have demonstrated a ZT ~0.1 with a highly stable p-type ICP synthesized from poly(phenylenevinylene) doped with iodine.[230-231]

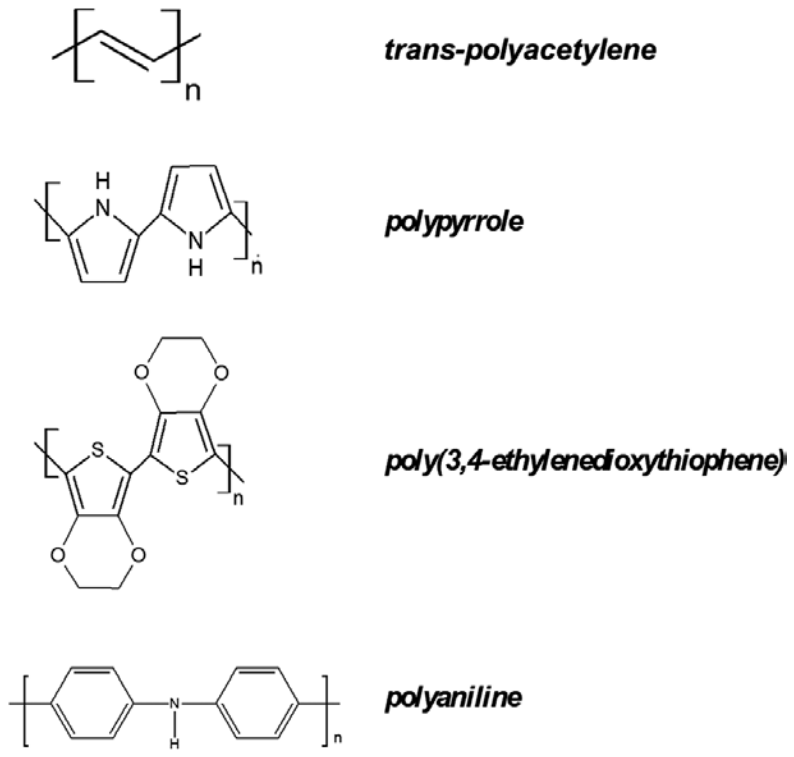

Figure 2.8. Repeat unit structures of conjugated polymers studied for thermoelectric behavior.[76]

PEDOT is one of the most commonly studied ICPs for electronic and thermoelectric applications.[76,211-212,215-220,233-240] This polythiophene can be reversibly doped,[233] has excellent chemical and thermal stability,[234] a low band gap between 1-1.6 eV,[235-237] and excellent electrochemical properties.[238-239] Highly doped conducting polymers are often insoluble in water unless they are combined with a soluble polymeric counterion to create a micelle-like particle (e.g., polystyrene sulfonate (PSS)) or by using an ionic surfactant stabilizer.[217, 240] Pristine PEDOT:PSS (**Figure 2.9**) is very soluble in water, but has poor thermoelectric properties (σ ~6 S m^{-1}, S ~12 μV K^{-1}, and $S^2\sigma$ ~0.001 μW m^{-1} K^{-2}).[219]

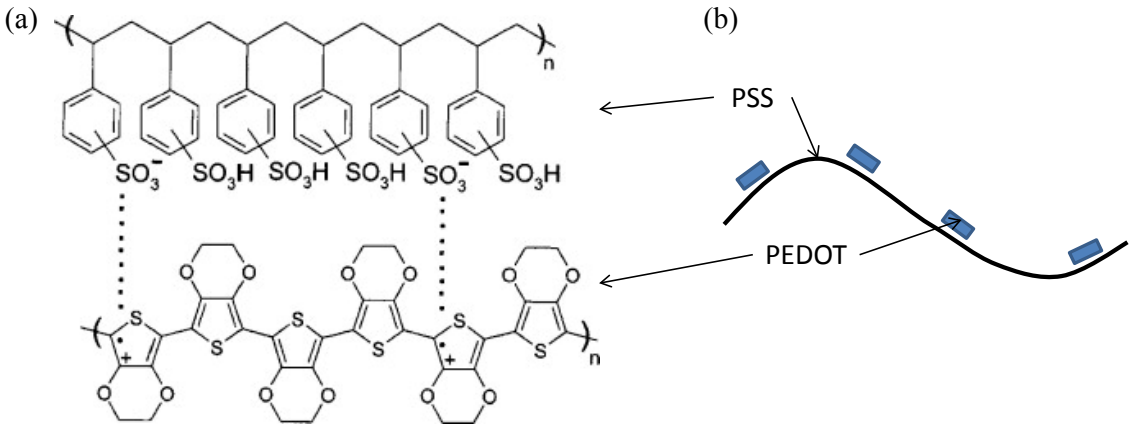

Figure 2.9. Chemical structure of PEDOT:PSS (a) with a schematic of the large polyanion dopant (PSS) PEDOT segments along its polymer chain (b) (adapted from [241]).

Table 2.1 summarizes the recent literature on the thermoelectric properties of PEDOT and its many derivatives. Doping commercially available PEDOT:PSS with a secondary dopant (e.g., dimethyl sulfoxide (DMSO)) causes a morphological reorganization in the structure, which ultimately increases the carrier mobility as the coil is transformed into a more linear conformation ($S^2\sigma$ ~45 μW m^{-1} K^{-2}).[218,242] When the insulating polyanion (PSS) is replaced by a smaller anion (e.g., iron (III) *tris*-p-toluenesulphonate (Tos)), PEDOT films can reach electrical conductivity values exceeding 100,000 S m^{-1}.[243] By controlling the oxidation levels of PEDOT-Tos using a reducing agent, $S^2\sigma$ was shown to reach ~320 μW m^{-1} K^{-2}.[216] A power factor of ~1,300 μW m^{-1} K^{-2} has been achieved for a film containing pyridine, a poly(ethylene glycol)-*block*-poly(propylene glycol)-*block*-poly(ethylene glycol) (PEPG) triblock copolymer,

and PEDOT (PP-PEDOT).[244] PEDOT:PSS, due to its aromatic structure and water solubility, can be used in conjunction with CNTs to create more electrically conductive, emulsion-based thermoelectric materials.

Table 2.1. Experimentally measured electrical conductivity, Seebeck coefficient, and power factor for PEDOT-containing materials and other conductive polymers (adapted from [244]).

Sample	σ (S m^{-1})	S (μV K^{-1})	$S^2\sigma$ (μW m^{-1} K^{-2})	Reference
Pristine PEDOT	~6	~12	~0.001	[219]
PP-PEDOT at 0.1 V	~92,300	~117	~1,270	[244]
Pristine PP-PEDOT	~135,400	~80	~960	[244]
PP-PEDOT at 1.1 V	~212,200	~50	~530	[244]
PEDOT:Tos films	~6,700	~220	~320	[216]
PEDOT nanowire	700 – 4,000	33 – 122	6 – 12	[245]
PEDOT films	320 – 1,830	33 – 57	0.5 – 4	[245]
PEDOT:PSS/DMSO/EG	22,000 – 29,800	13 – 14	3 – 6	[215]
PEDOT:PSS/5% DMSO	~94,500	~22	~45	[242]
PEDOT:PSS/5% DMSO	~29,900	~13	~5	[246]
PEDOT:PSS/urea	816 – 6,300	15 – 21	~3	[247]
PVAc/PEDOT:PSS/SWNT	~40,000	~25	~25	[65]
PEDOT:PSS/TE nanowire	~19,300	~160	~70	[248]
PA iodine doped	$3x10^6$ – $5x10^6$	15 – 20	1,200 – 1,500	[209]

Grunlan *et al* has recently shown the thermoelectric behavior of segregated network polymer composites and pioneered a field of light weight, water-processed thermoelectrics.[7] These CNT-filled composites were fabricated using gum arabic (GA), which is an insulating stabilizer for CNTs.[195] The electrical conductivity of these emulsion-based composites increases with CNT concentration (**Figure 2.10**a) due to the polymer particles forcing the CNT into the interstitial spaces between them (Figure 2.10b and c). As the electrical conductivity increases, the Seebeck coefficient (i.e., thermopower) remains insensitive to CNT concentration and is similar to those measured for metallic SWNT (~40 $\mu V\ K^{-1}$ at 300 K).[249-250] The junction between CNT is believed to play an important role in filtering low energy electrons, which is what keeps the Seebeck coefficient insensitive to the increase in conductivity. This study demonstrates a way to successfully decouple thermoelectric properties by creating electrically connected, but thermally disconnected, CNT junctions that promote electron hopping and impede phonon transport.[7]

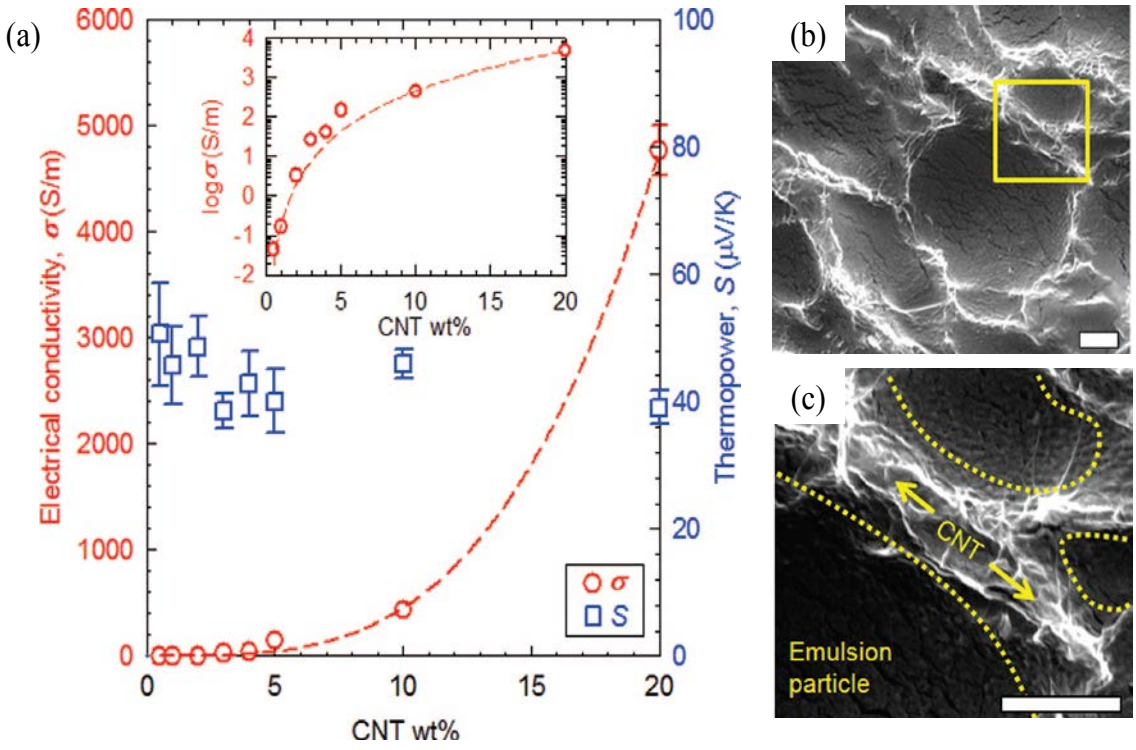

Figure 2.10. Electrical conductivity (circles) and Seebeck coefficient (squares) measured as a function of nanotube concentration at room temperature (a). The dashed red line and inset graph represent the data fitted to percolation power law (Eq. 2). The segregated network behavior is demonstrated in the freeze-fractured cross-sectional SEM of 5 wt% CNT (b), with the yellow square representing a high-magnification image (c). The scale bars in the images indicate 1 μm (adapted from [7]).

As CNT loading is increased to achieve higher electrical conductivity, the thermal conductivity in polymer composites remains in the insulating polymer regime (~0.1 – 0.4 W m^{-1} K^{-1}).[251-254] For ICPs and polymer composites, thermal conductivity is dominated by phonon transport.[183,251] An upper limit parallel resistor model (i.e., simple rule of mixtures) and a lower limit series model have been used to predict the thermal conductivity when CNTs (k ~1,000 – 3,000 W m^{-1} K^{-1})[249,255] are added to an insulating matrix (**Figure 2.11**). These composites, especially segregated networks, do

not exhibit the same percolation behavior as seen with electrical conductivity.[7,256-265] This small thermal conductivity can be primarily attributed to the high interfacial thermal resistance between the high aspect ratio CNTs and polymer matrix.[266] The interfacial resistance between CNTs and matrix represents a barrier for heat flow as scattering of phonons occurs due to mismatched vibrational frequencies.[267] This resistance was theoretically and experimentally quantified to be ~10^{-8} m^2 K W^{-1}, which corresponds to the resistance of a ~10 nm insulating layer.[267-268] A separate model reported an order of magnitude decrease in the composite thermal conductivity when the interfacial resistance was increased from 0 to $8x10^{-8}$ m^2 K W^{-1}.[269-270] The contact resistance between nanotubes is also high due to the small contact area and the Van der Waals interactions that bind CNT bundles/ropes together.[271] Gaps created by the misalignment of CNTs and CNT-stabilizer molecules acting as phonon scattering centers are additional factors that limit the composite thermal conductivity.[267]

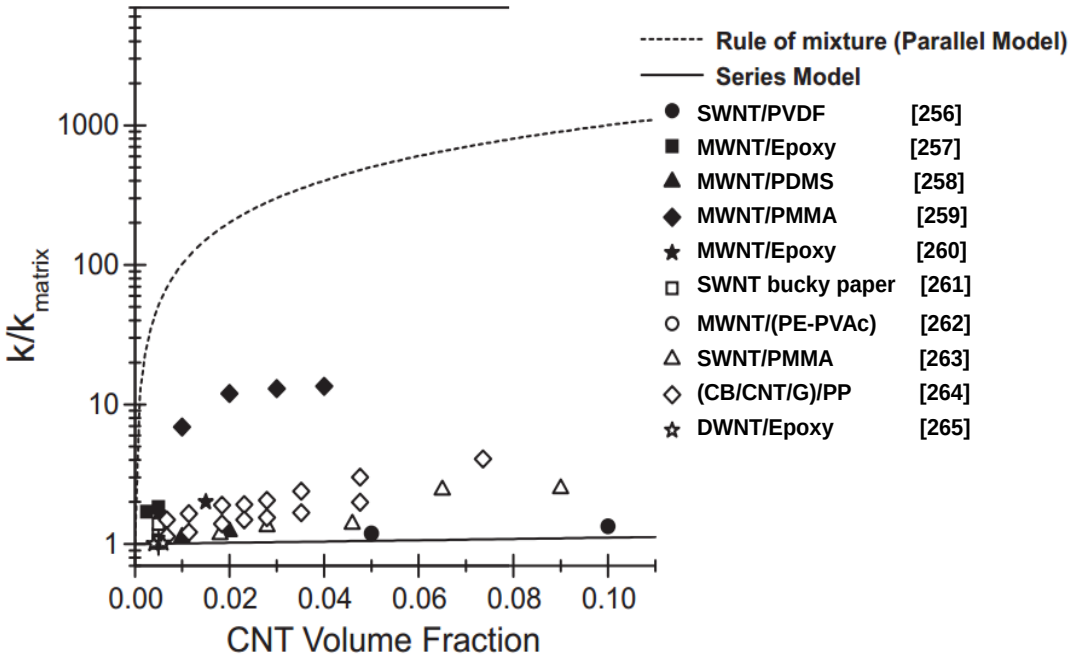

Figure 2.11. Thermal conductivity (of reported systems in literature) normalized by a reference matrix and represented as a function of CNT loading. These values were plotted in conjunction with the parallel (dotted line) and series (solid line) models (adapted from [251]).

To increase the electrical conductivity of CNT-filled segregated networks, intrinsically conductive polymers have been used to help tailor the numerous electrically-resistive CNT junctions. The use of PEDOT:PSS was shown to effectively stabilize CNT due to the aromatic rings in their respective chemical structures (Figure 2.7 and 2.9) creating noncovalent $\pi - \pi$ interactions.[162] The use of an ICP stabilizer reduces the energy barrier (e.g., lowers the band gap) between adjacent CNTs, thus creating less resistive junctions and increasing the composite electrical conductivity (**Figure 2.12**). By exchanging the stabilizer from the insulating GA to the conductive PEDOT:PSS, a four orders of magnitude increase in conductivity was observed and

results in $S^2\sigma$ ~25 μW m^{-1} K^{-2} (Figure 2.12a).[65] With a 60:30 CNT:(PEDOT:PSS) weight percent ratio, which minimizes the amount of insulating PVAc, the thermoelectric properties are optimized (S ~ 40 μV K^{-1}, σ ~100,000 S m^{-1}, and $S^2\sigma$ ~160 μW m^{-1} K^{-2}).[206] PANI has also been used in conjunction with CNT-filled composites,[272-276] exhibiting $S^2\sigma$ ~90 μW m^{-1} K^{-2} and maintaining a polymeric thermal conductivity of 0.27 W m^{-1} K^{-1}.[273] Combining CNT-filled composites with inorganic nanoparticles has helped to further manipulate the junctions and improve the thermoelectric properties.[64,207,277,280-284] Polymer composites have been predominately p-type thus far, as CNTs are very susceptible to oxygen doping (i.e., oxidation).[249,278-279] Carbon nanotube functionalized with polyethyleneimine (PEI) has been shown to exhibit an n-type Seebeck coefficient of -100 μV K^{-1}.[278] All of these results suggest that fully organic thermoelectric materials, with their light weight and environmentally-friendly composition, are becoming competitive with the common inorganic semiconductors used today.[285-288]

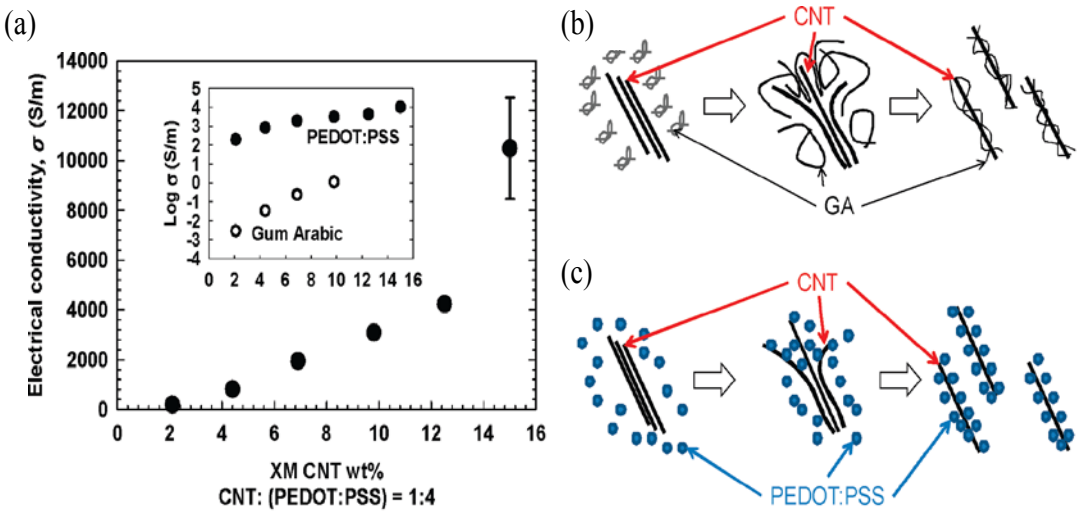

Figure 2.12. Electrical conductivity (measured at room temperature) of 1:4 XM-CNT:(PEDOT:PSS) composites (a). To show the role of stabilizer on electron transport across CNT junctions, electrical conductivity of GA-stabilized composites (hollow circles) (b) is plotted in the inset compared to those of PEDOT:PSS-stabilized composites (filled circles) (c) (adapted from [65]).

The ability to stabilize CNTs with different types of polymers and/or small molecules has led to the tailorability of their thermoelectric properties. Being able to manipulate electrical conductivity by using different composite constituents, while keeping the Seebeck coefficient (and thermal conductivity unaltered), was an important step for organic thermoelectrics. These studies led to the idea of simultaneously increasing both the electrical conductivity and Seebeck coefficient through the use of different stabilizers. Further studies presented in this dissertation (Chapters III, IV, V, and VI) lay the groundwork for the fully organic, flexible thermoelectric polymer composites.

CHAPTER III

INFLUENCE OF A SEMICONDUCTING CARBON NANOTUBE STABILIZER ON SEEBECK COEFFICIENT*

3.1 Introduction

Segregated network composites have been shown to increase in electrical conductivity with increasing CNT concentration. The thermoelectric properties of these polymer composites are dominated by the junctions between each tube.[7,65] In an effort to increase the Seebeck coefficient, a semiconducting molecule, *meso*-tetra(4-carboxyphenyl) porphine (TCPP), was used to stabilize MWNT. The capability of porphyrin derivatives to act as a surfactant, and also enhance electrical conductivity (or Seebeck coefficient),[42] suggests they can be used to make composites with improved ZT. A composite made with poly(vinyl acetate) latex and 12 wt% MWNT exhibits an increase in Seebeck coefficient, from 8 to 28 $\mu V\ K^{-1}$, when the stabilizer is changed from an insulating molecule, sodium deoxycholate (DOC), to TCPP. The porphyrin stabilizer is not as effective as DOC, so there is a slight reduction in electrical conductivity at a given MWNT concentration. The universality of this approach to

*Reprinted with permission from G. P. Moriarty, J. N. Wheeler, C. Yu, J. C. Grunlan. Increasing the thermoelectric power factor of polymer composites using a semiconducting stabilizer for carbon nanotubes, Carbon 50, 885-895, Copyright 2012 by Elsevier.

increase Seebeck coefficient (*S*) is demonstrated by replacing MWNT with DWNT in the composites. *S* increases from ~70 to ~80 μV K^{-1} when the stabilizer is changed from DOC to TCPP for DWNT-filled composites. Composite thermal conductivity did not significantly change from that of unfilled polymeric materials (0.2 – 0.4 W m^{-1} K^{-1}) as the stabilizer and CNT were exchanged. This use of a semiconducting stabilizer provides a new tool for enhancing the thermoelectric properties of polymer nanocomposites and provides greater potential for their use in harvesting waste heat, especially from places where inorganic semiconductors would be impractical (e.g., painted surfaces).

3.2 Experimental

3.2.1 Materials

A vinyl acetate/acrylic copolymer (PVAc) emulsion (Rovace TM 86 supplied by Rohm and Haas, Spring House, PA), that is 54.7 wt% solids in water, was used as the composite matrix starting material. This PVAc emulsion has an average particle diameter of 346 ±7nm. MWNT (Baytubes C 150P provided by Bayer MaterialScience, Leverkusen, Germany), with an average diameter of 14 nm and a length of 1 – 10 μm, was used as the model electrically conductive filler. DWNT (XBC1001 purchased from Continental Carbon Nanotechnologies, Inc., Houston, TX), with an average outer diameter of 3 nm and lengths of 0.5 – 2.0 μm, was used as high electrical conductivity filler. DOC (Sigma-Aldrich, Saint Louis, MO) or TCPP (Frontier Scientific, Logan, UT) were used to stabilize the nanotubes in water during composite preparation.

3.2.2 Composite Preparation

MWNT:stabilizer weight ratios of 1:1.57 and 1:3 were prepared using aqueous solutions of 3 wt% DOC and 2.67 wt% TCPP, respectively. These weight ratios were chosen to maintain equal moles of surfactant per gram of MWNT. These aqueous suspensions were then sonicated with a VirTis Virsonic 100 ultrasonic cell disrupter (SP Industries Inc., Warminster, PA) for 10 minutes at 50 W in an ice water bath. The PVAc emulsion and deionized water were adjusted (using a 0.1 M NaOH solution) to pH 10, as this was the pH value of the TCPP molecule needed in order to be stable in water. The polymer emulsion and pH-adjusted deionized water were then added to the MWNT:stabilizer mixture and sonicated again for another 10 minutes at 50 W. This final aqueous suspension contained 5 wt% total solids. Composites with seven different MWNT concentrations (2.5, 3, 4, 5, 7, 10, and 12 wt%) were prepared by drying suspensions in a 26 cm^2 plastic mold for 2 days under ambient conditions and then for 24 hours in a vacuum desiccator. This was done to ensure that all residual moisture within the composite materials was removed prior to testing. Concentrations are based upon the dry weight of PVAc, MWNT, and surfactant solids used in the composite. Composites containing 7, 10, and 12 wt% DWNT were prepared in the same manner, but with aqueous suspensions containing 2.5 wt% total solids. This was done to reduce the solution viscosity and ensure the complete exfoliation of CNT. Composite thicknesses ranged from ~0.15 to 0.24 mm and were measured with a table top micrometer.

3.2.3 Characterization

3.2.3.1 Electrical Conductivity

The in-plane electrical conductivity of these composites was measured with a custom built four-point probe system. This system consists of a Keithley 2000 multimeter (Cleveland, OH) for current measurement, an Agilent E3644A power supply (Santa Clara, CA), a mounted Signatone S-301 four-point probe (Gilroy, CA), and a LabView interface (National Instruments, Austin, TX) for recording voltage. This measurement technique is commonly used to obtain the electrical resistance of a thin material. **Figure 3.1** shows a schematic illustration of a four-point probe where a current is passed between the outer probes, while the drop in voltage is measured between the inner probes. Sheet resistance (R_s) of these composites is obtained by:

$$R_s = 2\pi \times d \times \left(\frac{V}{I}\right) \qquad (3.1)$$

where d (in cm) is the spacing between probes (i.e., d = 0.72 cm for this system), V is the voltage, and I is the current. The electrical conductivity is calculated by taking the inverse of the product of R_s and composite thickness. Five measurements were taken on each side (top and bottom surfaces of the composites) to confirm that a given specimen was isotropic.

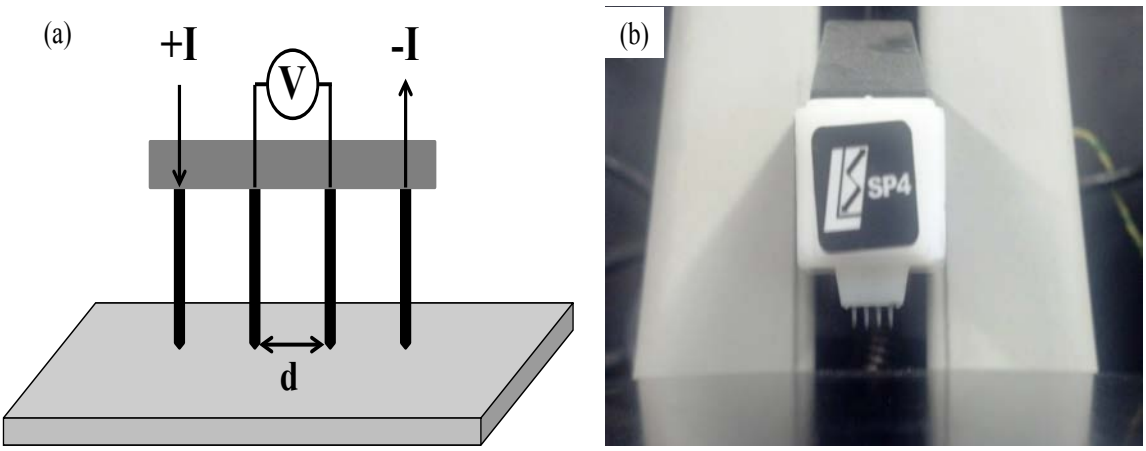

Figure 3.1. Schematic (a) and photograph (b) of a four-point probe apparatus.

3.2.3.2 Seebeck Coefficient

To measure the Seebeck coefficient (and consequently the in-plane electrical conductivity) of these polymer composites, a home-built, shielded four-point probe apparatus was used. This apparatus is equipped with a Keithley 2000 multimeter, a GW PPS-3635 power supply (Good Will Instrument Co., LTD), and operated with a LabView interface. Rectangular shape samples (~30 mm in length and 3 mm in width) were prepared with four electrically conductive metal lines painted onto the ends with silver-filled adhesive. The samples were suspended across two thermoelectric devices (TE, ~20 mm apart) that were used to create precise temperature gradients (**Figure 3.2**). R_s was then obtained by taking the slope of the sweeping I-V measurement curve, which also indicates if contact is ohmic, and converted into electrical conductivity by the same method as Section 3.2.3.1.

The two thermoelectric devices (TE_1 and TE_2) are electrically connected in series to allow one device to cool and one to heat (i.e., one is up-side-down compared to the

other). By switching the behavior of the side in contact with the sample (e.g., switching the polarity of the input current) and changing the amount of current supplied to the two devices, the temperature gradient across the sample can be altered. Two T-type thermocouples, in conjunction with two copper leads, were placed in contact with the silver-painted lines on both ends of the sample to simultaneously measure the temperature gradient (ΔT) and thermoelectric voltages (ΔV). The Seebeck coefficient was obtained by taking the slope of the V – T curve as the temperature gradient was varied up to 10°C and the thermoelectric voltages measured. Electrical conductivity and Seebeck coefficient measurements were done subsequently and achieved with the same sample, which minimizes the uncertainty that is potentially present in the samples due to differing composite microstructures.[7]

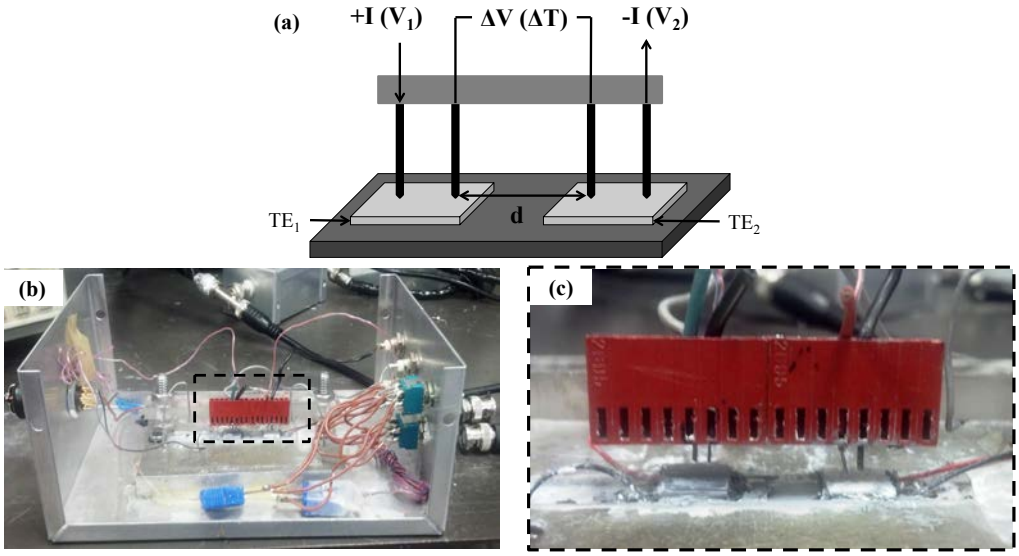

Figure 3.2. Schematic of the home-built four-point probe apparatus used to measure electrical conductivity (or Seebeck coefficients) (a) with photographs of the device in (b) and (c).

3.2.3.3 Thermal Conductivity

Thermal conductivity was measured in the through-thickness direction with a home-built ASTM D5470 steady-state standard setup (**Figure 3.3**). This setup was constructed with two brass blocks connected to a cartridge electrical heater and circulating water cooling bath (PolyScience, Niles, IL) to maintain a constant temperature gradient. The electrical heater was set to provide a constant temperature of 50°C, while the circulating water was set at 0°C. Meter bars, comprised of 1/2 inch diameter stainless steel, were then attached to the brass blocks and used as calorimeters. Ten T-type thermocouples (TC), each separated by ~7 mm, were then attached to both meter bars (i.e., five per calorimeter) to enable the extrapolation of the measured temperature profiles to the sample surfaces. The thermal conductivity (k) was then calculated by:

$$k = \frac{Q \times t}{A \times (T_H - T_C)} \tag{3.2}$$

where Q (in W) is the average heat flow through the sample, t (in m) is the sample thickness, A (in m^2) is the area of the meter bars, T_H (in K) is the temperature of the heated meter bar in contact with the sample, and T_C (in K) is the temperature of the cooled meter bar in contact with the sample. A silicon-based thermal paste was used to help increase the thermal conductivity of the interface between the meter bars and sample.

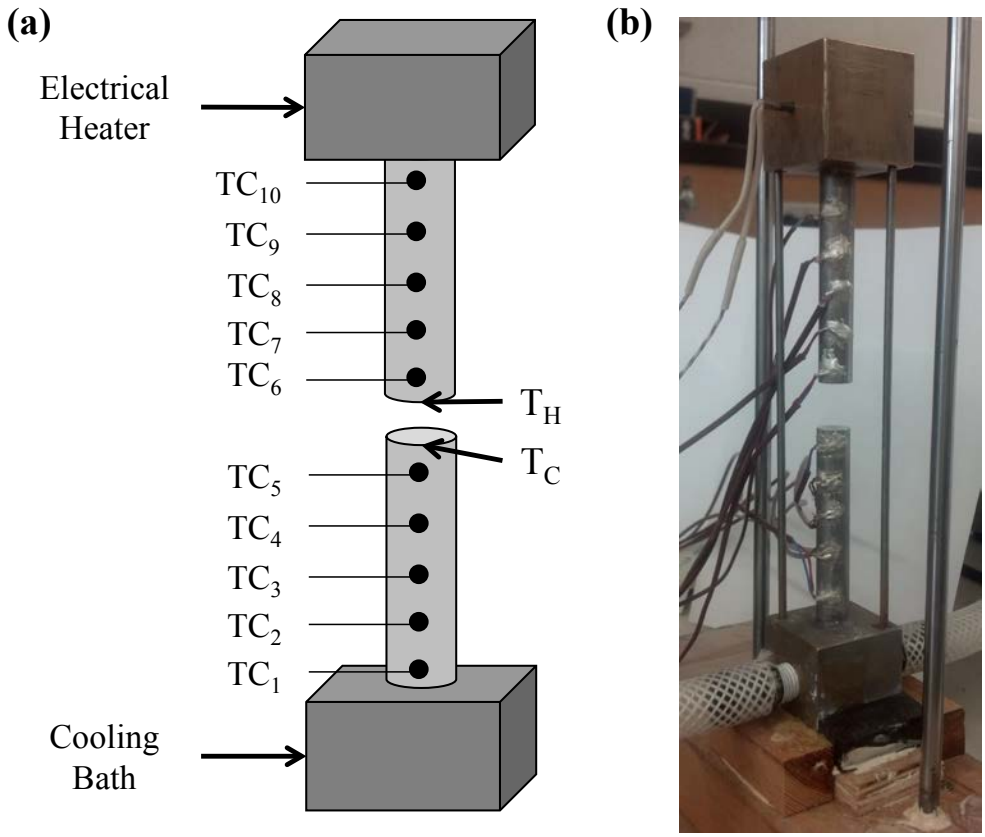

Figure 3.3. Schematic (a) and photograph (b) of a steady-state through-thickness thermal conductivity apparatus in accordance with ASTM D5470.

3.2.3.4 Thermomechanical Properties

Glass transition temperatures (T_g) and storage moduli were measured with a Q800 Dynamic Mechanical Analyzer (DMA) from TA Instruments (New Castle, DE). The composites were cut into strips (~27 mm in length and 4 mm in width) and measured in tensile mode, with amplitude of oscillation and frequency of 15 μm and 1 Hz, respectively. Temperature was ramped at a rate of 5°C min^{-1}, from -70 to 70°C, during testing. The T_g was taken as the peak in the loss modulus curve of each sample,

while the storage moduli were recorded at -60°C to ensure a measurement in the glassy state.

3.2.3.5 Composite Microstructure

The electron micrographs of composite cross-sections were taken with an FEI Quanta 600 FE-SEM (Hillsboro, OR). Samples were soaked in liquid nitrogen and freeze-fractured by hand, then sputter coated with 5 nm of platinum prior to imaging. During imaging, the accelerating voltage was 10 kV, with a spot size of 3.0 nm and a working distance of approximately 10 nm.

3.3 Results and Discussion

3.3.1 Composite Microstructure

Schematic representations of the dispersing behavior of DOC and TCPP are shown in **Figure 3.4**a and b, respectively. Both stabilizers exfoliate the MWNT in solution by adsorbing to their surfaces and changing them from hydrophobic to hydrophilic. DOC was chosen as a reference stabilizer because it is already known to effectively exfoliate CNT in water.[290-292] Porphyrin complexes have also been used as stabilizing agents for CNT and are believed to attach to nanotube surfaces through electrostatic[293] and/or $\pi - \pi$ interactions (i.e., secondary interactions that occur between aromatic or cyclohexane rings).[294-295] The chemical structures of each stabilizer reveal that DOC is an insulator and TCPP, with its conjugated backbone, is capable of conducting electrons. When the emulsion is added to this solution, the polymer particles

exclude volume during drying that the MWNT could otherwise occupy, thereby forcing the nanotubes into the interstitial spaces between them (Figure 2.5a).

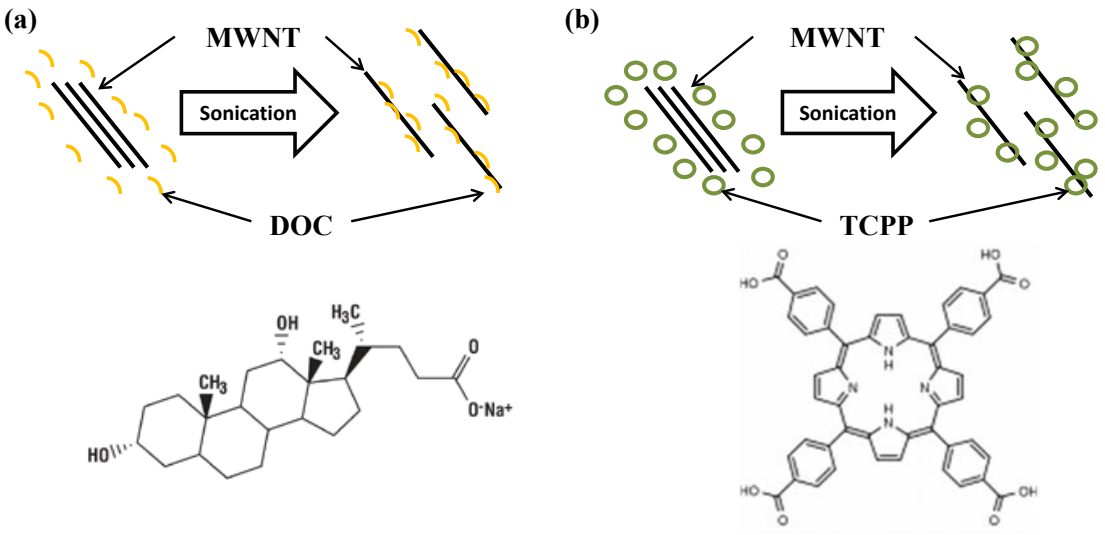

Figure 3.4. Schematic representations of the dispersed MWNT by the two stabilizing agents, DOC (a) and TCPP (b), with their respective chemical structures.

Figure 3.5 shows SEM cross-sectional micrographs of the 1:1.57 MWNT:DOC composites with varying MWNT concentrations. The 2.5 wt% MWNT composite (Figure 3.5a) does not clearly show the expected segregated network, which may be due to the sample being too close to the percolation threshold. There are relatively few long nanotube pathways in a composite with concentrations near the PTC (V_c) (Equation 2.2), making them difficult to find with SEM. At higher magnification (Figure 3.5b), the MWNT are shown to be aggregating in bundles by the polymer particles instead of being more evenly dispersed throughout the available interstitial space. Even with stabilizer

present, strong interactions exist among the nanotubes. Increasing the ratio of stabilizer to nanotube would likely improve dispersion, but it would be expected to simultaneously diminish electrical conductivity due to blocking of direct tube – tube contacts. When the MWNT concentration is increased to 10 wt% (Figure 3.5c), the segregated network becomes more visible. The polymer forms relatively large domains (> 10 μm) of many coalesced particles that the MWNT forms a network around. At higher magnification (Figure 3.5d), the MWNT are shown to be located in the regions between the large polymer particle domains. The MWNT do not appear to have significant interaction with the polymer, which contributes to higher conductivity. It is important to note that as the MWNT concentration is increased, the porosity of the network also increases. These microvoids form when the polymer particles can no longer fill the gaps between MWNT and contribute to degradation of mechanical properties at high concentration.[30] When the filler is changed to DWNT, at a concentration of 10 wt% (Figure 3.5e), the network appears more uniform and detached from the matrix. A possible reason for this could be due to the smaller DWNT not being stabilized as well by the DOC, allowing more bundles to form. Another possible reason for the irregular surfaces could be due to the DWNT being pulled out of the matrix instead of being fractured or embedded. This is evidence of the DWNT having a higher mechanical strength than the MWNT. There are still many tube – tube junctions (Figure 3.5f) that allow for increased electrical conductivity.

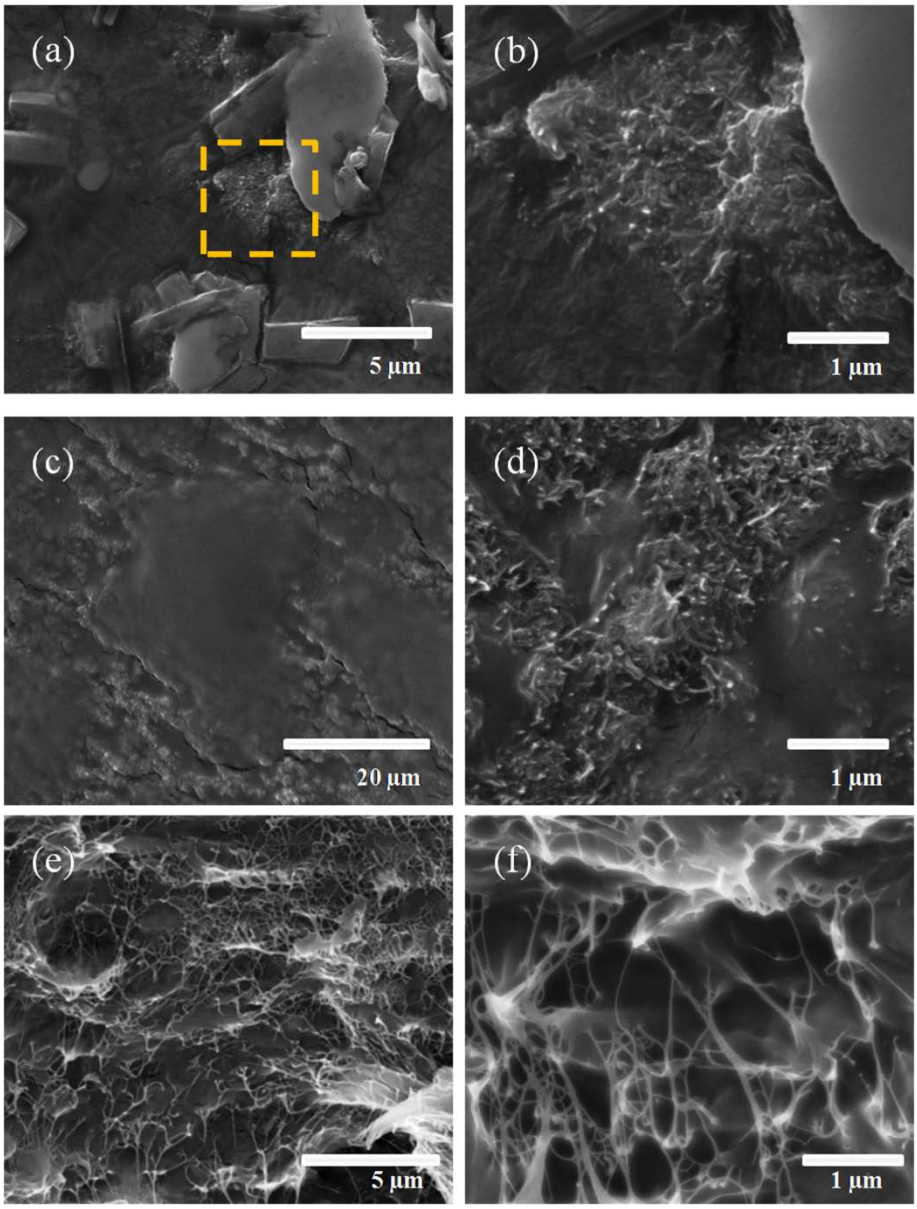

Figure 3.5. SEM cross-sectional images of 1:1.57 CNT:DOC composites containing 2.5 wt% MWNT (a) 10 wt% MWNT (c) and 10 wt% DWNT (e). (b), (d), and (f) are greater magnification images of (a), (c), and (e), respectively.

SEM cross-sectional images of the MWNT:TCPP system at varying MWNT concentrations are shown in **Figure 3.6**. Figure 3.6a is a 2.5 wt% MWNT composite,

with Figure 3.6b as the magnified image of the dotted-line box in Figure 3.6a. This system looks very similar to the MWNT:DOC in Figure 3.5a. The 2.5 wt% MWNT composite is again near the PTC, so there is little evidence of a segregated network. The same aggregation behavior is also observed, but the MWNT bundles look to be more evenly dispersed. Figure 3.6c shows the 10 wt% MWNT composite, which shows the true segregated network. As seen in the MWNT:DOC system (Figure 3.5d), porosity amongst the MWNT can be observed at higher magnification (Figure 3.6d). The pores seem more extensive here, which is believed to be related to the poorer stabilization by the higher molecular weight TCPP stabilizer. As already mentioned, this porosity becomes a factor in the mechanical properties that will be discussed in the next section and is linked to the critical pigment volume concentration (CPVC) phenomenon.[68,296-299] The microscopic voids seem to have begun connecting with each other, leading to large scale defects. This porosity is a significant issue for segregated networks due to the inability of the polymer to effectively fill voids between particles. Beyond the CPVC, often below 10 vol% for segregated networks, porosity becomes extensive and begins to degrade composite mechanical behavior.[53,68,295] This porosity is also seen when DWNT is used as the electrically conductive filler (Figure 3.6e). The DWNT appears to be better stabilized by the TCPP, when compared to the DOC-stabilized system. A reason for this behavior could be due to the larger TCPP molecule being able to sterically stabilize the DWNT.

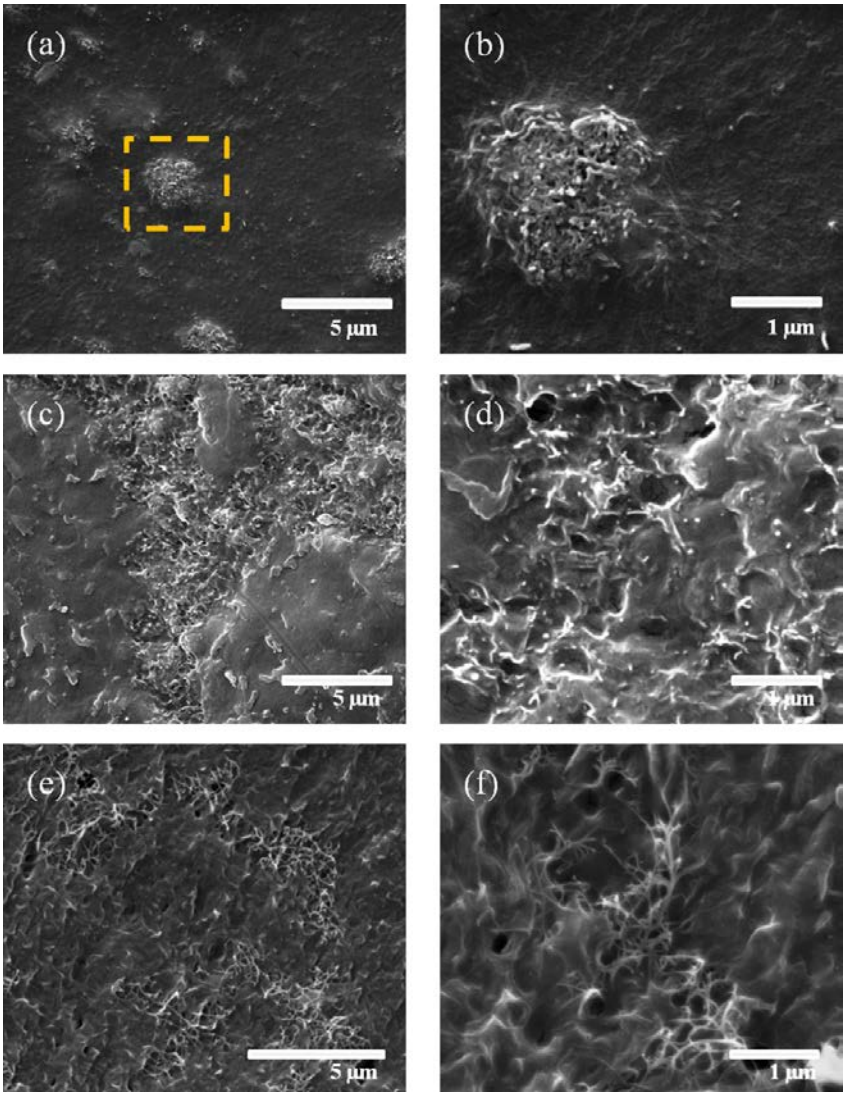

Figure 3.6. SEM cross-sectional images of 1:3 CNT:TCPP composites containing 2.5 wt% MWNT (a), 10 wt% MWNT (c), and 10 wt% DWNT (e). The highlighted region, marked by a dotted box in (a), is enlarged in (b). Higher magnification images of (c) and (e) are shown in (d) and (f), respectively.

3.3.2 Thermomechanical Behavior

Figure 3.7 shows the T_g for the MWNT:DOC and MWNT:TCPP composites.

These values were taken as the peak in the loss modulus curves measured with DMA.

The T_g of neat PVAc copolymer (0 wt% MWNT), is approximately 10°C. As the MWNT concentration increases (Figure 3.7a), the T_g increases only slightly. This confirms that the MWNT network does not interact strongly with the PVAc matrix. If there was a strong interaction between the filler and matrix, the T_g would be expected to increase more dramatically with increasing filler concentration due to the restriction of polymer chains.[300-304] In the MWNT:TCPP system (Figure 3.7b), the T_g increases to ~20°C at 7 wt% MWNT, with a drop to 15°C at 10 wt% MWNT. This increase may be attributed to some sort of molecular interaction of the TCPP with PVAc. Large error bars on these T_g values, especially at higher MWNT content, are likely due to the porosity in the structure. Even with TCPP, the T_g increase is very modest and again suggests that the MWNT has only weak interaction with the PVAc matrix.

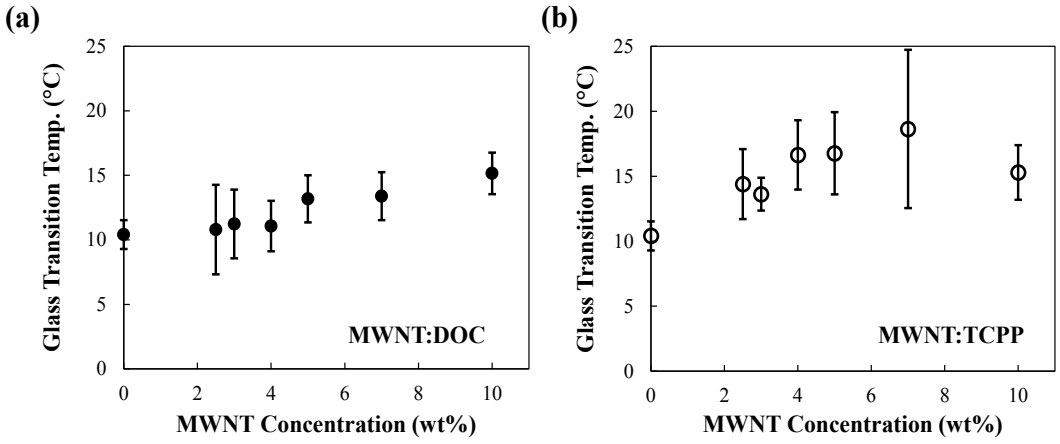

Figure 3.7. Glass transition temperatures, as a function of MWNT concentration, for DOC (a) and TCPP (b) stabilized systems.

The storage moduli, measured at -60°C, are shown in **Figure 3.8** for the DOC and TCPP stabilized systems. As expected, modulus increases with increasing MWNT concentration in the MWNT:DOC system (Figure 3.8a), from ~6 to 12 GPa (with 10 wt% MWNT). The storage modulus peaks at ~14 GPa for the MWNT:TCPP system at 7 wt% MWNT, then decreases at 10 wt% (Figure 3.8b). A more classical CPVC phenomenon is observed in the MWNT:TCPP system. This behavior was also seen in the T_g results (Figure 3.7b). Pores are very apparent in the composite containing 10 wt% MWNT (Figure 3.6c), which act as zero modulus filler. A CPVC is not observed in the MWNT:DOC system because the polymer matrix can still envelop the filler/stabilizer mixture. Better stabilization of MWNT by DOC, relative to TCPP, is believed to be the primary reason for this difference. As MWNT is better dispersed in the matrix, porosity will require a greater filler concentration to develop (i.e., higher CPVC). Latex-based films filled with 18 or 36 wt% TCPP, in the absence of MWNT, exhibited the same storage modulus as unfilled latex (~7 GPa).

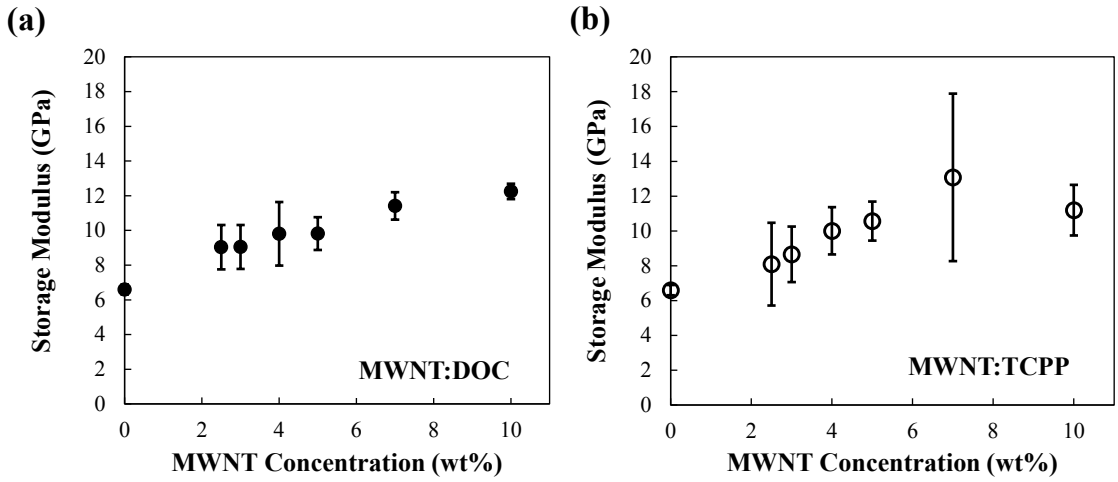

Figure 3.8. Storage moduli measured at -60°C, as a function of MWNT concentration, for DOC (a) and TCPP (b) stabilized systems.

3.3.3 Transport Properties

Unlike electrical conductivity, the thermal conductivity has been shown to be relatively insensitive to CNT concentration and stabilizer type for the 7, 10, and 12 wt% CNT:DOC and CNT:TCPP composites (**Figure 3.9**).[7,65] Thermal conductivities range from approximately 0.18 W m^{-1} K^{-1}, for the MWNT:DOC system, to 0.22 W m^{-1} K^{-1}, for the MWNT:TCPP system. When 12 wt% MWNT is replaced by DWNT, the thermal conductivity of the DOC composite is nearly identical to the TCPP composite at 0.17 W m^{-1} K^{-1}. The thermal conductivity (k) of a composite can best be described by a parallel resistor model:

$$k = k_m V_m + k_f V_f \tag{3.3}$$

where V is the volume fraction and subscripts, m and f, stand for the matrix and filler, respectively. It is important to note that weight fractions were used in place of volume

fractions due to the uncertain density of MWNT (and other composite ingredients).[305] Equation 3.3 provides a maximum thermal conductivity by maximizing the contribution of the conductive filler (i.e., it assumes perfect contact between each CNT). This assumption is not entirely correct, as a perfect contact between each tube is impossible for these composites. Due to the high thermal conductivity of the filler in comparison to the polymer matrix (i.e., 1,000 to 0.40 W m^{-1} K^{-1}, respectively), a large increase in composite thermal conductivity, as the CNT volume concentration is increased, would be expected.[7,256-265] At 12 wt% CNT, the predicted thermal conductivity of the composite would be ~120 W m^{-1} K^{-1}, which is nearly three orders of magnitude greater than the experimental results (~0.17 – 0.22 W m^{-1} K^{-1}). There is also a dramatic difference between the theoretical value of a single MWNT and the experimental value of the bulk measurement. This discrepancy is due to the numerous high thermal contact resistances between the tubes themselves, resulting in a reduced bulk measurement (~15 W m^{-1} K^{-1}).[306] If this value was chosen instead of the theoretical value, the thermal conductivity would be roughly 2.2 W m^{-1} K^{-1}, which is still an order of magnitude different than those reported experimentally.[7,65,206]

The stabilization of CNT by DOC or TCPP also suppresses the thermal conductivity by blocking tube – tube junctions, creating less favorable pathways for phonon transport. These organic stabilizers can also act as phonon scattering centers because they are embedded in the composite alongside the CNT.[267] This can be further explained by the increased thermal resistance, caused by the poor phonon coupling in vibrational modes of the polymer-filler and filler-filler at the interface, called the Kapitza

resistance.[266-268] Other possible reasons for such a low thermal conductivity include gaps present between adjacent tubes due to misalignment,[267] differing tube diameters and lengths,[307] morphology of the CNTs,[267] and defects introduced to the CNTs by functionalizing them during sonication with the dispersant.[251]

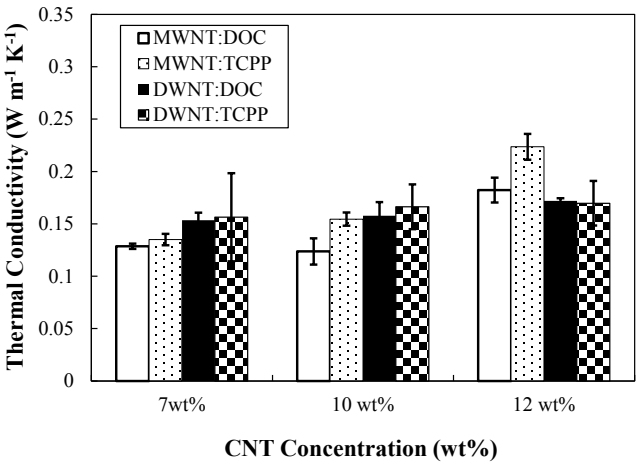

Figure 3.9. Thermal conductivity of DOC and TCPP stabilized systems containing 7, 10, and 12 wt% MWNT and DWNT.

Electrical conductivity, as a function of MWNT concentration, for the DOC and TCPP-stabilized composites are shown to increase exponentially at lower MWNT concentrations (**Figure 3.10**). A solid line fit to this data was performed using Kirkpatrick's percolation power law (Equation 2.2). Weight fractions are used here instead of volume fractions as already explained above. The PTC (V_c) for the MWNT:DOC system was calculated to be 1.6 wt% MWNT, while the MWNT:TCPP threshold was found to be approximately 2.2 wt% MWNT. These results support the

earlier assessment of composite microstructure at low MWNT concentrations. Higher PTC suggests higher CPVC due to a greater MWNT concentration required for strong network formation. Below 10 wt% MWNT, the DOC-stabilized composites exhibit slightly greater electrical conductivity due to better nanotube stabilization/exfoliation. The increased electrical conductivity at lower MWNT concentrations, with DOC stabilization, can be attributed to the tighter junctions that are formed relative to the bulkier TCPP.[308] The highest electrical conductivity of the MWNT:TCPP system was found to be approximately 128 S m^{-1}, at 12 wt% MWNT, which is 88% greater than the MWNT:DOC system. Control films containing 18 or 36 wt% TCPP, without any MWNT, were too insulating ($\sigma < 0.01$ S m^{-1}) to be measured using the standard four-point probe apparatus.

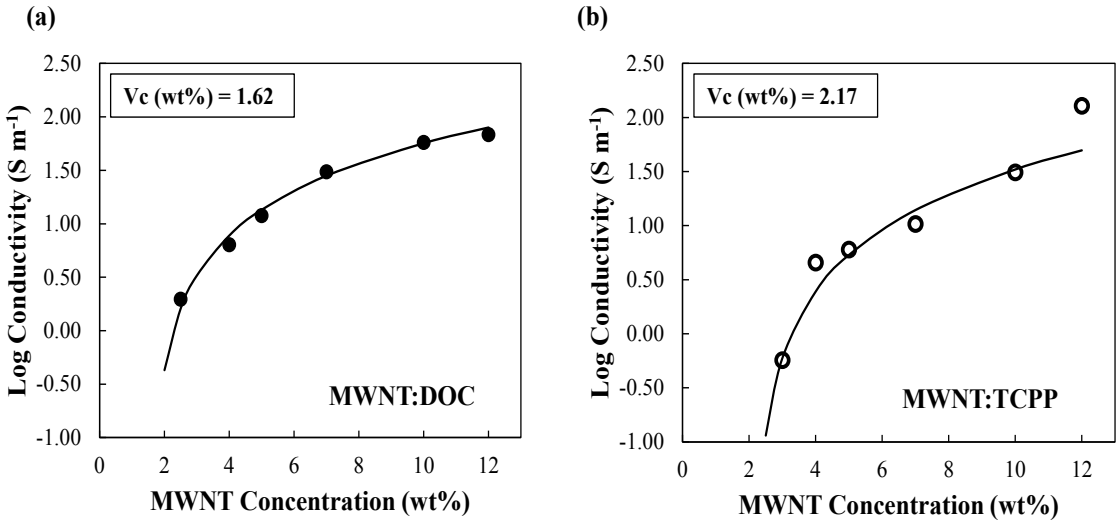

Figure 3.10. Electrical conductivity as a function of MWNT concentration for the DOC (a) and TCPP (b) systems. The solid line in both graphs is the percolation power law fit, with the percolation thresholds provided as insets.

Although electrical conductivity for a given MWNT concentration is quite similar between the two stabilizers, the TCPP stabilized composites have a much larger Seebeck coefficient (**Figure 3.11**a). In both MWNT:DOC and MWNT:TCPP composites, only the 7, 10, and 12 wt% MWNT samples were evaluated due to the need for relatively high conductivity for measurement. These composites exhibit an R^2 fit of 0.98 or higher for the voltage – temperature plot (not shown), which suggests an accurate Seebeck measurement. *S* range from approximately 8 $\mu V\ K^{-1}$, for the MWNT:DOC system, to 28 $\mu V\ K^{-1}$, for the MWNT:TCPP system. These values are much lower than those reported for composites filled with SWNT (40-60 $\mu V\ K^{-1}$).[7] The increased *S* with TCPP stabilization, relative to DOC, can be attributed to the manipulation of CNT junctions by providing increased electron transport with a modest intrinsic thermopower. The insulating nature of the DOC restricts the overall diffusion of charge carriers across the many junctions, therefore diminishing the Seebeck effect within the composite. The insensitivity of the Seebeck coefficient, in relation to the CNT concentration, is believed to be caused by a small energy barrier at the CNT junctions filtering the transport of low energy electrons. This barrier, and the junction between nanotubes, could be influenced by changing the stabilizer used to exfoliate the CNT (as seen here),[194] the interparticle distance,[65] the contact potential barrier,[310] differences in work functions,[309] or the electrostatic charges associated with the CNT and matrix.[162]

When 12 wt% MWNT is replaced by DWNT, the electrical conductivity of the DOC composite is 1,474 S m^{-1} and 7,108 S m^{-1} for the TCPP composite. DOC does not

provide as great an increase as TCPP because of the insulating nature of the stabilizer having a greater effect and inhibiting the electron transfer from tube – tube. For 12 wt% DWNT composites, the Seebeck coefficient is ~70 μV K^{-1} with DOC. This value increases to ~80 μV K^{-1} when TCPP replaces DOC as the stabilizer, demonstrating the universality of using semiconducting stabilizers to enhance the thermoelectric efficiency. The increased Seebeck coefficient with TCPP would increase ZT by nearly 30%, without even considering the simultaneous increase in electrical conductivity for the DWNT composite. DWNT exhibits these increased properties due to the fact that either one (or both) of the tubes are metallic in character, while the other is semiconducting, which creates a more highly conductive material. The increased electrical conductivity could also be explained by the DWNT having a higher structural stability, creating highly conductive π-conjugated pathways that remain undisturbed on the inner tube during functionalization (i.e., the inner tube is allowed to act as an independent SWNT).[188-192]

The increase in Seebeck coefficient with the addition of this semiconducting stabilizer results in an increase in the power factor ($S^2\sigma$) (Figure 3.11b). The power factor of these MWNT-filled composites increases more than an two orders of magnitude, from 0.004 to 0.1 μW m^{-1} K^{-2}, when TCPP is replaced by DOC. A more modest increase is observed for the DWNT-filled composites, with $S^2\sigma$ rising from 7.53 to 42.8 μW m^{-1} K^{-2}. This example demonstrates the significant improvement in thermoelectric performance that occurs with seemingly small changes in S and σ. Higher power factors have already been observed with higher nanotube concentrations,

using intrinsically conductive PEDOT:PSS as the stabilizer.[65] Much like with bulk semiconductors, a compromise between electrical conductivity and the Seebeck coefficient will produce the highest ZT values.

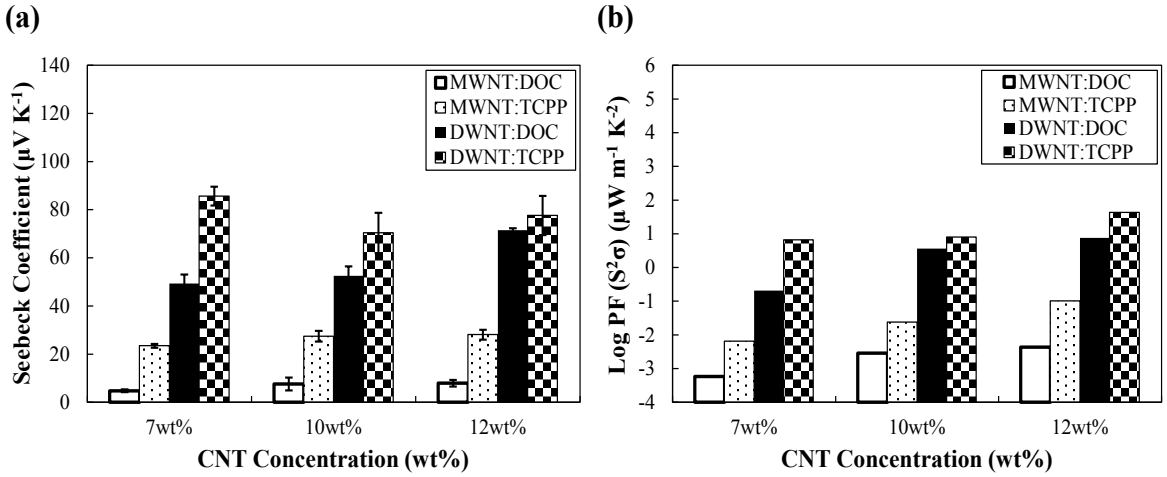

Figure 3.11. Seebeck coefficients (a) and power factors (b) of DOC and TCPP stabilized systems containing 7, 10, and 12 wt% MWNT and DWNT.

3.4 Conclusions

Two series of latex-based segregated-network polymer composites were prepared with insulating (DOC) or semiconducting (TCPP) stabilizing agents for CNT. Composite microstructure, mechanical, and transport properties were evaluated in an effort to understand the influence of using a porphyrin molecule as the stabilizer. Thermal conductivities were relatively unaffected by stabilizer, CNT type, or CNT concentration, and they were below those of typical polymeric materials (0.2 – 0.4 W m^{-1} K^{-1}). MWNT:DOC composites exhibited a lower PTC (1.6 wt% MWNT) than

MWNT:TCPP (2.2 wt% MWNT). This threshold difference is attributed to the latex particles being able to envelop the better stabilized MWNT:DOC more effectively than the more weakly stabilized MWNT:TCPP. Seebeck coefficients were relatively unaffected by MWNT concentration, but TCPP-stabilized composites had *S* values that were five times as large as DOC-stabilized. *S* and σ both increased for composites containing DWNT instead of MWNT, further demonstrating the utility of semiconductor stabilizers for improving thermoelectric behavior. These improvements can be explained by the semiconducting nature of TCPP molecules effectively manipulating CNT junctions. Further improvements in Seebeck coefficient and/or electrical conductivity are expected with higher DWNT concentration and the use of an intrinsically conductive polymer stabilizer (e.g., PEDOT:PSS) in combination with TCPP (or other semiconducting stabilizers).

CHAPTER IV

ENHANCEMENT OF THERMOELECTRIC PROPERTIES WITH AN INTRINSICALLY CONDUCTIVE STABILIZER

4.1 Introduction

In the previous chapter, the ability to successfully tailor their thermoelectric properties of fully organic polymer nanocomposites was shown. In this chapter, a segregated network was created with a PVAc latex, in combination with highly conductive DWNT, stabilized by intrinsically conductive PEDOT:PSS. PEDOT:PSS, doped with DMSO, has been previously shown to effectively disperse carbon nanotubes in an aqueous solution and increase the electrical conductivity of the mixture as a whole.[65,162] By combining the highly conductive behavior of DWNT with a conductive stabilizer, less resistive nanotube junctions are expected to be created and result in a dramatic increase in composite conductivity. A 40 wt% DWNT composite, at a 1:1 DWNT:(PEDOT:PSS) dry weight ratio, obtained metallic-like electrical conductivity (~200,000 S m^{-1}) and a modest Seebeck coefficient (~45 μV K^{-1}). These fully organic composites were shown to exhibit power factors (~400 μW m^{-1} K^{-2}) within an order of magnitude of commercially available inorganic semiconductors. These composites, however, developed anisotropic thermal conductivity, with in-plane values ~40 times

greater than those measured in the through-thickness direction (~16 and 0.40 W m^{-1} K^{-1}, respectively). A demonstration of the thermoelectric behavior is shown as a ~3.5°C temperature gradient is applied. This work demonstrates that organic composites are now becoming competitive with the traditional inorganic semiconductors.

4.2 Experimental

4.2.1 Materials

A vinyl acetate/ethylene copolymer emulsion (Vinnapas EP 401 supplied by Wacker Chemical Corporation, Munchen, Germany), that is 54 – 56 wt% solids in water, was used as the composite matrix. The PVAc latex has an average particle diameter of 650 nm with a T_g of -15ºC. DWNT (XBC 1001), stabilized by intrinsically conductive PEDOT:PSS (Clevios PH1000, Heraeus Precious Metals, Hanau, Germany) doped with 5 wt% dimethyl sulfoxide (DMSO), was used as the model electrically conductive filler.

4.2.2 Composite Preparation

A DWNT:(PEDOT:PSS) dry weight ratio of 1:1 was prepared by using an aqueous solution of 1.23 wt% PEDOT:PSS. The suspensions were sonicated for 15 min at 50 W in an ice water bath. The aqueous suspension was then added to the PVAc emulsion and pH 2-adjusted deionized water (using 0.1 M HCl). The resulting solutions were then sonicated for another 5 min at 50 W in an ice water bath to homogenize. A series of composites, containing 0.1, 0.25, 0.5, 0.75, 1, 10, 20, 30, and 40 wt% DWNT, was prepared by drying the suspensions in 26 cm^2 plastic molds. The final aqueous

suspensions contained 0.5 wt% solids to reduce viscosity. The composites were dried for 36 hours under ambient conditions in a vented hood, heated for 6 hours at 80°C in an oven, and then dried 24 hours in a vacuum desiccator. Concentrations are based upon the dry weight of PVAc, DWNT, and PEDOT:PSS solids used in the composite. Composite thicknesses ranged from ~0.045 to 0.070 mm.

4.2.3 Characterization

In-plane electrical conductivity and Seebeck coefficients were measured with a home-built device, as previously described (Section 3.2.3.2). Through-thickness thermal conductivity measurement was also described in Chapter III (Section 3.2.3.3), along with scanning electron microscope imaging of composite cross-sections (Section 3.2.3.5). In-plane thermal diffusivity measurements (D in $mm^2\ s^{-1}$) were performed by Netzsch Instruments North America, LLC (Burlington, MA), on circular disks (~25 mm in diameter) at 25ºC and converted to thermal conductivity (k) using:

$$k = D \times C_p \times \rho \tag{4.1}$$

where C_p (in $J\ g^{-1}\ K^{-1}$) is the specific heat and ρ (in $g\ cm^{-3}$) is composite density. A radial heat flow method, utilizing a Netzsch LFA 447 Nanoflash instrument and its analysis software, was performed on the test samples in accordance with ASTM E1461. This method involves pulse heating a 5 mm diameter spot on one surface of the disk and monitoring the arrival of the resulting radial temperature wave on the opposite surface with a diameter of approximately 10.7 mm. The area heated by the pulse and the area viewed by the IR detector are defined by masks sandwiching the sample.

Specific heats of the samples were measured using ASTM E1269 with a Q20 Differential Scanning Calorimeter (DSC) from TA Instruments (New Castle, DE). This method involved running three separate tests per composite (an empty pan, sapphire standard, and loaded pan) to eliminate any influence from the instrument during testing. The temperature was ramped at a rate of 20°C min^{-1}, from -60 to 60°C. To ensure accurate results, three tests were done for each sample. The heat flows of the sapphire standard (D_{st}) and loaded pan (D_s) were subtracted from an empty pan to cancel out the pan influence. The C_p was then calculated using:

$$C_{p,\,s} = C_{p,\,st}\frac{D_s W_{st}}{D_{st} W_s} \qquad (4.2)$$

where W_{st} is the weight of the sapphire standard, W_s is the weight of sample, and the resulting data was extrapolated to 25°C.

4.3 Results and Discussion

4.3.1 Composite Microstructure

The ability of PEDOT:PSS to stabilize DWNT and increase the thermoelectric properties of polymer-based composites is believed to be the result of more favorable junctions between the nanotubes after drying (**Figure 4.1**a). PEDOT:PSS effectively stabilizes the DWNT by decorating the nanotube surfaces through $\pi - \pi$ stacking interactions.[162] During the drying of the stabilized nanotube and latex suspension, the polymer particles exclude volume and force the DWNT into the interstitial space between them, as shown schematically in Figure 4.1b. As the water evaporates and the latex particles coalesce together, an electrically connected, but thermally disconnected,

three-dimensional network of nanotubes is created.[197,300] When the composites are placed in an atmosphere with elevated temperatures, a reduction of the porosity in the network occurs by the polymer particles having a higher degree of coalescence. This behavior tightens the DWNT network and forces more intimate contacts between tubes, therefore increasing the electrical conductivity and retaining the flexibility of the composite (Figure 4.1c).

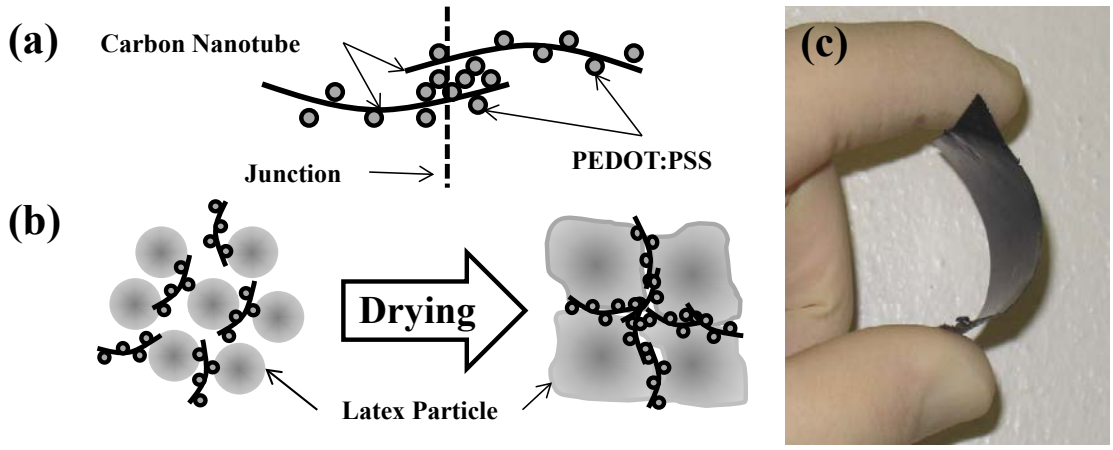

Figure 4.1. Schematic of carbon nanotubes decorated by PEDOT:PSS particles and the junction formed between them (a). Schematic of the segregated network formation upon drying and polymer coalescence (b). A fully dried, free standing, flexible composite is held between two fingers (c).

The segregated network microstructure of a 0.5 wt% DWNT-filled composite is clearly observed in the freeze-fractured cross-sectional SEM micrograph (**Figure 4.2**a). The nanotubes appear as bright spaghetti-like strands trapped between the darker coalesced latex particles. The nanotubes do not appear to have significant interaction with the coalesced polymer particles (Figure 4.2b), which further contributes to high

electrical conductivity and retention of film flexibility.[67] At 10 wt% DWNT (Figure 4.2c), a well-defined DWNT network around relatively large domains of coalesced polymer particles is created with distinct filler and matrix regions. It should be noted that DWNT concentrations well above the PTC of the composite system will create extensive porosity in the composite. This is primarily due to the inability of polymer particles to adequately envelop the nanotubes and consequently incomplete coalescence. At these higher filler concentrations, the polymer particles act more as a binder to retain the mechanical integrity of the entangled DWNT network. Striations begin to form at 40 wt% DWNT within the microstructure, which can contribute to some anisotropic transport properties (Figure 4.2d). This microstructure is believed to be a result of the simple stationary drying during network formation and the lack of greater amounts of exclusionary polymer particles to interrupt this layering behavior. Porosity created by the incomplete coalescence will not only affect the mechanical properties of the composite, but it will also influence the transport properties.

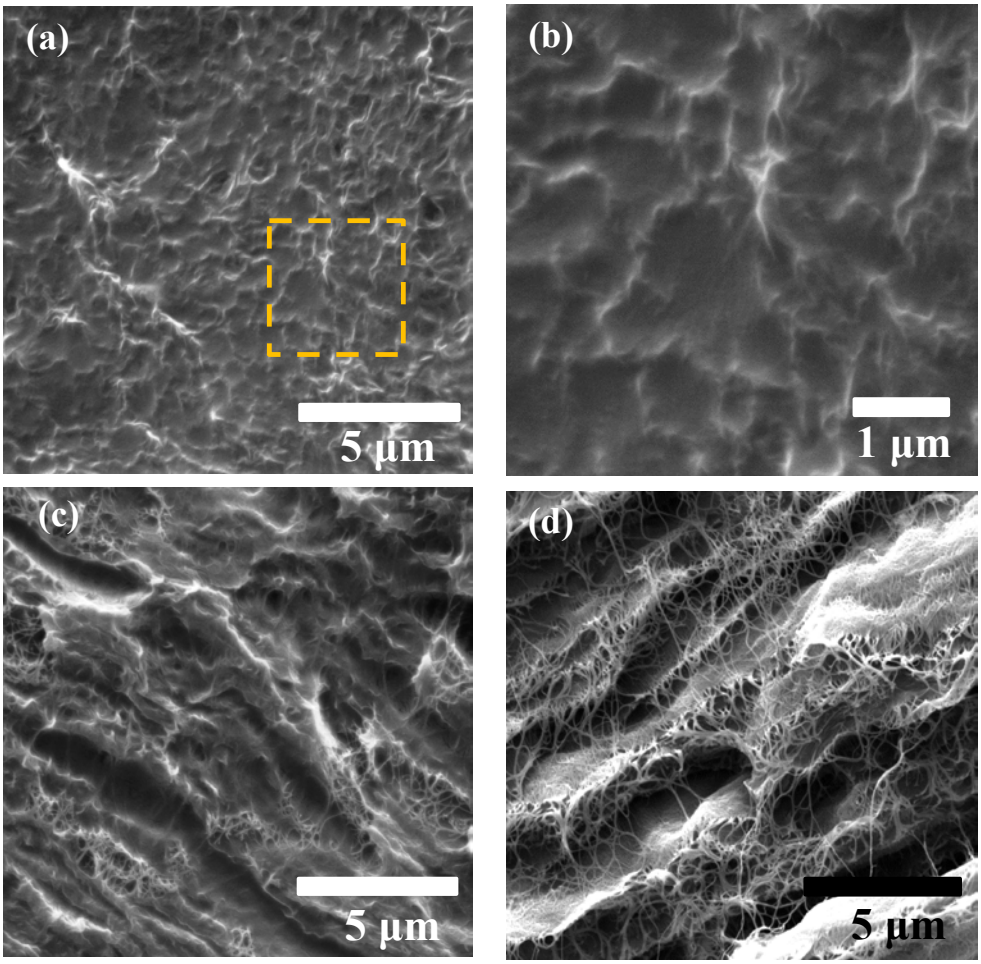

Figure 4.2. SEM cross-sectional images of 1:1 DWNT:(PEDOT:PSS) composites containing 0.5 wt% DWNT (a) 10 wt% DWNT (c), and 40 wt% DWNT. The highlighted region, marked by a dotted box in (a), is enlarged in (b).

4.3.2 Transport Properties

Figure 4.3 compares the through-thickness and in-plane thermal conductivity of these DWNT-filled composites. These composites resulted in polymer-like through-thickness thermal conductivity (Figure 4.3a), ranging from 0.15 – 0.4 W m^{-1} K^{-1}.[7,65,206,256-265] As mentioned previously, a significant increase in the thermal

conductivity would be expected as the DWNT concentration increased because of the difference in thermal conductivity between the PVAc matrix and that of a single CNT.[7,28,65,249] At 40 wt% CNT, the thermal conductivity for the composite could have been as large as ~400 W m^{-1} K^{-1}, based upon Equation 3.3.[7,249,251] The low experimental values (~0.40 W m^{-1} K^{-1} for the 40 wt% DWNT composite) can be attributed to the numerous high interfacial thermal contact resistances occurring between the nanotubes, PEDOT:PSS, and latex particles.[266-270] This low k may also be credited to the increased porosity accompanied by the high concentration of DWNT, which further disrupts phonon transport through the composite. These experimental through-thickness values are similar to those presented in Chapter II for CNT-filled polymer composites.

In-plane thermal conductivity shows a clear increasing trend with DWNT concentration (Figure 4.3b). The more than order of magnitude difference between through-thickness and in-plane thermal conductivity values (~0.40 and 16 W m^{-1} K^{-1} for 40 wt% DWNT, respectively) is likely due to the orientation of DWNT in the in-plane direction, as shown in Figure 4.2d. This orientation could be due to the high aspect ratios of the nanotubes and the use of simple stationary evaporation drying. In the direction of orientation (i.e., in-plane), fewer tube – tube junctions are necessary to travel a given distance and greater overlap exists amongst nanotubes, which dramatically improves phonon transport.[266] These values correlate with the thermal conductivity predicted by Chalopin *et al* (~10 W m^{-1} K^{-1}),[206,266,311] who modeled the interfacial thermal conductance between crossing carbon nanotubes (i.e., one vertically aligned and

the other horizontally) and found that heat flow across the interface was dominated by low frequency phonons. Although this anisotropic behavior is interesting, it should be noted that in-plane thermal conductivity is rarely reported in the literature due to measurement difficulty and limitations associated with composite thicknesses.[312]

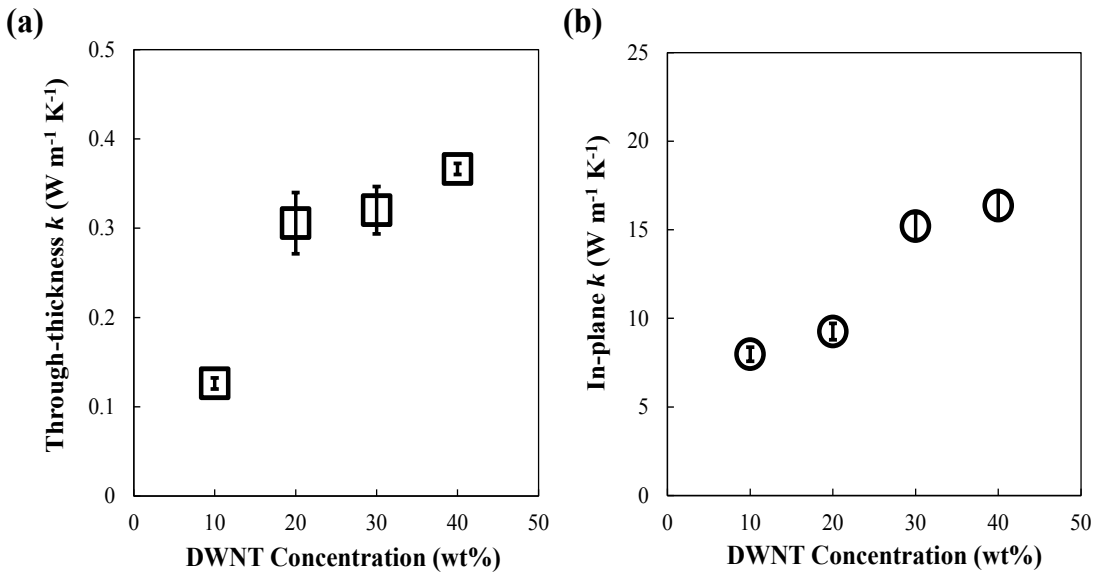

Figure 4.3. Thermal conductivity measurements reported as a function of DWNT concentration in the through-thickness (a) and in-plane (b) composite orientations.

Figure 4.4 shows the in-plane electrical conductivities and Seebeck coefficients as a function of DWNT concentration. The percolation threshold behavior of these DWNT-filled composites fit well with Kirkpatrick's percolation power law (solid line in Figure 4.4a)[121-122] and exhibit a PTC of 0.025 wt% DWNT. This low PTC is well below those previously reported and demonstrates the highly conductive nature of this particular composite system.[165-176] As the DWNT concentration is increased, the

electrical conductivity increases exponentially (Figure 4.4b) and reaches ~200,000 S m^{-1} with 40 wt% DWNT. This metallic-like conductivity for a fully organic, flexible composite is orders of magnitude greater than previously reported values for similar segregated network systems.[7,65,206,165-176] The primary reason for this large improvement is attributed to the DWNT having an intrinsically high electrical conductivity, due to its highly conductive π-conjugated pathways.[188] As both concentric tubes are believed to act as independent SWNT, the high electrical conductivity is maintained because the inner tube remains undisturbed during stabilization.[188-192] This high electrical conductivity is also believed to be due to the oven drying process creating tighter tube – tube junctions during the initial segregated network formation.[65] Drying at a temperature well above the T_g of the latex particles softens the polymer and allows for improved coalescence that forces more intimate contacts by narrowing any potential gaps that may exist between nanotubes.[313] Additionally, PEDOT:PSS enhances the electrical conductivity of the composites by producing less resistive tube – tube junctions. Increasing the PEDOT:PSS concentration, in relation to the DWNT, would simultaneously enhance the stabilization of the nanotubes and produce electrical conductivities similar to > 10 wt% CNT composites at < 10 wt% CNT concentrations.[65] However, the CNT concentration is still the dominating factor in determining the upper bound of the electrical conductivity in the composite.

Even as electrical conductivity of these composites is significantly altered by varying DWNT concentration, the in-plane Seebeck coefficient (Figure 4.4b) remains

relatively constant (35 – 50 μV K^{-1}). These *S* values are similar to those previously reported for segregated network composites containing SWNT and a different derivation of PEDOT:PSS (20 – 60 μV K^{-1}).[65,206,310] The PEDOT:PSS formulation used here exhibits larger intrinsic Seebeck coefficients than other commercially available PEDOT:PSS derivatives.[206,242,244,246] The consistency in the Seebeck coefficient is believed to be caused by a small energy barrier filtering low energy electron transport at the tube junctions, leaving the Seebeck coefficient insensitive to changes in electrical conductivity. This barrier, and the junctions between nanotubes, could be influenced by changing the stabilizer used to exfoliate the CNT,[194] altering the distance between particles,[65] decreasing the contact potential barrier,[310] or the electrostatic charges associated with the CNTs and matrix.[162] This behavior separates these polymer composites from traditional semiconductor thermoelectric materials, which show a large reduction in the Seebeck coefficient as the electrical conductivity increases with carrier concentration.[80-85]

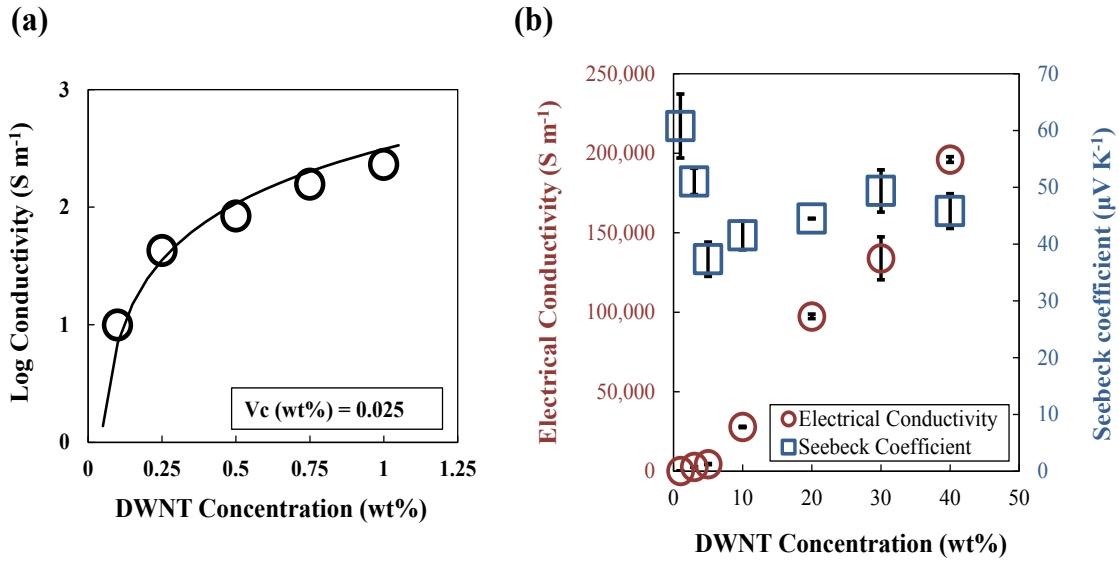

Figure 4.4. The in-plane electrical conductivity plotted as a function of DWNT concentration and the percolation power law (solid line) (a). The in-plane electrical conductivity (circles) and Seebeck coefficient (squares) as a function of DWNT concentration (b).

The increased electrical conductivity and Seebeck coefficient exhibited by these composites results in among the highest power factors ($PF = S^2\sigma$) reported for an all organic system,[7,65,67,197,206,248,276,285] and within an order of magnitude of commercially available inorganic materials.[15,82-83] **Figure 4.5**a shows that power factors increase linearly with DWNT concentration and reach a value ~400 μW m^{-1} K^{-2} for a composite filled with 40 wt% DWNT. This is a level of thermoelectric performance that makes these flexible, organic materials viable competition for the commonly used inorganic materials (e.g., PbTe ~500 μW m^{-1} K^{-2}).[82-83] To demonstrate the thermoelectric behavior, an edge of 40 wt% DWNT-filled composite was sandwiched between two flexible heaters while the other was left open to the ambient atmosphere (Figure 4.5b).

As the heaters were connected in parallel and supplied 1.5 V, a steady state temperature gradient of ~3.5°C developed from one end of the sample to the other (Figure 4.5c). This small heat gradient was chosen to closely resemble those potentially developed when placed in contact with a human body. The voltage output is seen to increase as the temperature gradient becomes larger, which is demonstration that these organic materials are thermoelectric (Figure 4.5d). A steady-state power output of ~18.2 nW was obtained as this material was placed in a circuit containing a 0.15 Ω resistor (voltage drop measured across this resistor). This efficiency would dramatically increase when placed in series with an n-type leg to create a thermoelectric junction (Figure 2.1).

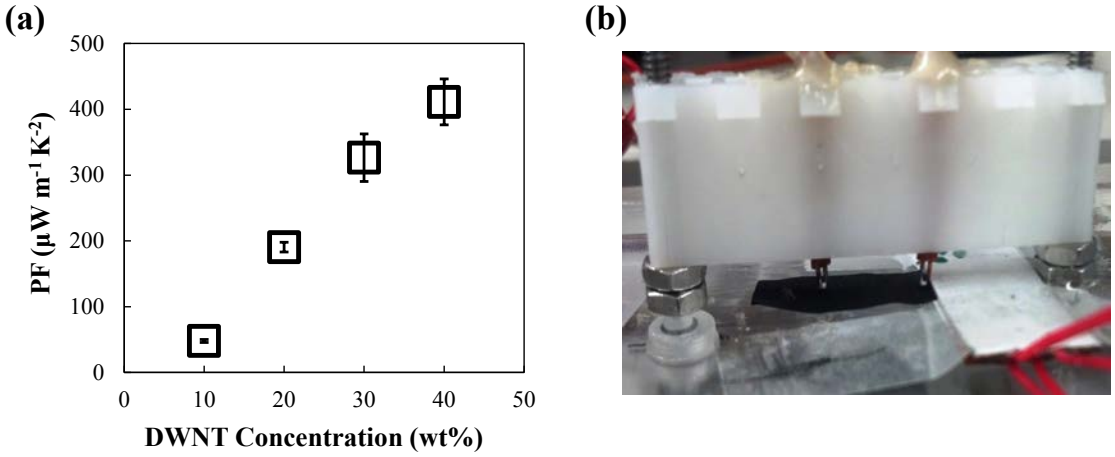

Figure 4.5. The power factor is plotted against the DWNT concentration (a). Photographic image of a 40 wt% DWNT composite as it is sandwiched between two flexible heaters (b). The temperature profile (c) and voltage output (d) are given across the sample.

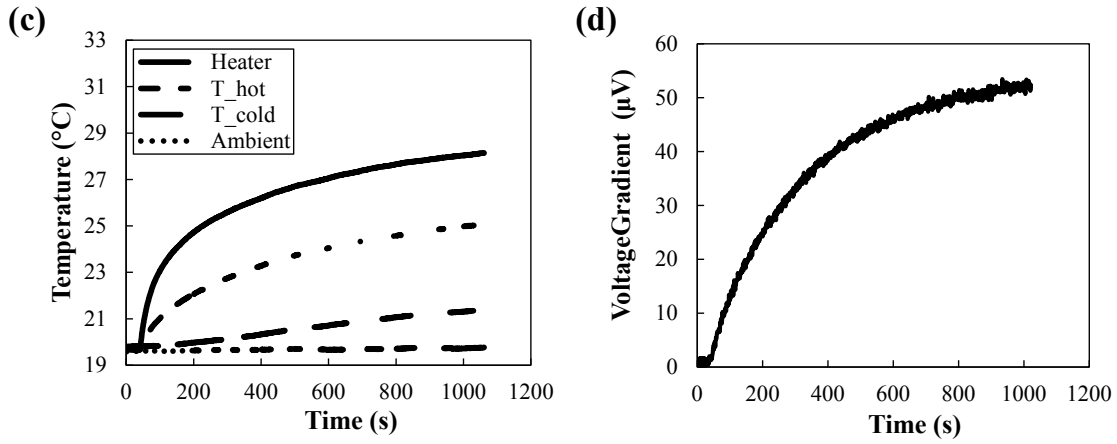

Figure 4.5. Continued.

4.4 Conclusions

Fully organic (i.e., completely carbon-based) polymer nanocomposites have numerous advantages over traditional inorganic semiconductors, including mechanical flexibility and the ability to be painted onto a given surface, as a new class of thermoelectric material. A 40 wt% DWNT composite, at 1:1 DWNT:(PEDOT:PSS) dry weight ratio, reached metallic-like conductivity at ~200,000 S m^{-1} and maintained a modest Seebeck coefficient of ~45 μV K^{-1}. Carbon nanotube-filled latex composites were shown to exhibit power factors similar to single crystal PbTe and within an order of magnitude of nanocrystalline Bi_2Te_3. Anisotropic thermal conductivity was developed, however, as the in-plane values were more than an order of magnitude greater than the polymeric values in the through-thickness direction (~16 to 0.40 W m^{-1} K^{-1}, respectively). A proof of thermoelectric behavior was demonstrated as a ~3.5°C temperature gradient was placed across the sample and the power output was measured

to be ~18 nW. With additional work aimed at increasing Seebeck coefficient with the addition of inorganic nanoparticles and/or multiple stabilizers,[64,68] these water-based composites have the potential to eventually exceed their inorganic semiconductor counterparts in thermoelectric efficiency.

CHAPTER V

HIGH THERMOELECTRIC POWER FACTORS FROM A DUAL-STABILIZER COMPOSITE PREPARATION*

5.1 Introduction

In an effort to further improve the thermoelectric properties of fully organic nanocomposites, PEDOT:PSS and TCPP were used together. Combining the high Seebeck coefficients of the TCPP-stabilized composites, with the enhanced electrical conductivity of the PEDOT:PSS, the power factor could become even more competitive with common inorganic semiconductors. The electrical conductivity of these dual-stabilizer organic composites approximately 9,500 S m^{-1} as the concentrations of both

MWNT and PEDOT:PSS were increased. The Seebeck coefficient and thermal conductivity, however, remained relatively unaffected by the increase in concentration (~40 μV K^{-1} and ~0.12 W m^{-1} K^{-1}, respectively). Replacing MWNT with DWNT increased σ and *S* to ~96,000 S m^{-1} and 70 μV K^{-1}, respectively, at 40 wt% DWNT and a 1:1:0.25 DWNT:(PEDOT:PSS):TCPP dry weight ratio. This work suggests that σ and S can be simultaneously improved by using multiple stabilizing agents to alter transport properties of the junctions between nanotubes. Combining semiconducting and intrinsically conductive molecules as CNT-stabilizers has led to a power factor that

*Reprinted with permission from G. P. Moriarty, K. Briggs, C. Yu, J. C. Grunlan. Dual Stabilizer Approach to High Thermoelectric Power Factor Nanocomposites: Fully Organic Materials for Waste Heat Recovery. *Energy Technology* **2013**, *1*, 265.

is among the best ever reported for a completely organic, free-standing film (~500 μW m^{-1} K^{-2}). The use of this dual-stabilizer system provides a new tool for enhancing the thermoelectric properties of polymer nanocomposites and provides a way to create high-efficiency organic materials for harvesting waste heat from previously inconceivable places (e.g., fibers in clothing that convert body heat to a voltage that can recharge batteries).

5.2 Experimental

5.2.1 Materials

Vinnapas EP 401 PVAc copolymer emulsion was used as the composite matrix material. MWNT (Baytubes C 150P) was used as the model electrically conductive filler, while DWNT (XBC 1001) was used to show the universality of this approach and create higher PF composites. PEDOT:PSS (Clevios PH1000) doped with 5 wt% DMSO, and TCPP were used to stabilize the CNTs in water during composite preparation. All of these materials are described in greater detail in Sections 3.2.1 and 4.2.1.

5.2.2 Composite Preparation

CNT:(PEDOT:PSS):TCPP weight ratios of 1:1:0.25, 1:2:0.25, 1:3:0.25, and 1:4:0.25 were prepared using aqueous solutions of 1.23 wt% PEDOT:PSS and 2.67 wt% TCPP, respectively. The aqueous suspensions were then sonicated for 15 minutes at 50 W in a water bath. All solutions were left at their unaltered pH values. The polymer emulsion and deionized water were then added to the CNT:(PEDOT:PSS):TCPP mixture

and sonicated again for another 5 minutes at 50 W to homogenize. This final aqueous suspension contained 5 wt% total solids. Composites with four different CNT concentrations (10, 20, 30, and 40 wt%) were prepared by drying suspensions in a 26 cm^2 plastic mold for 2 days under ambient conditions and then for 24 hours in a vacuum desiccator. Composites containing 10, 20, 30, and 40 wt% CNT, stabilized at a 1:1:0.25 CNT:(PEDOT:PSS):TCPP weight ratio, were prepared in the same manner, but dried in a vented hood for 36 hours and then in an oven at 80°C for 6 hours. These final aqueous suspensions contained 0.5 wt% total solids. Concentrations are based upon the dry weight of PVAc, CNTs, and stabilizer solids used in the composite. Composite thicknesses ranged from ~0.06 to 0.15 mm.

5.2.3 Characterization

In-plane electrical conductivity and Seebeck coefficients were measured with a home-built device, as previously described (Section 3.2.3.2). Through-thickness thermal conductivity measurement and scanning electron imaging were also previously described in Sections 3.2.3.3 and 3.2.3.5, respectively.

5.3 Results and Discussion

5.3.1 Composite Microstructure

The dual-stabilizer CNT-filled composite recipes that were studied are summarized in Table 5.1. In the first set of composites (A1 – A4), four different MWNT concentrations with a fixed MWNT:(PEDOT:PSS):TCPP weight ratio of 1:1:0.25, were

used to show the influence of filler concentration on thermoelectric properties. Subsequent composite sets (B – D) were fabricated to compare thermoelectric properties of composites made with different amounts of PEDOT:PSS in relation to MWNT and TCPP. The PEDOT:PSS concentration affects the CNT dispersion and transport behavior at tube junctions.[65,206] For the two remaining sets of samples (E – F), a mixed-drying condition was performed in a vented hood for 36 hours and then in an oven at 80°C for 6 hours. The elevated temperature removes excess dopant (DMSO) and helps strengthen the segregated network.[65]

Table 5.1. Thermoelectric polymer nanocomposite recipes.

Sample Name	CNT Conc. (wt%)	CNT Type	CNT:(PEDOT:PSS):TCPP ratio	Drying Temp.[a]
A1	10	MWNT	1:1:0.25	RT
A2	20	MWNT	1:1:0.25	RT
A3	30	MWNT	1:1:0.25	RT
A4	40	MWNT	1:1:0.25	RT
B1	10	MWNT	1:2:0.25	RT
B2	20	MWNT	1:2:0.25	RT
B3	30	MWNT	1:2:0.25	RT
C1	10	MWNT	1:3:0.25	RT
C2	20	MWNT	1:3:0.25	RT

Table 5.1. Continued.

D1	10	MWNT	1:4:0.25	RT
E1	10	MWNT	1:1:0.25	RT + 80°C
E2	20	MWNT	1:1:0.25	RT + 80°C
E3	30	MWNT	1:1:0.25	RT + 80°C
E4	40	MWNT	1:1:0.25	RT + 80°C
F1	10	DWNT	1:1:0.25	RT + 80°C
F2	20	DWNT	1:1:0.25	RT + 80°C
F3	30	DWNT	1:1:0.25	RT + 80°C
F4	40	DWNT	1:1:0.25	RT + 80°C

[a] RT is room temperature

Cross sectional SEM images of freeze-fractured composites are shown in **Figure 5.1** for different MWNT concentrations and MWNT:(PEDOT:PSS):TCPP weight ratios (Samples A1, A4, and D1). MWNT are shown as light-colored spaghetti-like flexible cylinders. Figure 5.1a and b (Sample A1) clearly shows the segregated network behavior previously described, with the MWNT forced into the interstitial spaces between the nonconductive, coalesced polymer particles (dark regions). As the MWNT:(PEDOT:PSS):TCPP ratio is increased to 1:4:0.25 (Figure 5.1c, Sample D1), the MWNT appear better stabilized due to their more homogeneous dispersion throughout the composite cross section. At higher magnification (Figure 5.1d), the junctions between the MWNT are more visible, but somewhat obscured by their

clustering. It is nearly impossible to completely exfoliate every nanotube because of their high affinity to each other through secondary interactions.[314] As the MWNT concentration is increased to 40 wt% (Figure 5.1e and f, Sample A4), the network becomes thicker and there is a dramatic increase in porosity. This porosity is the result of the polymer's inability to envelop the stabilized MWNT, creating microvoids that act as barriers for complete polymer coalescence.

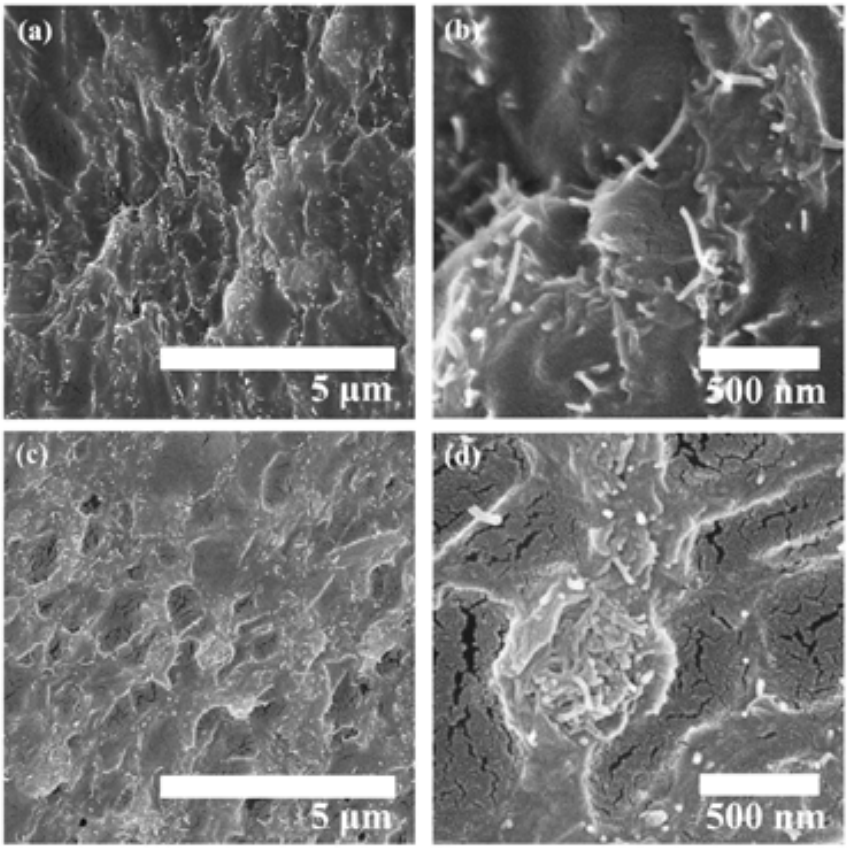

Figure 5.1. SEM cross-sectional images of composites containing 10 wt% MWNT with 1:1:0.25 MWNT:(PEDOT:PSS):TCPP (Sample A1) (a), 10 wt% MWNT with 1:4:0.25 MWNT:(PEDOT:PSS):TCPP (Sample D1) (c), and 40 wt% MWNT with 1:1:0.25 MWNT:(PEDOT:PSS):TCPP (Sample A4) (e). Higher magnification images of the composites shown in (a), (c), and (e) are displayed in (b), (d), and (f), respectively.

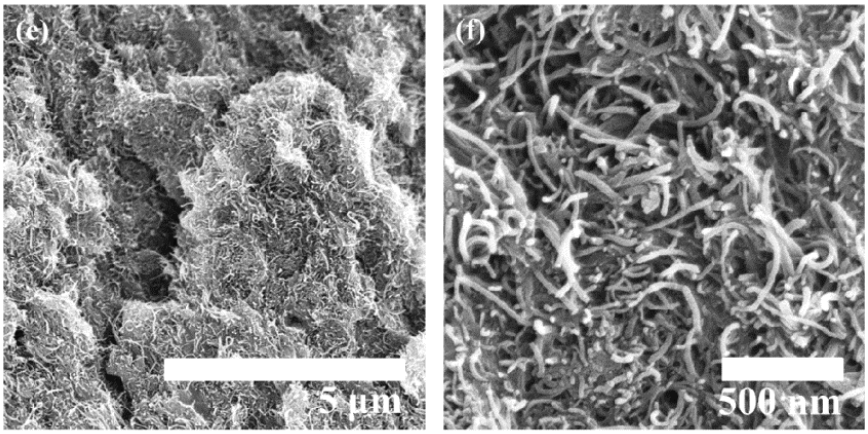

Figure 5.1. Continued.

SEM cross-sectional images of the DWNT:(PEDOT:PSS):TCPP system are shown in **Figure 5.2** with varying DWNT concentrations. Figure 5.2a shows a 10 wt% DWNT composite (Sample F1), which is shown at higher magnification in Figure 5.2b. The nanotube network appears more uniform and detached from the matrix than that observed for MWNT. The DWNT were pulled out from the composite rather than fractured or embedded in the matrix, which is due to their high mechanical strength. A possible reason for the irregular surfaces seen here is that the smaller and less-aggregated bundles of DWNT are easier to bend. The porosity seems to be slightly decreased when compared to the MWNT-filled composites (Figure 5.2) which is because the composites were heated to a temperature above the T_g of the latex, which allows for increased coalescence. As the DWNT concentration is increased to 40 wt% (Sample F4, Figure 5.2b), the porosity dramatically increases and becomes a factor in the degradation of the mechanical properties, which are linked to the critical pigment volume concentration (CPVC) phenomenon commonly seen in this type of polymer

nanocomposite.[29,67-68,297-299] The CPVC describes the maximum amount of filler that can be added to the matrix and still maintain sufficient wetting of the filler by the polymer. Above the CPVC, the mechanical properties can deteriorate to such a degree that it will affect the transport properties.

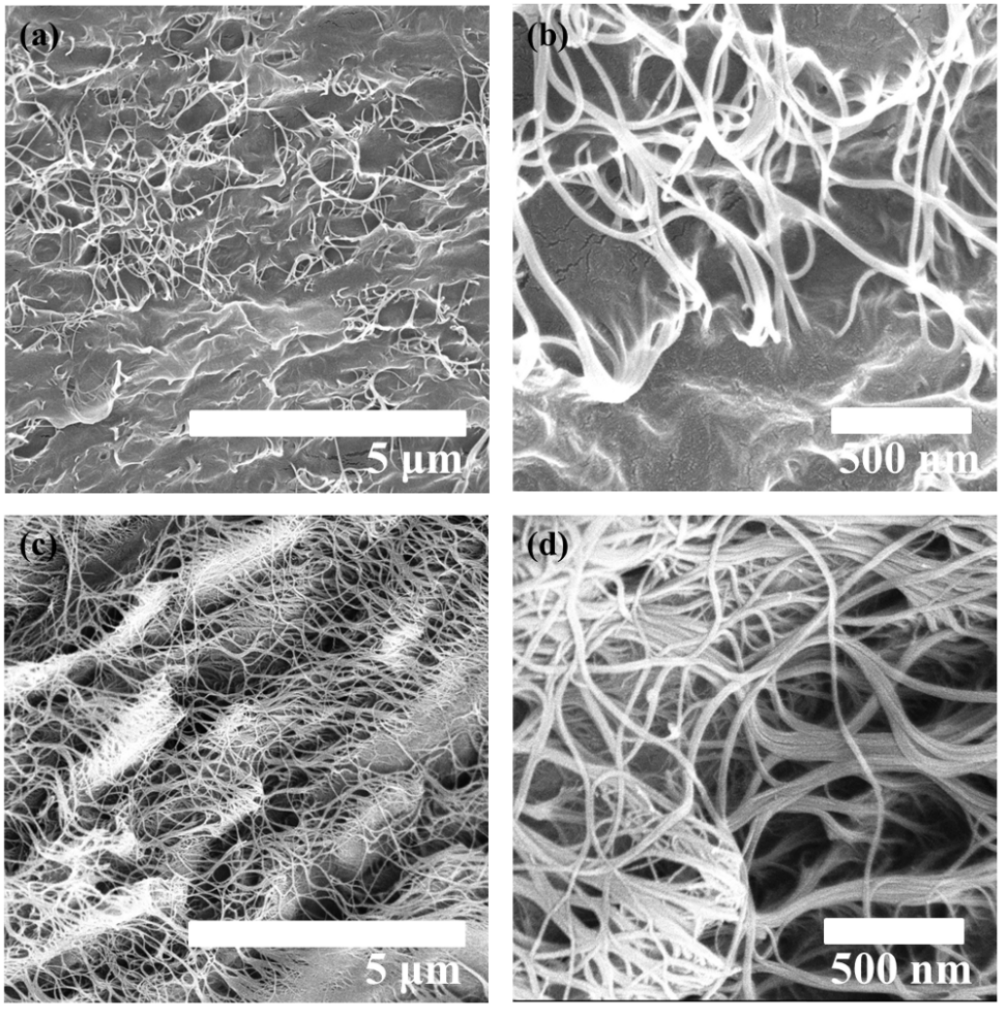

Figure 5.2. SEM cross-sectional images of 1:1:0.25 DWNT:(PEDOT:PSS):TCPP composites containing 10 wt% (Sample F1) (a) and 40 wt% DWNT (Sample F4) (c). Higher magnification images of (a) and (c) are shown in (b) and (d), respectively.

5.3.2 Transport Properties

The through-thickness thermal conductivities of these segregated network polymer composites are shown in **Figure 5.3**. Figure 5.3a shows the results for a CNT:(PEDOT:PSS):TCPP weight ratio of 1:1:0.25 as the CNT concentration is increased (Samples A1–A4 and F1–F4). Unlike the electrical conductivity, the thermal conductivity has been shown to be relatively insensitive to CNT and stabilizer concentration.[7,65,67,251] The thermal conductivities of MWNT-filled composites increase from 0.08 to 0.12 W m^{-1} K^{-1} as the concentration is increased from 10 to 40 wt%. When MWNT are replaced by DWNT, the thermal conductivity does not show a dramatic increase (0.10 – 0.14 W m^{-1} K^{-1}). It should also be noted that the thermal conductivity is not affected by the amount of PEDOT:PSS used to stabilize the MWNT (Figure 5.3b). These composites (Samples A1, B1, C1, and D1), range in thermal conductivity from 0.09 – 0.12 W m^{-1} K^{-1} with no discernible trend. The thermal conductivity of these composites correlates well with those materials previously reported but are lower than those reported in Chapters III – IV. These low experimental values (~0.12 W m-1 K^{-1} for the 40 wt% MWNT composite) can be attributed to the numerous high thermal contact resistances occurring between the nanotubes, PEDOT:PSS, TCPP, and the latex particles.[267-271] The addition of the small amount of TCPP adds another interface with differing vibrational frequency, which reduces the conductivity seen in similar single stabilizer CNT-filled composites. This low *k* can be attributed to the increased porosity, accompanied by the high concentration of CNT, which further disrupts phonon transport through the composite. These organic stabilizers can also act

as phonon-scattering centers because they are embedded in the composite alongside the MWNT.[268]

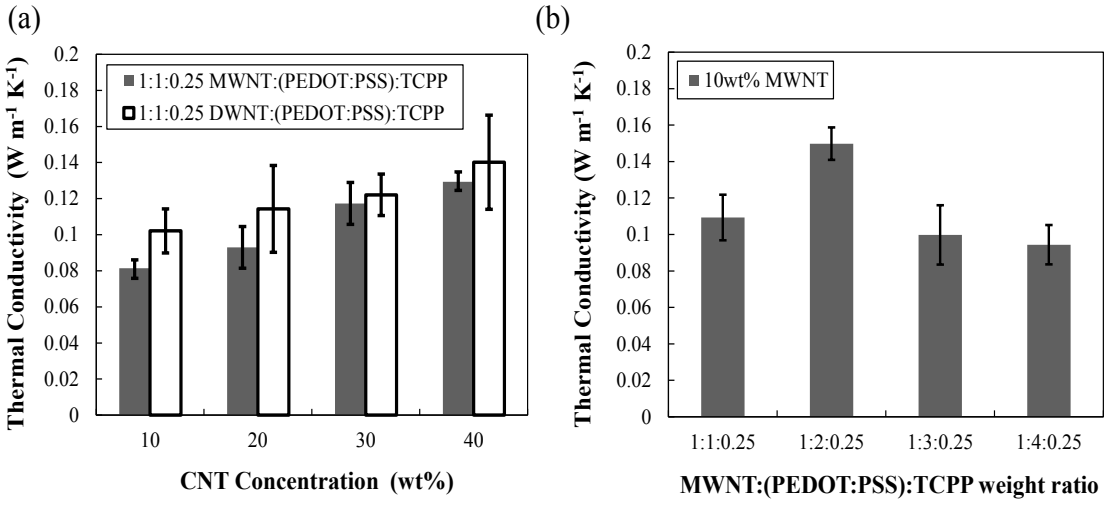

Figure 5.3. Through-thickness thermal conductivity values of 1:1:0.25 CNT:(PEDOT:PSS):TCPP as a function of CNT concentration (Samples A1 – A4, F1 – F4) (a) and 10 wt% MWNT as a function of MWNT:(PEDOT:PSS):TCPP weight ratio (Samples A1, B1, C1, and D1) (b).

The in-plane electrical conductivities of these composites as a function of MWNT:(PEDOT:PSS):TCPP ratio and MWNT concentration are shown in **Figure 5.4**a. As the MWNT concentration increases for each MWNT:(PEDOT:PSS):TCPP ratio, the electrical conductivity increases. A composite containing a MWNT:(PEDOT:PSS):TCPP ratio of 1:1:0.25 and 40 wt% MWNT (Sample A4) reaches an electrical conductivity of approximately 9,500 S m^{-1}, which is comparable to that of a composite with 10 wt% MWNT and a 1:4:0.25 MWNT:(PEDOT:PSS):TCPP

(Sample D1, ~8,500 S m^{-1}). PEDOT:PSS is believed to create less electrically resistive junctions between tubes, so increasing the amount of PEDOT:PSS within the composite will help stabilize more MWNT and create a large number of electrically bridged junctions. This behavior enables higher electrical conductivity to be reached without having to add more filler.

Increasing the MWNT concentration and altering the MWNT:(PEDOT:PSS):TCPP ratio does not have a dramatic effect on the Seebeck coefficient (25 – 50 μV K^{-1}) (Figure 5.4b). The consistency in the Seebeck coefficient is believed to be caused by a small energy barrier hindering low-energy electron transport at the tube junctions, which leaves it insensitive to changes in electrical conductivity. The Seebeck coefficients appear to decrease slightly as the concentration of PEDOT:PSS is increased, which could be due to its intrinsically small *S* (~20 μV K^{-1}).[242,246] The Seebeck coefficients reported here are greater than MWNT:TCPP composites (~28 μV K^{-1}),[67] and similar to values previously reported for SWNT:(PEDOT:PSS) composites (20 – 60 μV K^{-1}).[7,65] As the dual stabilizers potentially shift the Fermi level, these composites maintain the high electrical conductivity of PEDOT:PSS-stabilized composites.[65,67,206] The addition of the semiconducting TCPP might also create sharper features in the density of states, creating more asymmetry and increasing *S*. The charge transport across the junctions can be easily influenced by the stabilizer(s) used to stabilize the CNT,[194] the interparticle distance,[65] the contact potential barrier,[310] and the electrostatic charges associated with the CNTs and matrix.[162] This is a strong indication that the thermoelectric properties of

these polymer composites can be manipulated by tailoring the junctions between nanotubes with different combinations of stabilizing agents.

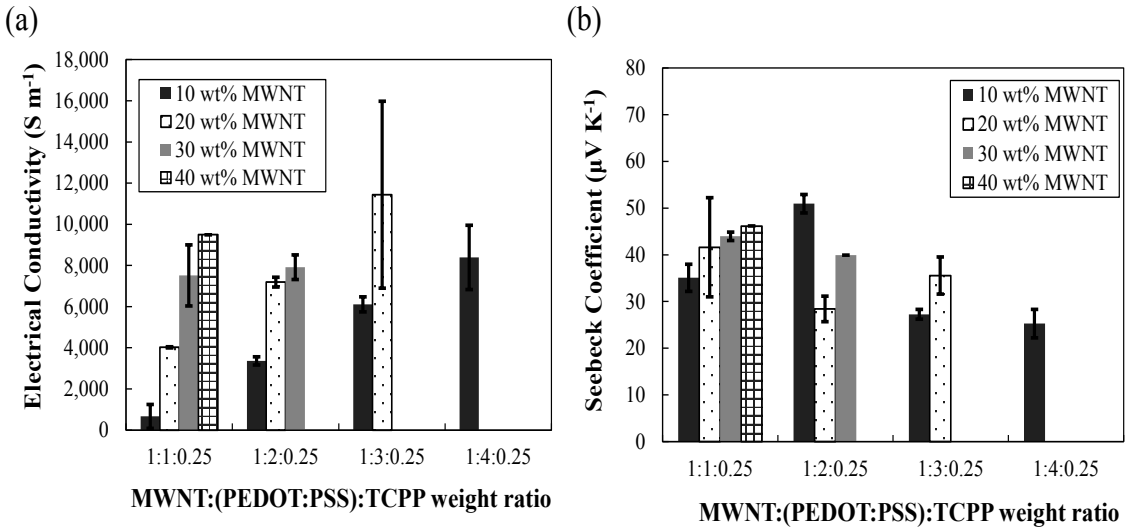

Figure 5.4. In-plane electrical conductivity values (a) and Seebeck coefficients (b) as a function of both MWNT concentration and MWNT:(PEDOT:PSS):TCPP weight ratio.

In an effort to further enhance electrical conductivity, two sets of composites were placed in an oven for 6 hours at 80°C (**Figure 5.5**a, Samples E and F). This elevated temperature softens the polymer particles (T_g = –15°C), allowing them to better tighten the electrically conductive network that exists between the nanoparticles.[30,65] Comparing MWNT- and DWNT-filled composites, the electrical conductivities increase roughly by an order of magnitude at each CNT concentration. At 40 wt% CNT, the electrical conductivity reaches approximately 96,000 and 9,500 S m^{-1} for DWNT-filled and MWNT-filled composites, respectively. This conductivity for DWNT-filled

composites is comparable to the highest values reported for completely organic, free-standing composites and can be attributed to the high intrinsic conductivity of this type of CNT.[206] The increased electrical conductivity can be explained by the DWNT having a higher structural stability, which creates highly conductive π-conjugated pathways that remain undisturbed on the inner tube during functionalization and allow it to act as an independent SWNT.[67,188-192] This large conductivity in DWNT-filled composites can also be explained by the tube lengths appearing longer compared to the MWNT, as evidenced in the SEM images (Figures 5.1 and 5.2, respectively). The MWNT could have been mechanically degraded (i.e., scission of the tubes) during sonication, reducing their lengths. The longer tube lengths reduce the frequency of CNT – CNT junctions, which dominate the resistivity throughout the conductive network.[192,197,251] As one of the tubes within a DWNT is always metallic in character, the other semiconducting tube will help to enhance the Seebeck coefficient (Figure 5.5b), which remains insensitive to the CNT concentration and is not directly affected by the increased drying temperature. MWNT-filled composites maintain values of approximately 40 $\mu V\ K^{-1}$, which are comparable to those reported previously (Figure 5.5b). As MWNT-filled composites are compared to DWNT-filled composites, the Seebeck coefficients increase by roughly 50% (~40 to 70 $\mu V\ K^{-1}$). This large increase has been previously observed with DWNT-filled composites and is directly related to the intrinsic properties of this type of nanotube.[67]

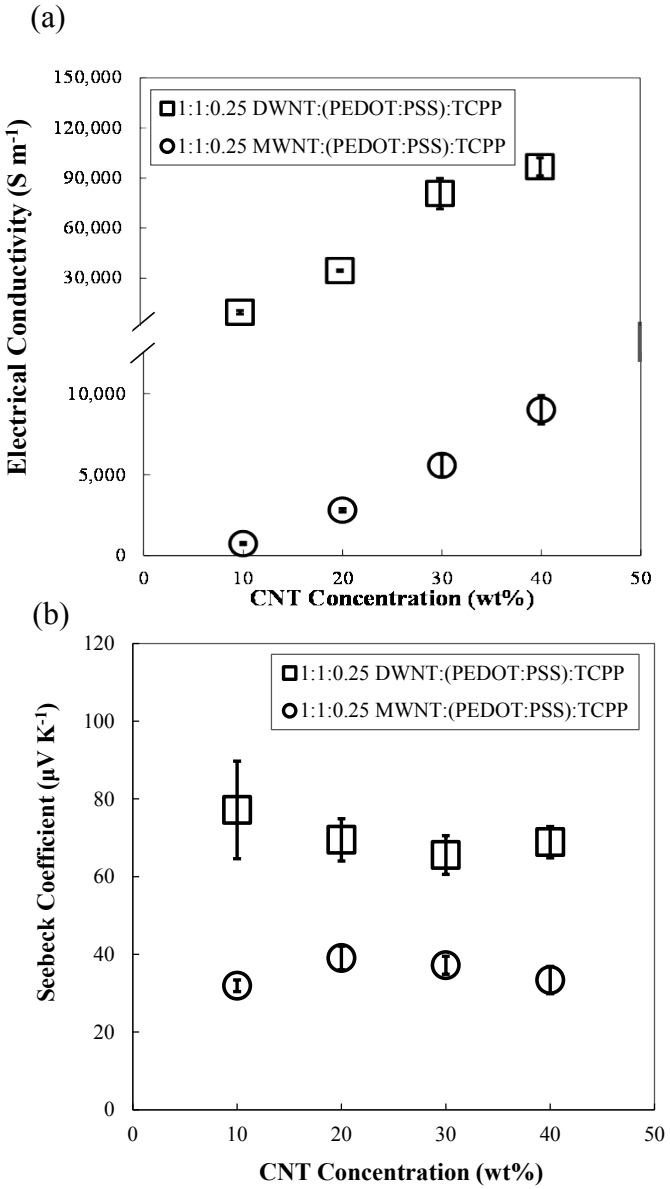

Figure 5.5. In-plane electrical conductivity (a) and Seebeck coefficients (b) as a function of CNT concentration and type (Samples E – F).

The ability to maintain relatively constant electrical conductivities, while simultaneously increasing Seebeck coefficient, results in power factors ($PF = S^2\sigma$)

among the largest reported for a fully organic material. **Figure 5.6a** shows PF as a function of MWNT concentration and MWNT:(PEDOT:PSS):TCPP ratio. With a 1:1:0.25 MWNT:(PEDOT:PSS):TCPP ratio, the power factor increases linearly as the MWNT concentration is increased from 10 to 40 wt% (1.24 to 20.2 $\mu W\ m^{-1}\ K^{-2}$, respectively). This behavior is consistent with the increasing electrical conductivity and relatively constant Seebeck coefficient (Figure 5.5). Increasing the PEDOT:PSS concentration, and holding the other components constant, produces no discernible trend in the values of *S* (Figure 5.5b). Replacing MWNT with DWNT (Figure 5.6b, Samples F1 – F4), results in a 25× improvement in PF. The 40 wt% DWNT 1:1:0.25 DWNT:(PEDOT:PSS):TCPP composite achieves a power factor of approximately 500 $\mu W\ m^{-1}\ K^{-2}$ at room temperature. This is among the highest values ever reported for a fully organic free-standing composite, and is within a factor of five of traditional single-crystal inorganic thermoelectric materials (e.g., PbTe [$S^2\sigma$ ~500 $\mu W\ m^{-1}\ K^{-2}$][82-83]).[7,65,67,197,206,248,276,285] This level of performance makes these flexible, organic materials viable for practical applications.

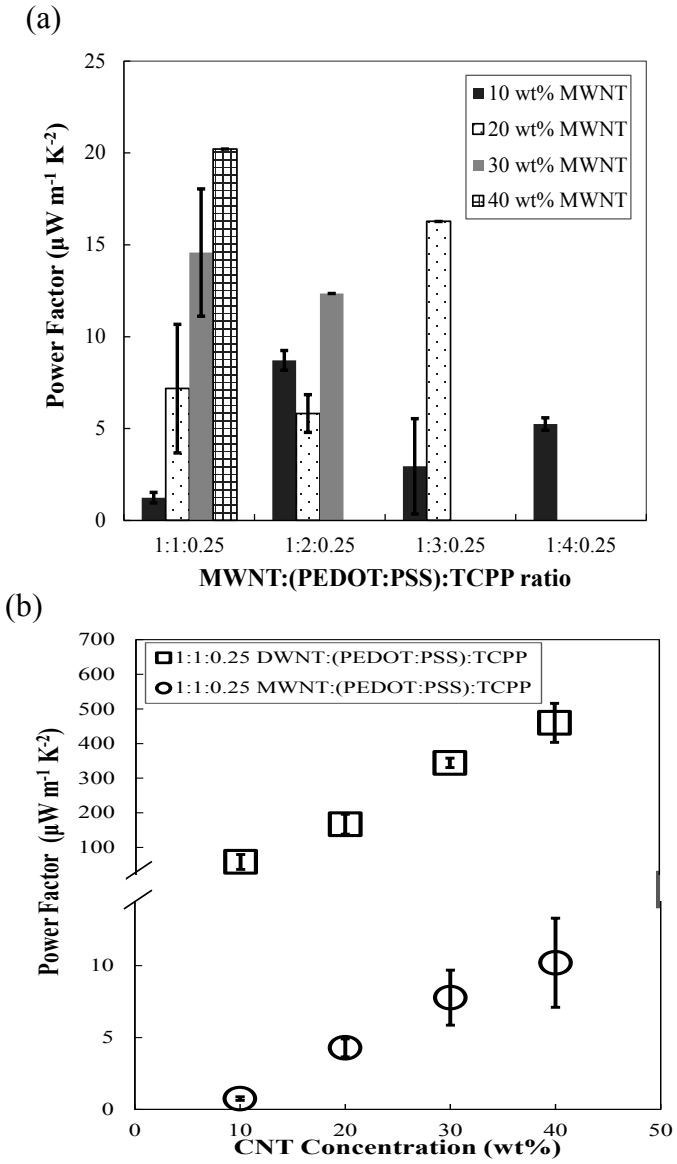

Figure 5.6. Composite power factor measured as a function of both MWNT concentration and type (samples A – D) (a) and as a function of both CNT concentration and type (samples E – F) (b).

5.4 Conclusions

Thermoelectric polymer nanocomposites were prepared with two different nanotubes (MWNT and DWNT), two CNT-stabilizers (PEDOT:PSS and TCPP), and

four different CNT:(PEDOT:PSS):TCPP weight ratios, each dried at 80°C and/or room temperature. This study reveals the influence of CNT type and concentration, PEDOT:PSS concentration, and drying condition on thermoelectric properties. The stabilization by PEDOT:PSS and TCPP, presumably by π-π stacking, bridges nanotubes and helps charge carriers (i.e., holes) to travel more efficiently in these composites, resulting in high electrical conductivity. Thermal conductivity (0.09 – 0.14 W m^{-1} K^{-1}) was relatively unaffected by stabilizer concentration (ranging from 1:1:0.25 to 1:4:0.25 MWNT:(PEDOT:PSS):TCPP), CNT concentration (10 – 40 wt^%), and CNT type. This likely resulted from the mismatches in vibrational spectra at the many interfaces within the composite, which impeded phonon transport. At 40 wt% MWNT, the 1:1:0.25 MWNT:(PEDOT:PSS):TCPP composite exhibited an electrical conductivity of approximately 9,500 S m^{-1} and the Seebeck coefficient remained relatively insensitive to MWNT concentration and MWNT:(PEDOT:PSS):TCPP weight ratio (~40 μV K^{-1}). Using DWNT at 40 wt% in a 1:1:0.25 DWNT:(PEDOT:PSS):TCPP composite, produced electrical conductivity of 96,000 S m^{-1} and nearly doubled the Seebeck coefficient (~70 μV K^{-1}) of the comparable MWNT composite. These thermoelectric properties are much greater than those of typical polymer composites containing CNTs, yielding power factors ($S^2\sigma$) that are among the highest reported for a completely organic, flexible material (~500 μW m^{-1} K^{-2}). These composites have the potential to eventually exceed commonly used inorganic semiconductors in thermoelectric efficiency (and already do when normalized by the mass).

CHAPTER VI

LATEX FREE THERMOELECTRIC THIN FILMS PRODUCED BY LIQUID-PHASE EXFOLIATION*

6.1 Introduction

Organic thin film nanocomposites prepared by liquid-phase exfoliation of SWNT, stabilized by intrinsically conductive PEDOT:PSS, were examined without the use of an insulating polymer emulsion matrix. This thin film preparation method as it has been shown to effectively produce coherent, flexible composites at high CNT concentrations (> 70 wt%). The goal of this chapter is to investigate the thermoelectric properties of thin films as the SWNT concentration is increased to 95 wt%. Without the use of the insulating polymer emulsion as a binder for the SWNT network, electrical conductivity for these fully organic films is shown to increase from 50,000 to 400,000 S m^{-1} as the SWNT concentration is increased. While these thin films exhibit metallic electrical conductivity, the thermal conductivity and Seebeck coefficient remain relatively unaffected with higher concentrations of electrically conductive filler. The high interfacial thermal resistances seen in segregated network composites are still

*Reprinted with permission from G. P. Moriarty, S. De, P. J. King, U. Khan, M. Via, J. A. King, J. N. Coleman, J. C. Grunlan. Thermoelectric behavior of organic thin film nanocomposites. *J. Polym. Sci. B* **2013**, *51*, 119-123. Copyright © 2012 Wiley Periodicals, Inc.

prevalent within these thin films and keep the thermal conductivity relatively low (< 0.6 W m^{-1} K^{-1}). Power factors of these thin film nanocomposites reach a maximum of 115 μW m^{-1} K^{-2} at 85 wt% SWNT, which is similar to previously reported.[65] The ability of a completely organic, flexible material to reach metallic electrical conductivity, and maintain low thermal conductivity, is an important tool for harnessing energy from thermal gradients.

6.2 Experimental

6.2.1 Materials

High purity arc-discharge single walled carbon nanotubes (purchased from Iljin Nanotech Co., Seoul, Korea) were used as the electrically conductive filler. Dispersions were prepared by adding the nanotubes to a 10 mL cylindrical vial containing an aqueous solution of 5 mg mL^{-1} PEDOT:PSS (Clevios PH500, purchased from Heraeus Precious Metals, Leverkusen, Germany). The nanotube concentration was maintained at 1 mg mL^{-1} to keep the resultant solution viscosity low during sonication.

6.2.2 Composite Preparation

This dispersion was subjected to 5 min of high-power tip sonication (VibraCell CVX, 750 W, 20% amplitude, 60 kHz) before being placed in a sonic bath (Branson 2510-MT) for 1 hour and subjected to another 5 min of high-power sonication. These dispersions were blended in the ratio required to give the desired SWNT:(PEDOT:PSS) mass fraction. The mixtures were then sonicated for 15 min to homogenize. The

resulting dispersions were vacuum-filtered using 0.45 μm poly(vinylidene fluoride) (PVDF) filter membranes (MF-Millipore membrane, 47 mm diameter) to produce thick films. The thickness of these films was controlled by the volume of dispersion filtered and hence the deposited mass. Deposited films were washed with 200 mL of deionized water, dried under vacuum for 24 hours at 60°C, and peeled from the filter membrane to give a robust free standing film. Thin film thicknesses ranged from ~0.01 to 0.45 mm.

6.2.3 Characterization

Samples were cut into a rectangular shape (~15 mm in length and 2 mm in width) to measure the in-plane electrical conductivity and Seebeck coefficients with a home-built, shielded four-point probe apparatus (see Section 3.2.3.2). The scanning electron micrographs of composite cross-sections were taken with an FEI Quanta 600 FE-SEM (see Section 3.2.3.5). Through-thickness thermal conductivity at 25°C was measured with a Nanoflash LFA 447 in accordance with ASTM E1461-07. For a single through-plane thermal conductivity measurement, a 25.4 mm diameter disk (cut from the center of the thin film composites) was placed in the device. A Xenon flash lamp was then used to direct a short heat pulse of 10 J to the front side of the sample, as the temperature rise on the back surface of the disk was recorded as a function of time. For each sample, five separate heat pulses were used and the resulting thermal conductivities for each test were averaged. Additionally, at least three thin films were measured for each SWNT concentration. Specific heats were measured with a Q20 DSC in conjunction with ASTM E1269-05 (see Section 4.2.3).

6.3 Results and Discussion

6.3.1 Composite Microstructure

In this chapter, SWNT was combined with intrinsically conductive PEDOT:PSS to create organic thermoelectric thin films. **Figure 6.1**(a) depicts an exfoliated solution of SWNT with PEDOT:PSS attached to its surface. The surfactant helps prevent the hydrophobic SWNT from aggregating together through enhanced hydrophilicity. As the solution is allowed to dry, electrically conductive junctions form between CNT (Figure 6.1b), which is believed to be the source of exceptional electronic properties.[315] These junctions are easily influenced by the interparticle distance, contact potential barriers, and electronic states of CNT, but can be tailored by stabilizer type and concentration.[65,67]

Figure 6.1c shows a freeze-fractured cross-sectional SEM micrograph of a thin film made of 20 wt% SWNT and 80 wt% PEDOT:PSS. The bright spaghetti-like strands that appear here are nanotubes that have pulled out of the darker PEDOT:PSS matrix. At higher magnification (Figure 6.1d), designated by the dotted-line box in Figure 1c, PEDOT:PSS at SWNT junctions are more clearly seen as brighter spots. These junctions are believed to impart metal-like electrical conductivity to the thin films. As the SWNT concentration is increased to 60 wt% (Figure 6.1e and f), porosity within the microstructure is shown to increase as well. These microvoids are formed by the SWNT aggregation that increases as the PEDOT:PSS concentration is reduced. This porosity will affect the mechanical and transport properties of these thin films.

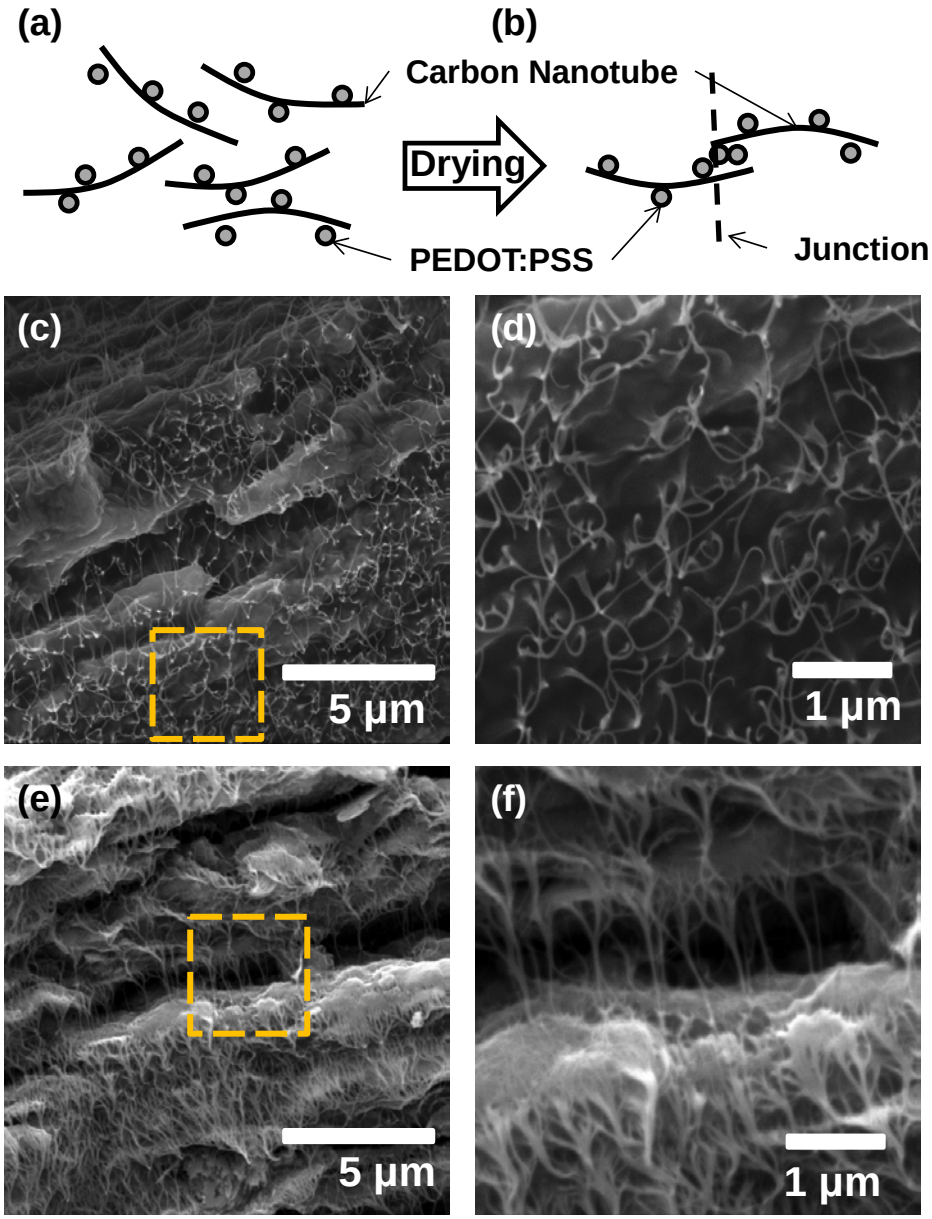

Figure 6.1. Schematics of carbon nanotubes coated by PEDOT:PSS particles in their exfoliated state (a) and an electrically conductive junction formed between carbon nanotubes upon drying of the exfoliated solution (b). SEM cross-sectional images of a 20 wt% SWNT film (c) and a 60 wt% SWNT film (e). Images (d) and (f) are higher magnification images, marked by dotted boxes in (c) and (e), respectively. The balance of each film is PEDOT:PSS.

6.3.2 Transport Properties

Table 6.1 summarizes the through-thickness thermal conductivity for the SWNT-filled thin films. These measurements were obtained using the transient method (ASTM E1461-07), where thermal conductivity is calculated from Equation 4.1. As expected, the specific heat decreases with increasing SWNT concentration. These data agree with a simple rule of mixtures calculation, which is conceptually accurate because it would take less energy to raise the temperature as more conductive filler is introduced. These thin films have a slightly elevated polymer-like thermal conductivity (~0.4 W m^{-1} K^{-1}),[7,65,67] ranging from 0.4 – 0.7 W m^{-1} K^{-1}, despite displaying metal-like electrical conductivity (**Figure 6.2**a). At 95 wt% SWNT, the thermal conductivity for the composite could have been as large as ~950 W m^{-1} K^{-1}, based upon the parallel resistor model presented in Chapter III,[7,249,251] but the low experimental values (0.53 W m^{-1} K^{-1} for the 95 wt% SWNT) can be attributed to the numerous high thermal contact resistances and differing vibrational frequencies occurring between the nanotubes and PEDOT:PSS.[266-270] This low *k* is also linked to increased porosity that accompanies the increase in SWNT concentration and further disrupts phonon transport.[67]

Table 6.1. Thermal properties of SWNT:(PEDOT:PSS) thin films.

SWNT Conc. (wt%)	Density (g cm^{-3})	Specific Heat (J g^{-1} K^{-1})	Thermal Conductivity (W m^{-1} K^{-1})
20	0.970	1.714	0.560 ± 0.068
40	1.171	1.503	0.444 ± 0.031
60	0.910	1.309	0.638 ± 0.29
77.5	0.610	1.183	0.687 ± 0.0054
85	0.685	0.960	0.664 ± 0.0082
95	0.636	0.956	0.526 ± 0.046

Figure 6.2a shows the electrical conductivity and Seebeck coefficient as a function of SWNT concentration for these thin films. Electrical conductivity appears to increase linearly with SWNT concentration. The highest conductivity of approximately 400,000 S m^{-1}, obtained with 95 wt% SWNT, is orders of magnitude greater than previously reported values for other organic composite systems.[7,65,206,165-176] This high conductivity is attributed to the SWNT having an intrinsically high electrical conductivity, due to its highly conductive π-conjugated pathways that promote electron transport.[65,206] Additionally, PEDOT:PSS enhances the electrical conductivity of the thin films by creating less resistive tube – tube junctions.[65,206] As electrical conductivity of these composites is significantly altered by increasing SWNT concentration, the Seebeck coefficient remains relatively unaltered (~14 to 26 μV K^{-1}) (Figure 6.2a). The Seebeck coefficient remains insensitive to changes in electrical conductivity, as observed in Chapters III-VI, and effectively decouples these two properties.[7,65,206,174] While the indirect contact of SWNT, and the weak bonding between SWNT – PEDOT:PSS at the junctions, effectively impede phonon transport, electrical conductivity can be maintained without direct contact between SWNT through hopping and tunneling of the energetic electrons.[162,174] These thin films display the general behavior of traditional semiconductors in a very weak sense, showing a slight reduction in Seebeck coefficient with increasing electrical conductivity.[5-6,9-12]

The high electrical conductivity exhibited by these thin films results in above average power factors ($S^2\sigma$) commonly reported for all organic systems.[7,65,67,242,244-246,272-276] These values are roughly an order of magnitude lower than commercially

available inorganic semiconductors[21] and are similar to other inorganic thin films.[283-284] Figure 6.2b shows that power factors do not show a distinct trend as the SWNT concentration is increased due to the large variability in electrical conductivity and slight deviations in Seebeck coefficient measurements. However, a thin film composed of 85 wt% SWNT achieves a power factor of ~115 $\mu Wm^{-1} K^{-2}$, which is competitive with other types of good organic thermoelectric materials.[7,65,67,206] A calculated ZT value of ~0.04, from the power factor and through-plane thermal conductivity at 300 K for a 40 wt% SWNT film, makes these fully organic thin films viable for converting waste heat into useful electricity. By incorporating another stabilizer to further tailor the Seebeck coefficient could increase the efficiency of these thin films.

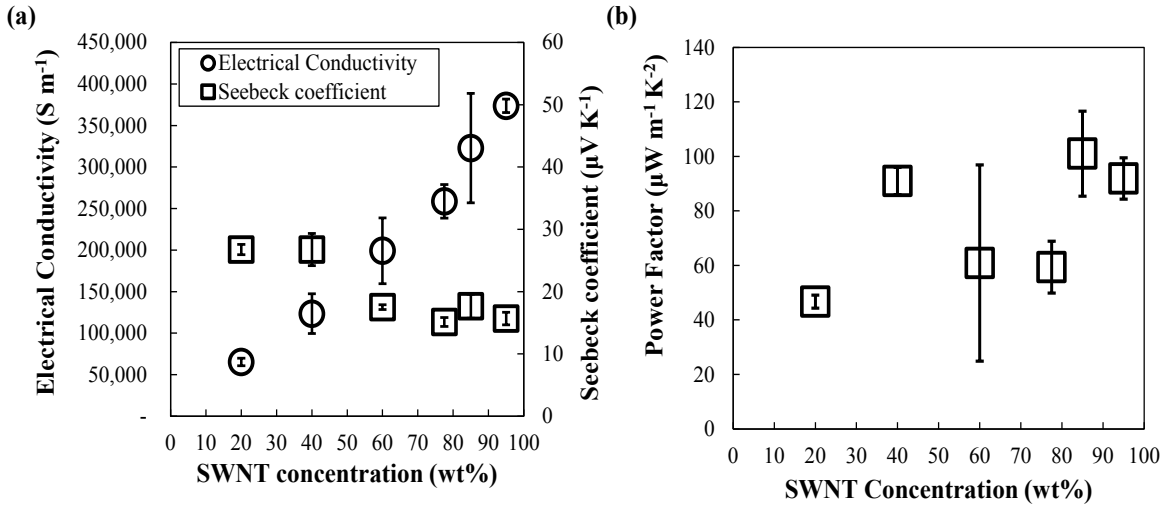

Figure 6.2. Electrical conductivity, Seebeck coefficient (a) and power factor (b) of SWNT:(PEDOT:PSS) thin films as a function of nanotube concentration.

6.4 Conclusions

These fully organic, water-processable and flexible thin films have many advantageous properties for thermoelectric applications. It has been demonstrated that single-walled carbon nanotubes can be easily exfoliated with PEDOT:PSS and dried into thin, coherent films. These films can achieve among the highest reported electrical conductivity for an all organic system (~400,000 S m^{-1}), while still maintaining a thermal conductivity similar to a heat insulating polymer (0.4 – 0.7 W m^{-1} K^{-1}). A thin film composed of 85 wt% SWNT achieves a power factor of ~115 μW m^{-1} K^{-2}, which is competitive with other types of good organic thermoelectric materials. These results present a method to produce thin organic films for applications in thermoelectric devices or as metallic replacements. More work is underway to further improve the waste heat conversion efficiency of these thin films (i.e., produce greater ZT).

CHAPTER VII

CONCLUSIONS AND FUTURE WORK

The ultimate goal of this dissertation was to create fully organic, emulsion-based thermoelectric composites that would be competitive with traditional inorganic semiconductors. By incorporating different types of stabilizers into these materials, carbon nanotube junctions were manipulated and thermoelectric properties were optimized. In addition to using insulating, semiconducting, and intrinsically conductive stabilizers for carbon nanotubes, this dissertation explored the use of using multiple stabilizers within the same composite. Latex-less thin films were also investigated to create organic nanocomposites with ultra-high electrical conductivity.

7.1 Semiconducting Stabilizer Effects for CNTs

Segregated network polymer composites were prepared with a poly(vinyl acetate) emulsion and carbon nanotubes (CNT) as the matrix and electrically conductive filler, respectively. Composite microstructure, mechanical, and transport properties were evaluated in an effort to understand the influence of using a semiconducting molecule, *meso*-tetra(4-carboxyphenyl) porphine (TCPP), as a stabilizer for multi-walled carbon nanotubes (MWNT). The porphyrin was not as effective as an insulating molecule, sodium deoxycholate (DOC), for CNT stabilization, resulting in greater amounts of porosity in the microstructure. Thermal conductivities were relatively unaffected by stabilizer type, CNT type, and concentration, remaining in the polymeric

regime (0.2 – 0.4 W m^{-1} K^{-1}). The DOC-stabilized composites also exhibited a percolation threshold ~30% lower than the TCPP-stabilized, but electrical conductivities (σ) increased with MWNT concentration for both systems. Seebeck coefficients (*S*) were relatively unaffected by MWNT concentration, but TCPP-stabilized composites had *S* values that were five times as large as the DOC-stabilized systems. *S* and σ both increased for composites containing double-walled carbon nanotubes (DWNT) instead of MWNT, further demonstrating the utility of semiconducting stabilizers for improving thermoelectric behavior. These results demonstrate that incorporating semiconducting CNT-stabilizers is a useful tool for increasing the thermoelectric properties of fully organic composites.

7.2 Intrinsically Conductive Stabilizer for High Performance Composites

DWNT, stabilized by intrinsically conductive poly(3,4-ethylenedioxythiophene):poly(styrene sulfonate) (PEDOT:PSS), dramatically influences the thermoelectric properties by more effectively linking the numerous CNT junctions in the microstructure. By creating less resistive junctions, a 40 wt% DWNT composite exhibits metallic electrical conductivity while maintaining constant Seebeck coefficients. Even with the increased electronic properties, the composite thermal conductivity remains in the polymer regime. The combination of high σ and modest *S* results in a power factor ($S^2\sigma$ ~400 μW m^{-1} K^{-2}) that is similar to single crystal semiconductors and is within an order of magnitude of more commonly used inorganics like bismuth telluride.[15,86-87] When a small temperature gradient was applied across this flexible

composite, the thermoelectric behavior was successfully demonstrated with the generation of ~18 nW of power.

7.3 Synergistic Behavior Using a Dual CNT-Stabilizer Approach

Thermoelectric polymer composites were prepared with carbon nanotubes (MWNT or DWNT) and stabilized by the combination of an intrinsically conductive polymer (PEDOT:PSS) and a semiconducting molecule (TCPP). The synergistic behavior of PEDOT:PSS and TCPP helps electrically bridge nanotubes, which results in high electrical conductivity and Seebeck coefficients similar to TCPP-stabilized systems. The thermal conductivity remained relatively insensitive to the stabilizer concentration, CNT concentration, and CNT type. Thermoelectric properties greater than those of typical polymer composites containing CNTs yield power factors ($S^2\sigma \sim 500$ $\mu W\ m^{-1}\ K^{-2}$) that are among the highest reported for a completely organic, flexible material. These composites have the potential to eventually exceed commonly used inorganic semiconductors in thermoelectric efficiency.

7.4 Latex-less Thin Films for High Electrical Conductivity

Thin, coherent films composed of single-walled carbon nanotubes (SWNT) and PEDOT:PSS were created by liquid-phase exfoliation. These fully organic, water-processable thin films do not require the insulating polymer matrix used in the emulsion-based composites and have many advantageous properties for thermoelectric applications. These films exhibit among the highest reported electrical conductivity for

an all organic system, while still maintaining a Seebeck coefficient that is insensitive to SWNT concentration. Even with the metallic electrical conductivity, the thermal conductivity is similar to an insulating polymer. These thin films have power factors that are competitive with other types of good organic thermoelectric materials ($S^2\sigma \sim 120\ \mu W\ m^{-1}\ K^{-2}$), but are limited by low *S* (~20 $\mu V\ K^{-1}$). These results present a method to produce organic thin films that are light weight and could be used for applications in thermoelectric devices or as metallic replacements.

7.5 Future Research Directions

From the results in Chapter IV, V, and VI, it is known that PEDOT:PSS can manipulate the numerous CNT junctions within a composite to enhance the thermoelectric behavior. There are still opportunities to advance the thermoelectric properties further and drive the efficiencies of these fully organic composites closer to (and eventually exceed) traditional inorganic semiconductors. The overall thermoelectric performance of PEDOT is limited by the insulating nature of the large polyanion, PSS, but can be tailored by exploring other smaller anions. Oxidation issues of carbon nanotubes and/or n-type polymers are a concern that needs to be resolved in order to create a completely organic thermoelectric device. One option is to encapsulate an organic n-type composite using layer-by-layer deposition that will restrict the flow of oxygen.[278,309,317] It is also important to try and combine these organic p-type thermoelectric composites with inorganic n-type semiconductors into a working

retrofitted device to show the conversion efficiencies of these materials. These three areas of future work are described in more detail below.

7.5.1 Smaller Anions for Water-Based PEDOT

Chapters IV – VI showed that incorporating PEDOT into a composite system as a CNT stabilizer can improve thermoelectric performance, primarily by increasing electrical conductivity. The ability of this polymer to effectively manipulate the numerous CNT junctions has brought fully organic composites into direct competition with common inorganic semiconductors. Despite this improvement, the large PSS polyanion hinders the overall potential of PEDOT due to its insulating nature.[76] Replacing this insulating polymer with smaller anions, such as a tosylate (e.g., iron (III) *tris*-p-toluenesulphonate (Tos)), will allow for increased electrical conductivity of the resultant conductive polymer (**Figure 7.1**).[216] Crispin *et al* successfully polymerized PEDOT:Tos through an oxidative polymerization process, which precisely controlled the oxidation levels of the polymer and finely tuned the thermoelectric properties. By controlling oxidation, the power factors of the resultant films were optimized to ~320 $\mu W\ m^{-1}\ K^{-2}$. The replacement of PSS by Tos led to roughly an order of magnitude improvement in $S^2\sigma$.[216,242] The potential ability of PEDOT:Tos to stabilize carbon nanotubes in water should be investigated. Several tosylates would need to be studied to produce the most water-stable derivative of this new polymer. Due to the aromatic rings still present, it is assumed stabilization of CNTs will still occur through $\pi - \pi$ interactions. For this approach, the effects of PEDOT:Tos on the thermoelectric

properties would be studied in a manner similar to Chapter V. The ultimate goal would be to achieve $S^2\sigma$ above 800 $\mu W\ m^{-1}\ K^{-2}$. If successful, this approach would make fully organic, water-based, flexible composites that rival many inorganic semiconductors and could be used to efficiently scavenge energy from small temperature gradients.

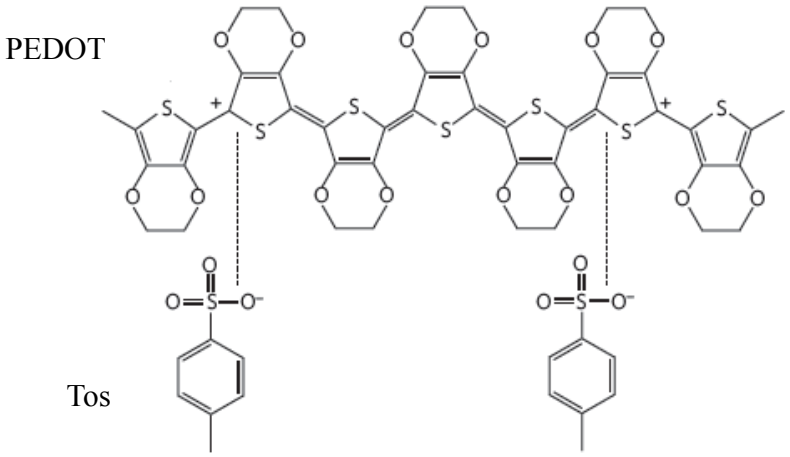

Figure 7.1. Chemical structure of PEDOT as it associates with the smaller anion, Tos, after oxidative polymerization (adapted from [216]).

7.5.2 Encapsulating N-Type Polymer Composites

Organic n-type composites have recently been investigated and developed. Traditionally, these materials are difficult to preserve, as carbon nanotubes and polymers suffer from oxidation.[249,278-279] One such production method to convert the conducting properties of CNTs from p-type back to n-type has been demonstrated by the physical adsorption of branched polyethyleneimine (PEI) onto carbon nanotubes surfaces.[309] By incorporating the numerous electron-donating amine groups of PEI onto the SWNT

surface, n-type composites maintained Seebeck coefficients of roughly -60 μV/K for several days in air before transitioning back to p-type due to oxidation (**Figure 7.2**a). A possible approach to eliminate the oxidation issues is to apply a nano-coating to composite surfaces that will act as an oxygen barrier. Using water-based layer-by-layer assembly (LbL), which is the building of a thin film by alternating exposure of a substrate to cationic and anionic mixtures,[316] a flexible polymeric super gas barrier can be used to stop oxygen doping of n-type composites. One approach would involve using a three component system consisting of cationic PEI, anionic poly(acrylic acid) (PAA) and montmorillonite clay (MMT) in a deposition sequence of PEI/PAA/PEI/MMT (Figure 7.2b and c). This quadlayer (QL) system has been shown to reduce the oxygen transmission rate (OTR) and effectively stop the flow of oxygen with only 4 QL (Figure 7.2d).[317] As LbL is a simple deposition process that can be done under ambient conditions, this thin film can be applied to composites after they have completely dried within an argon atmosphere. The goal of this study would be to create a conformal barrier on polymer composites so as to maintain the n-type behavior for extended periods of time. If successful, a fully organic n-type composite would be realized for use in a fully organic thermoelectric module.

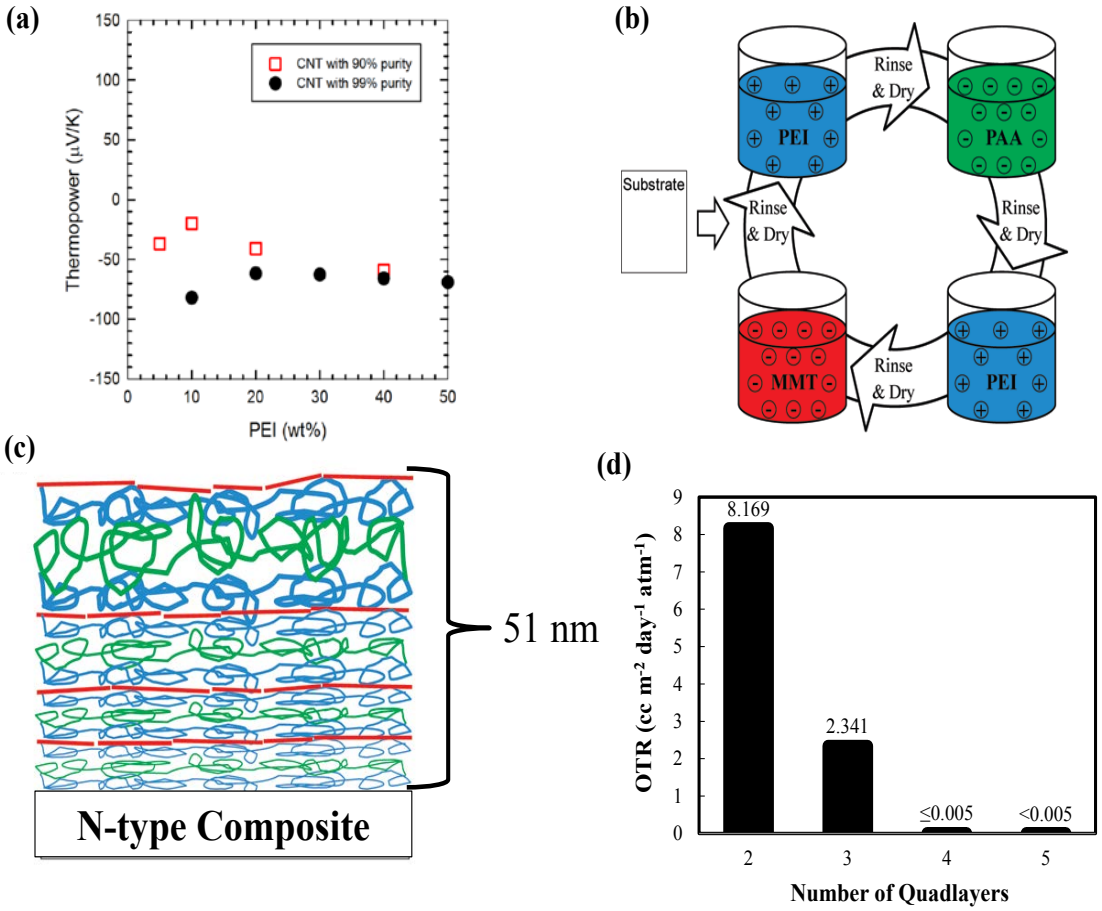

Figure 7.2. Seebeck coefficients of 20 wt% SWNT composites as a function of PEI concentration and CNT purity (a).[309] Cartoon illustrations of layer-by-layer assembly (b) and the nano-brick wall structure resulting from the alternate adsorption of PEI (blue), PAA (green), and MMT (red), onto an n-type composite (c). Oxygen transmission rate reported as a function of the number of quadlayers deposited on 179 μm thick PET film (d) (adapted from [317]).

7.5.3 Combining Organic P-Type with Inorganic N-Type

Chapter V revealed the ability of organic composites to produce a reasonable amount of useful power that can be captured from a small temperature gradient. To increase the efficiency of this power output, and to further show proof that they are capable of converting heat into electricity, p-type organic composites can be paired with

inorganic n-type legs. This could be accomplished using silver-filled conductive epoxy to bind both thermoelectric legs to a copper laden lattice (**Figure 7.3**a). Preliminary results of this module, which is composed of 40 junctions, show that the voltage outputs increase with higher temperature gradients (Figure 7.3b), but the efficiency is still quite low when compared to a commercially available module. In order to make the retrofitted module more comparable, the internal resistance resulting from poor electrical contacts and high contact resistance from the epoxy has to be dramatically reduced. One way to reduce the internal resistance would be to solder the inorganic legs onto the copper pads and increase the electrical conductivity of the epoxy by adding other electrically conductive fillers (e.g., carbon black, carbon nanotubes, graphene). The goal would be to obtain efficiencies similar to a commercial device. Additionally, a simple demonstration could be done by using this module to power an LED or another low power consumption device (e.g., send a wireless signal).

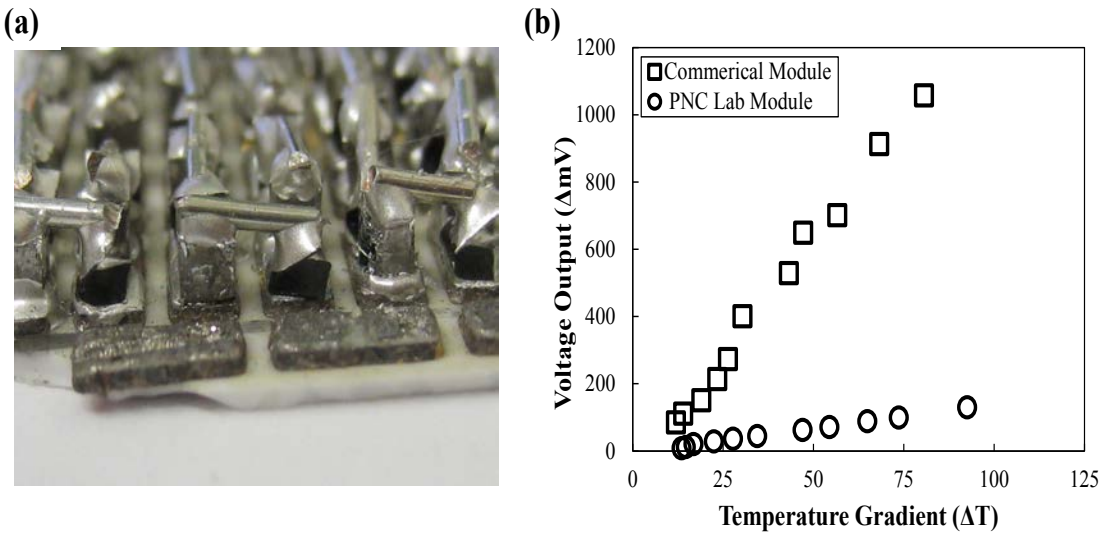

Figure 7.3. A retrofitted device, containing 40 junctions connected electrically in series and composed of inorganic n-type and organic p-type legs (a). Voltage outputs of the retrofitted device, compared to a commercial device, as the temperature gradient is increased (b).

REFERENCES

[1] Lawrence Livermore National Laboratory, August 2010. DOE/EIA – 0384 (2009).

[2] Keping Yan, in *Electrostatic Precipitation: 11th International Conference on Electrostatic Precipitation*. Hangzhou, **2008**, pp. 28.

[3] D. M. Wu, P. L. Hagelstein, P. Chen, K. P. Sinha, A. Meulenberg. *J. Appl. Phys.* **2009**, *106*, 094315.

[4] Natl. Renew. Energy Lab. Energy technology cost and performance data. **http://www.nrel.gov/analysis/tech_costs.html** (accessed 3/13/2011)

[5] G. J. Synder, E. S. Toberer, *Nat. Mater*. **2008**, *7*, 105.

[6] T. M. Tritt, M. A. Subramanian, *MRS Bull*. **2006**, *31*, 188.

[7] C. Yu, Y. S. Kim, D. Kim, J. C. Grunlan, *Nano Lett*. **2008**, *8*, 4428.

[8] W. Thomson, *Proc. Roy. Soc. Edinburgh* **1851**, 91.

[9] G. S. Nolas, J. Sharp, J. Goldsmid, in *Thermoelectric: Basic Principles and New Materials Developments,* Springer-Verlag Berlin, Heidelberg, Germany **2001**, pp. 38.

[10] D. M. Rowe, in *Handbook of Thermoelectrics*, CRC Press, Boca Raton, USA **1995**.

[11] A. Majumdar, *Science* **2004**, *303*, 777.

[12] T. C. Harman, P. J. Taylor, M. P. Walsh, B. E. LaForge, *Science* **2002**, *297*, 2229.

[13] R. Venkatasubramanian, E. Siivola, T. Colpitts, B. O'Quinn, *Nature* **2001**, *413*, 597.

[14] K. F. Hsu, S. Loo, F. Guo, W. Chen, J. S. Dyck, C. Uher, T. Hogan, E. K. Polychroniadis, M. G. Kanatzidis, *Science* **2004**, *303*, 818.

[15] B. Poudel, Q. Hao, Y. Ma, Y. C. Lan, A. Minnich, B. Yu, X. Yan, D. Z. Wang, A. Muto, D. Vashaee, X. Y. Chen, J. M. Liu, M. S. Dresselhaus, G. Chen, Z. Ren, *Science* **2008**, *320*, 634.

[16] J. Winters, *Mech. Eng.* **2008**, *130*, 30.

[17] L. E. Bell, *Science* **2008**, *321*, 1457.

[18] C. J. Vineis, A. Shakouri, A. Majumdar, M. G. Kanatzidis, *Adv. Mater.* **2010**, *22*, 3970.

[19] V. Leonov, R. J. M. Vullers, *J. Electron. Mater.* **2009**, *38*, 1491.

[20] R. Amatya, R. J. Ram, *J. Electron. Mater.* **2010**, *39*, 1735.

[21] A. Shakouri, *Annu. Rev. Mater. Res.* **2011**, *41*, 399.

[22] D. Frankenfield, C. Compher, *J. Amer. Diet. Assoc.* **2005**, *105*, 775.

[23] M. D. Mifflin, S. T. St Jeor, L. A. Hill, B. J. Scott, S. A. Daugherty, Y. O. Koh. *Am. J. Clin. Nutr.* **1990**, *51*, 241.

[24] M. A. McDowell, C. D. Fryar, C. L. Ogden, K. M. Flegal. Anthropometric Reference Data for Children and Adults: United States, 2003-2006. *Nat. Health Stat. Reports* **2008**, *10*.

[25] J. I. Gersten, F. W. Smith, in *The Physics and Chemistry of Materials*, John Wiley & Sons, Inc., New York **2001**. Ch. 14.

[26] G. M. Brown, in *Thermal Characterization Techniques*, (Eds. P. E. Slade, L. T. Jenkins), Marcel Dekker, New York, **1970.** Ch. 5.

[27] J. M. G. Cowie, in *Polymers: Chemistry and Physics of Modern Materials*, 2nd Ed., Chapman and Hall, New York, **1994**.

[28] R. G. Gilbert, in *Emulsion Polymerization: a Mechanistic Approach*, Academic Press, London, **1996**.

[29] G. P. Moriarty, K. A. Sun, J. H. Whittemore, J. W. Rawlins, J. C. Grunlan, *J. Poly. Sci. B* **2011**, *49*, 1547.

[30] Y. S. Kim, J. B. Wright, J. C. Grunlan, *Polymer* **2008**, *49*, 570.

[31] I. Chodak, M. Omastova, J. Pionteck, *J. Appl. Poly. Sci.* **2001**, *82*, 1903.

[32] G. J. Lee, K. D. Suh, S. S. Im, *Polym. Eng. Sci.* **1998**, *38*, 471.

[33] J. F. Feller, I. Linossier, G. Levesque, *Polym. Advan. Technol*. **2002**, *13*, 714.

[34] P. Potschke, A. R. Bhattacharyya, A. Janke, *Polymer* **2003**, *44*, 8061.

[35] D.-X. Yan, H.-D. Huang, J.-F. Gao, K. Dai, W.-Q. Zhang, Z.-M. Li, *J. Macromol. Sci. B* **2013**, *52*, 167.

[36] K. Dai, X. B. Xu, Z. M. Li, *Polymer* **2007**, *48*, 849.

[37] H. Tang, X. F. Chen, Y. X. Luo, *Eur. Polym. J.* **1996**, *32*, 963.

[38] R. Schueler, J. Petermann, K. Schulte, H. P. Wentzel, *J. Appl. Polym. Sci.* **1997**, *63*, 1741.

[39] C.-J. Lee, I.-S. Tsai. *Adv. Mat. Res.*, **2012,** *608-609*, 1318.

[40] M. Shao, Y. He, K. Hong, C. M. Rouleau, D. B. Geohegan, K. Xiao, *Polym. Chem*. **2013**, DOI:10.1039/c2py21020g.

[41] O. Breuer, R. Tchoudakov, M. Narkis, A. Siegmann, *J. Appl. Polym. Sci.* **1997**, *64*, 1097.

[42] J. Y. Feng, C. M. Chan, J. X. Li, *Polym. Eng. Sci.* **2003**, *43*, 1058.

[43] P. Potschke, A. R. Bhattacharyya, A. Janke, *Carbon* **2004**, *42*, 965.

[44] S. H. Foulger, *J Polym Sci B* **1999**, *37*, 1899.

[45] J. C. Grunlan, W. W. Gerberich, L. F. Francis, *J. Mater. Res*. **1999**, *14*, 4132.

[46] F. G. Souza, M. E. Sena, B. G. Soares, *J. Appl. Polym. Sci*. **2004**, *93*, 1631.

[47] H. Scher, R. Zallen, *J. Chem. Phys.* **1970**, *53*, 3759.

[48] X. S. Yi, G. Wu, D. Ma, *J. Appl. Polym. Sci.* **1998**, *67*, 131.

[49] R. P. Kusy, *J. Appl. Phys.* **1977**, *48*, 5301.

[50] D. P. Dharaiya, S. C. Jana, S. F. Lyuksyutov, *Polym. Eng. Sci.* **2006**, *46*, 19.

[51] J. L. Keddie, *Mater. Sci. Eng., R* **1997**, *21*, 101.

[52] J. Sun, W. W. Gerberich, L. F. Francis, *J. Polym. Sci. Part B.* **2003**, *41*, 1744.

[53] J. C. Grunlan, W. W. Gerberich, L. F. Francis, *J. Polym. Sci. Part B.* **2001**, *80*, 692.

[54] S. M. Miriyala, Y. S. Kim, L. Liu, J. C. Grunlan, *Macromol. Chem. Phys.* **2008**, *209*, 2399.

[55] A. Mierczynska, J. Friedrich, H.-E. Maneck, G. Boiteux, J. K. Jeszka, *Cent. Euro. J. Chem.* **2004**, *2*, 363.

[56] P. Vandervorst, C. H. Lei, Y. Lin, O. Dupont, A. B. Dalton, Y. P. Sun, J. L. Keddie, *Prog. Org. Coat.* **2006**, *57*, 91.

[57] N. Grossiord, H. E. Miltner, J. Loos, J. Meuldijk, B. Van Mele, C. E. Koning, *Chem. Mater.* **2007**, *19*, 3787.

[58] H. Pang, T. Chen, G. Zhang, B. Zeng, Z.-M. Li, *Mat. Lett.* **2010**, *20*, 2226.

[59] A. Malliaris, D. T. Turner, *J. Appl. Phys.* **1971**, *45*, 614.

[60] P. A. Lovell, M. S. El-Aasser, in *Emulsion Polymerization and Emulsion Polymers*, John Wiley & Sons, Inc., New York **1997**.

[61] J. F. Auchter, in *Chemical Economics Handbook: Carbon Black*, SRI Consulting, Menlo Park, CA **2005**.

[62] X. Wang, Q. Li, J. Xie, Z. Jin, J. Wang, Y. Li, K. Jiang, S. Fan, *Nano Lett*. **2009**, *9*, 3137.

[63] S. Iijima, T. Ichihashi, *Nature* **1993**, 363, 603.

[64] K. Choi, C. Yu, *PLoS ONE* **2012**, 7, e44977.

[65] D. Kim, Y. S. Kim, K. Choi, J. C. Grunlan, C. Yu, *ACS Nano* **2010**, *4*, 513.

[66] K. R. Anilkumar, A. Parveen, G. R. Badiger, M. V. N. A. Prasad, *Ferroelectrics* **2009**, *386*, 88.

[67] G. P. Moriarty, J. N. Wheeler, C. Yu, J. C. Grunlan, *Carbon* **2012**, *50*, 885.

[68] J. C. Grunlan, A. R. Mehrabi, M. V. Bannon, J. L. Bahr, *Adv. Mater.* **2004**, *16*, 150.

[69] T. J. Seebeck, *Abh. K. Akad. Wiss. Berlin* **1821**, 289.

[70] T. J. Seebeck, *Abh. K. Akad. Wiss. Berlin* **1823**, 265.

[71] T. J. Seebeck, *Ann. Phys. (Leipzig)* **1826**, *6*, 1.

[72] T. J. Seebeck, *Schweigger's J. Phys.* **1826**, *46*, 101.

[73] D. D. Pollock, in *Thermocouples, Theory and Properties*, CRC Press, Boca Raton, FL, **1991**, Ch. 5.

[74] J. C. A. Peltier, *Ann. Chem. Phys.* **1834**, *56*, 371.

[75] A. L. Rockwood, *Phys. Rev. A.* **1984**, *30*, 2843.

[76] O. Bubnova, X. Crispin, *Ener. Environ. Sci.* **2012**, *5*, 9345.

[77] S. B. Shastry, *Rep. Prog. Phys.* **2009**, *72*, 016501.

[78] F. J. DiSalvo, *Science* **1999**, *285*, 703.

[79] A. Shakouri, *Annu. IEEE Semicond. Therm. Meas. Manag. Symp., 20th* **2004**, 1.

[80] A. J. Minnich, M. S. Dresselhaus, Z. F. Ren, G. Chen, *Energy Environ. Sci.* **2009**, *2*, 466.

[82] A. Todosiciuc, A. Nicorici, E. Condrea, J. Warchulska, *2012 Inter. Semicond. Conf.* **2012**, *2*, 269.

[83] J. Martin, G. S. Nolan, W. Zhang, L. Chen, *Appl. Phys. Lett.* **2007**, *90*, 222112.

[84] T. M. Tritt, *Annu. Rev. Mater. Res.* **2011**, *41*, 433.

[85] L. Hicks, M. Dresselhaus, *Phys. Rev. B* **1993**, *47*, 16631.

[86] H. J. Goldsmid, R. W. Douglas, *Br. J. Appl. Phys.* **1954**, *5*, 386.

[87] H. J. Goldsmid, A. R. Sheard, D. A. Wright, *Br. J. Appl. Phys*. **1958**, *9*, 365.

[88] T. C. Harman, D. L. Spears, M. J. Manfra, *J. Electron. Mater.* **1996**, *25*, 1121.

[89] D.-Y. Chung, T. Hogan, P. Brazis, M. Rocci-Lane, C. Kannewurf, M. Bastea, C. Uher, M. G. Kanatzidis, *Science* **2000**, *287*, 1024.

[90] A. I. Boukai, Y. Bunimovich, J. Tahir-Kheli, J. K. Yu, W. A. Goddard, J. R. Heath, *Nature* **2008**, *451*, 168.

[91] A. I. Hochbaum, R. K. Chen, R. D. Delgado, W. J. Liang, E. C. Garnett, M. Najarian, A. Majumdar, P. D. Yang, *Nature* **2008**, *451*, 163.

[92] P. F. P. Poudeu, J. D'Angelo, A. D. Downey, J. L. Short, T. P. Hogan, M. G. Kanatzidis, *Angew. Chem. Int. Ed.* **2006**, *45*, 3835.

[93] J. Androulakis, C. H. Lin, H. J. Kong, C. Uher, C. I. Wu, T. Hogan, B. A. Cook, T. Caillat, K. M. Paraskevopoulos, M. G. Kanatzidis, *J. Am. Chem. Soc.* **2007**, *129*, 9780.

[94] J.-S. Rhyee, K. H. Lee, S. M. Lee, E. Cho, S. I. Kim, E. Lee, Y. S. Kwon, J. H. Shim, G. Kotliar, *Nature* **2009**, *459*, 965.

[95] J. P. Heremans, V. Jovovic, E. S. Toberer, A. Saramat, K. Kurosaki, A. Charoenphakdee, S. Yamanaka, G. J. Snyder, *Science* **2008**, *321*, 554.

[96] A. Saramat, G. Svensson, A. E. C. Palmqvist, C. Stiewe, E. Mueller, D. Platzek, S. G. K. Williams, D. M. Rowe, J. D. Bryan, G. D. Stucky, *J. Appl. Phys*. **2006**, *99*, 023708.

[97] X. W. Wang, H. Lee, Y. C. Lan, G. H. Zhu, G. Joshi, D. Z. Wang, J. Yang, A. J. Muto, M. Y. Tang, J. Klatsky, S. Song, M. S. Dresselhaus, G. Chen, Z. F. Ren, *Appl. Phys. Lett*. **2008**, *93*, 193121.

[98] A. Shakouri, in *Proc. of the Int. Conf. Thermoelectrics* **2005**, 492.

[99] R. Yang, G. Chen and M. Dresselhaus, *Phys. Rev. B* **2005**, *72*, 125418.

[100] E. J. Winder, A. B. Ellis, G. C. Lisensky. *J. Chem. Educ.* **1996**, *73*, 940.

[101] W. Steplewski, T. Serzysko, G. Koziol, A. Dziedzic, *Microelect. Reliab.* **2012**, *52*, 1719.

[102] Y. Wan, D. J. Wen, *Smart Mater. Struct.* **2004**, *13*, 983.

[103] N. C. Das, T. K. Chaki, D. Khastgir, A. Chakraborty, *Adv. Polym. Tech.* **2001**, *20*, 226.

[104] D. M. Mihut, K. Lozano, S. C. Tidrow, H. Gracia, *Thin Solid Films* **2012**, *520*, 6547.

[105] Y. S. Kim, S. C. Ha, Y. Yang, Y. J. Kim, S. M. Cho, H. Yang, Y. T. Kim, *Sensor. Actuat. B* **2005**, *108*, 285.

[106] A. Graham, P. J. Laughlin, D. Bloor, *Sensor. Actuat. B* **2013**, *177*, 507.

[107] M. Castro, J. Lu, S. Bruzaud, B. Kumar, J. F. Feller, *Carbon* **2009**, *47*, 1930.

[108] E. Llobet, *Sensor. Actuat. B* **2013**, *179*, 32.

[109] J. F. Feller, Y. Grohens, *Synth. Met.* **2005**, *154*, 193.

[110] P. Murugaraj, D. E. Mainwaring, T. Jakubov, N. E. Mora-Huertas, N. A. Khelil, R. Siegele, *Solid State Commun.* **2006**, *137*, 422.

[111] P. Potschke, A. R. Bhattacharyya, A. Janke, H. Goering, *Compos. Interfaces* **2003**, *10*, 389.

[112] R. Tchoudakov, O. Breuer, M. Narkis, A. Siegmann, *Polym Eng Sci* **1996**, *36*, 1336.

[113] K. Levon, A. Margolina, A. Z. Patashinsky, *Macromolecules* **1993**, *26*, 4061.

[114] K. Cheah, M. Forsyth, G. P. Simon, *J. Polym. Sci. B* **2000**, *38*, 3106.

[115] S. R. Broadbent, J. M. Hammersley, *Proc. Camb. Phil. Soc.* **1957**, *53*, 629.

[116] D. J. A. Welsh, *Sci. Prog. Oxf.* **1977**, *64*, 65.

[117] L. H. Sperling, in *Introduction to Physical Polymer Science, 2nd* ed., John Wiley & Sons, New York, **1992**, Ch. 12.

[118] J. C. Grunlan, *Ph.D. Dissertation*, University of Minnesota, MN **2001**.

[119] A. I. Medalia, *Rubb. Chem. Technol.* **1986**, *59*, 432.

[120] H. Kawamoto, in *Carbon black-polymer composites*, (Ed. K. Sichel), Marcel Dekker, New York **1982**, Ch. 5.

[121] S. Kirkpatrick, *Rev. Mod. Phys.* **1973**, *45*, 574.

[122] G. Deutscher, A. Kapitulnik, M. Rappaport, in *Annals of the Israel Physical Society, Vol 5: Percolation Structures and Processes* (Eds. G. Deutscher, R. Zallen, J. Adler), American Institute of Physics, New York **1983**, Ch. 10.

[123] S. Etemad, X. Quan, N. A. Sanders, *Appl. Phys. Lett.* **1986**, *48*, 607.

[124] S. Hotta, S. D. D. V. Rughooputh, A. J. Heeger, *Synth. Met.* **1987**, *22*, 79.

[125] J. Janzen, *J. Appl. Phys.* **1975**, *46*, 966.

[126] C. H. Bennet, *J. Appl. Phys.* **1972**, *43*, 2727.

[127] T. Slupkowski, *Phys. Status Solidi A* **1984**, *83*, 329.

[128] F. Bueche, *J. Appl. Phys.* **1972**, *43*, 4837.

[129] M. Sumita, S. Asai, N. Miyadera, E. Jojima, K. Miyasaka, *Colloid Polym. Sci.* **1986**, *264*, 212.

[130] B. Wessling, *Polym. Eng. Sci.* **1991**, *31*, 1200.

[131] L. E. Nielsen, *Ind. Eng. Chem. Fund.* **1974**, *13*, 17.

[132] J. Bouchet, C. Carrot, J. Guillet, G. Boiteux, G. Seytre, M. Pineri, *Polym. Eng. Sci.* **2000**, *40*, 36.

[133] J. C. Huang, *Adv. Polym. Tech.* **2002**, *21*, 299.

[134] K. Miyasaka, K. Watanabe, E. Jojima, H. Aida, M. Sumita, K. Ishikawa, *J. Mater. Sci.* **1982**, *17*, 1610.

[135] S. C. Tjong, G. D. Liang, S. P.Bao, *Scripta Mater.* **2007**, *57*, 461.

[136] S. B. Kharchenko, J. F. Douglas, J. Obrzut, E. A. Grulke, K. B. Migler, *Nat. Mater*. **2004**, *3*, 564.

[137] M. K. Seo, S. J. Park, *Chem. Phys. Lett*. **2004**, 395, 44.

[138] G. Gorrasi, V. Romeo, D. Sannino, M. Sarno, P. Ciambelli, V. Vittoria, B. De Vivo, V. Tucci, *Nanotechnology* **2007**, *18*, 275703.

[139] M. Sumita, H. Abe, H. Kayaki, K. Miyasaka, *J. Macromol. Sci. Phys. B* **1986**, *25I,* 171.

[140] A. Mierczynska, M. Mayne-L'Hermite, G. Boiteux, *J. Appl. Polym. Sci*. **2007**, *105*, 158.

[141] M. O. Lisunova, Y. P. Mamunya, N. I. Lebovka, A. V. Melezhyk, *Europ. Polym. J.* **2007**, *43*, 949.

[142] G. Gorrasi, M. Sarno, A. Di Bartolomeo, D. Sannino, P. Ciambelli, V. Vittoria, *J. Polym. Sci. B* **2007**, *45*, 597.

[143] Q. H. Zhang, S. Rastogi, D. J. Chen, D. Lippits, P. J. Lemstra, *Carbon* **2006**, *44*, 778.

[144] T. McNally, P. Pötschke, P. Halley, M. Murphy, D. Martin, S. E. J. Bell, G. P. Brennan, D. Bein, P. Lemoine, J. P. Quinn, *Polymer* **2005**, *46*, 8222.

[145] D. Zhao, Q. Lei, C. Qin, X. Bai, *Pigment Resin Technol*. **2006**, *35*, 341.

[146] J. Fournier, G. Boiteux, G. Seytre, G. Marichy, *Synth. Met.* **1997**, *84*, 839.

[147] G. Boiteux, J. Fournier, D. Issotier, G. Seytre, G. Marichy, *Synth. Met.* **1999**, *102*, 1234.

[148] L. Flandin, T. Prasse, R. Schueler, K. Schulte, W. Bauhofer, J. Y. Cavaille, *Phys. Rev. B* **1999**, *59*, 14349.

[149] J. Sandler, M. S. P. Shaffer, T. Prasse, W. Bauhofer, K. Schulte, A. H. Windle, *Polymer* **1999**, *40*, 5967.

[150] J. K. W. Sandler, J. E. Kirk, I. A. Kinloch, M. S. P. Shaffer, A. H. Windle, *Polymer* **2003**, *44*, 5893.

[151] Y. J. Kim, T. S. Shin, H. D. Choi, J. H. Kwon, Y. C. Chung, H. G. Yoon, *Carbon* **2005**, *43*, 23.

[152] A. P. Yu, M. E. Itkis, E. Bekyarova, R. C. Haddon, *Appl. Phys. Lett*. **2006**, *89*, 133102.

[153] B. Kim, J. Lee, I. Yu, *J. Appl. Phys*. **2003**, *94*, 6724.

[154] S. Barrau, P. Demont, C. Maraval, A. Bernes, C. Lacabanne, *Macromol. Rapid Commun*. **2005**, *26*, 390.

[155] N. Yousefi, M. M. Gudarzi, Q. Zheng, X.Lin, X. Shen, J. Jia, F. Sharif, J.-K. Kim, *Comp. A.*, **2013**, in press.

[156] G. Long, C. Tang, K. Wong, C. Man, M. Fan, W. Lau, T. Xu, B. Wang, *Green Chem.* **2013**, *3*, 821.

[157] H. Pang, C. Chen, Y. Bao, J. Chen, X. Ji, J. Lei, Z.-M. Li, *Mater. Lett.* **2012**, *79*, 96.

[158] J. Kaur, J. H. Lee, D. G. Bucknall, M. L. Shofner, *ACS Appl. Mater. Inter*. **2012**, *6*, 3111.

[159] S. Zhang, H. Wang, G. Wang, Z. Jiang, *Appl. Phys. Lett*. **2012**, *101*, 012904.

[160] H. Pang, Y. Bao, J. Lei, J.-H. Tang, X. Ji, W.-Q. Zhang, C. Chen, *Polym.-Plast. Tech. Eng.* **2012**, *14*, 1483.

[161] B. P. Grady, *Macromol. Rapid Comm*. **2010**, *31*, 3.

[162] M. C. Hermant, B. Klumperman, A. V. Kyrylyuk, P. van der Schoot, C. E. Koning, *Soft Matter* **2009**, *4*, 878.

[163] M.-J. Jiang, Z.-M. Dang, S.-H. Yao, J. Bai, *Chem. Phys. Lett*. **2008**, *4-6*, 352.

[164] M. L. P. Ha, B. P. Grady, G. Lolli, D. E. Resasco, W. T. Ford, *Macromol. Chem. Phys*. **2007**, *208*, 5.

[165] H. Pang, Y. Bao, L. Xu, D.-X. Yan, W.-Q. Zhang, J.-H. Wang, Z.-M. Li, *J. of Mater. Chem. A*, **2013**, *13*, 4177.

[166] Z. S. Levin, C. Robert, J. F. Feller, M. Castro, J. C. Grunlan, *Smart Mater. Struct.* **2013**, *22*, 015008.

[167] Y. Bao, L. Xu, H. Pang, D.-X. Yan, C. Chen, W.-Q. Zhang, J.-H. Tang, Z.-M. Li, *J. Mater. Sci.*, **2013**, in press.

[168] G. Pandey, E. T. Thostenson, *Polym. Rev*. **2012**, *3-4*, 355.

[169] H. Jiang, Q. Ni, H. Wang, J. Liu, *Polym. Comp*. **2012**, *33*, 9.

[170] Y. Bao, J. Wang, P. Xue, Q. Li, W. Guo, C. Wu, J. *Mater. Sci*. **2012**, *3*, 1289.

[171] M. H. Kang, S. J. Lee, *Korea-Australia Rheol. J.* **2012**, *2*, 97.

[172] J. Lu, J.F. Feller, B. Kumar, M. Castro, Y.S. Kim, Y.T. Park, J.C. Grunlan, *Sensor. Actuat. B* **2011**, *1*, 28.

[173] N. Grossiord, M. E.L. Wouters, H. E. Miltner, K. Lu, J. Loos, B. Van Mele, C. E. Koning, *Euro. Polym. J.* **2010**, *9*, 1833.

[174] Y. S. Kim, D. Kim, K. J. Martin, C. Yu, J. C. Grunlan, *Macromol. Mater. Eng.* **2010**, *295*, 5.

[175] D. C. Wu, L. Shen, J. E. Low, S. Y. Wong, X. Li, W. C. Tjiu, Y. Liu, C. B. He, *Polymer* **2010**, *10*, 2155.

[176] C. Min, X. Shen, Z. Shi, L. Chen, Z. Xu, *Polym.-Plast. Tech. Eng*. **2010**, *12*, 1172.

[177] C. Min, X. Shen, Z. Zhi, L. Chen, Z. Xu, *Polym.-Plast. Techn. Eng.* **2010**, *49*, 117.

[178] M. S. Dresselhaus, G. Dresselhaus, A. P. Eklund, in *Science of Fullerenes and Carbon Nanotubes*, Academic Press, New York **1996**.

[179] T. W. Ebbesen, H. J. Lezec, H. Hiura, J. W. Bennett, H. F. Ghaem, T. Thio, *Nature* **1996**, *382*, 54.

[180] M. S. Dresselhaus, G. Dresselhaus, R. Saito, *Carbon* **1995**, *33*, 883.

[181] D. S. Bethune, C. H. Kiang, M. S. De Vries, G. Gorman, R. Savoy, J. Vazquez, R. Beyers, *Nature* **1993**, *363*, 605.

[182] J. N. Coleman, U. Khan, W. J. Blau, Y. K. Gun'ko, *Carbon* **2006**, *44*, 1624.

[183] M. Moniruzzaman, K. I. Winey, *Macromol.* **2006**, *39*, 5194.

[184] C. A. Dyke, J. M. Tour, *J. Phys. Chem. A* **2004**, *108*, 11151.

[185] J. A. Elliott, J. K. W. Sandler, A. H. Windle, R. J. Young, M. S. P. Shaffer, *Phys. Rev. Lett.* **2004**, *92*, 1.

[186] K. Awasthi, A. Srivastava, O. N. Srivastava, *J. Nanosci. Nanotechnol*. **2005**, *5*, 1616.

[187] S. Iijima, *Nature* **1991**, *354*, 56.

[188] R. Pfeiffer, T. Pichler, Y. A. Kim, H. Kuzmany, *Topics Appl. Phys.* **2008**, *111*, 495.

[189] J. C. Charlier, J. P. Michenaud, *Phys. Rev. Lett.* **1993**, *70*, 1858.

[190] W. Ren, F. Li, J. Chen, S. Bai, H.-M. Cheng, *Chem. Phys. Lett.* **2002**, *359*, 196.

[191] S. Bandow, M. Takizawa, K. Hirahara, M. Yudasaka, S. Iijima, *Chem. Phys. Lett*. 2001, *337*, 48.

[192] M. Scaraselli, P. Castrucci, M. De Crescenzi, *J. Phys.: Condens. Matter* **2012**, *24*, 313202.

[193] F. Laoutid, L. Bonnaud, M. Alexandre, J.-M. Lopez-Cuesta, P. Dubois, *Mat. Sci. Eng. R.* **2009,** *63,* 100.

[194] L. Vaisman, H. D. Wagner, G. Marom, *Adv. Colloid Interfac*. **2006**, *128*, 37.

[195] R. Bandyopadhyaya, E. Nativ-Roth, O. Regev, R. Yerushalmi-Rozen, *Nano Lett*. **2002**, *2*, 25.

[196] N. R. Tummala, A. Striolo, *ACS Nano* **2009**, *3*, 595.

[197] N. Grossiord, J. Loos, O. Regev, C. E. Koning, *Chem. Mater*. **2006**, *18*, 1089.

[198] H. Wang, W. Zhou, D. L. Ho, K. I. Winey, J. E. Fischer, C. J. Glinka, *Nano Lett*. **2004**, *4*, 1789.

[199] V. C. Moore, M. S. Strano, E. H. Haroz, R. H. Hauge, R. E. Smalley, J. Schmidt, *Nano Lett.* **2003**, *3*, 1379.

[200] J. C. Grunlan, L. Liu, O. Regev, *J. Colloid Interf. Sci*. **2008**, *317*, 346.

[201] Y. Dror, W. Pyckhout-Hintzen, Y. Cohen, *Macromolecules* **2005**, *38*, 7828.

[202] B. Y. Ouyang, C. W. Chi, F. C. Chen, Q. F. Xi, Y. Yang, *Adv. Funct. Mater*. **2005**, *15*, 203.

[203] J. Ouyang, Q. F. Xu, C. W. Chu, Y. Yang, G. Li, J. Shinar, *Polymer* **2004**, *45*, 8443.

[204] Y. C. Tsai, C. C. Chiu, M. C. Tsai, J. Y. Wu, T. F. Tseng, T. M. Wu, *Carbon* **2007**, *45*, 2823.

[205] L. Liu, J. C. Grunlan, *Adv. Funct. Mater*. **2007**, *17*, 2343.

[206] C. Yu, K. Choi, L. Yin, J. C. Grunlan, *ACS Nano* **2011**, *5*, 7885.

[207] Y. Du, S. Z. Shen, K. Cai, P. S. Casey, *Prog. Polym. Sci.* **2012**, *37*, 820.

[208] Y. W. Park, W. K. Han, C. H. Choi, H. Shirakawa, *Phys. Rev.* B **1984**, *30*, 5847.

[209] Y. Nogami, H. Kaneko, T. Ishiguro, A. Takahashi, J. Tsukamoto, N. Hosoito, *Solid State Commun.* **1990**, *76*, 583.

[210] J. P. W. Pukacki, S. Rothc, in *Anisotropy of Charge Transport Properties in Highly Conductive Oriented Polyacetylene*, Capri, Italy **1993**.

[211] H. Yan, N. Toshima, *Chem. Lett.* **1999**, *28*, 1217.

[212] N. Toshima, *Macromol. Symp.* **2002**, *186*, 81.

[213] J. Liu, L.-M. Zhang, L. He, X.-F. Tang, *J. Wuhan Uni. Tech. Mater. Sci.* **2003**, *18,* 53.

[214] C. O. Yoon, M. Reghu, *Synth. Met.* **1995**, *69*, 273.

[215] C. C. Liu, B. Y. Lu, J. Yan, J. K. Xu, R. R. Yue, Z. J. Zhu, S. Y. Zhou, X. J. Hu, Z. Zhang, P. Chen, *Synth. Met.* **2010**, *160*, 2481.

[216] O. Bubnova, Z. U. Khan, A. Malti, S. Braun, M. Fahlman, M. Berggren, X. Crispin, *Nat. Mater*. **2011**, *10*, 429.

[217] L. Groenendaal, F. Jonas, D. Freitag, H. Pielartzik, J. R. Reynolds, *Adv. Mater*. **2000**, *12*, 481.

[218] X. Crispin, F. L. E. Jakobsson, A. Crispin, P. C. M. Grim, P. Andersson, A. Volodin, C. van Haesendonck, M. Van der Auweraer, W. R. Salaneck, M. Berggren, *Chem. Mater*. **2006**, *18*, 4354.

[219] F.-X. Jiang, J.-K. Xu, B.-Y. Lu, Y. Xie, R.-J. Huang, L.-F. Li, *Chin. Phys. Lett.* **2008**, *25*, 2202.

[220] T.-C. Tsai, H.-C. Chang, C.-H. Chen, W.-T. Whang, *Org. Electron.* **2011**, *12*, 2159.

[221] T. Hasan Gilani, T. Masui, G. Yu. Logvenov, T. Ishiguro, *Synth. Met*. **1996**, *78*, 327.

[222] Y.-J. Cheng, S.-H. Yang, C.-S. Hsu, *Chem. Rev*. **2009**, *109*, 5868.

[223] R. Reynolds, *Chemtech* **1988**, *18*, 440.

[224] T. O. Poehler, H. E. Katz, *Energy Environ. Sci.* **2012**, *5*, 8110.

[225] K. Gurunathan, A. V. Murugan, R. Marimuthu, U. P. Mulik, D. P. Amalnerkar, *Mater. Chem. Phys.* **1999**, *61*, 173.

[226] K. P. Pernstich, B. Rossner, B. Batlogg, *Nat. Mater*. **2008**, *7*, 321.

[227] M. Pfeiffer, A. Beyer, T. Fritz, K. Leo, *Appl. Phys. Lett*. **1998**, *73*, 3202.

[228] A. J. Epstein, H. Rommelmann, R. Fernquist, H. W. Gibson, M. A. Druy, T. Woerner, *Polymer* **1982**, *23*, 1211.

[229] A. Pron, C. Budrowski, J. Przyluski, *Polymer* **1983**, *24*, 1294.

[230] Y. Hiroshige, M. Ookawa, N. Toshima, *Synth. Met.* **2006**, *156*, 1341.

[231] Y. Hiroshige, M. Ookawa, N. Toshima, *Synth. Met*. **2007**, *157*, 467.

[232] Y. Wang, *J. Phys.: Conf. Ser.* **2009**, *152*, 012023.

[233] J. R. Reynolds, A. Kumar, J. L. Reddinger, B. Sankaran, S. A. Sapp, G. A. Sotzing, *Synth. Met.* **1997**, *85*, 1295.

[234] H. J. Ahonen, J. Lukkari, J, Kankare, *Macromolecules* **2000**, *33*, 6787.

[235] Q. Pei, G. Zuccarello, M. Ahskog, O. Inganäs, *Polymer* **1994**, *35*, 1347.

[236] J. Cornil, D. A. dos Santos, D. Beljonne, J. L. Brédas, *J. Phys. Chem*. **1995**, *99*, 5604.

[237] G. Heywang, F. Jonas, *Adv. Mater*. **1992**, *4*, 116.

[238] M. Dietrich, J. Heinze, G. Heywang, F. Jonas, *J. Electroanal. Chem*. **1994**, *369*, 87.

[239] C. Kvarnström, H. Neugebauer, S. Blomquist, H. J. Ahonen, J. Kankare, A. Ivaska, N. S. Sariciftci, *Synth. Met*. **1999**, *101*, 66.

[240] K. Lee, S. Cho, S. H. Park, A. J. Heeger, C.-W. Lee, S.-H. Lee, *Nature* **2006**, *441*, 65.

[241] A. M. Nardes, M. Kemerink, M. M. de Kok, E. Vinken, K. Maturova, R. A. J. Janssen, *Organic Electronics* **2008**, *9*, 727.

[242] B. Zhang, J. Sun, H. E. Katz, F. Fang, R. L. Opila, *ACS Appl. Mater. Inter.* **2010**, *2*, 3170.

[243] B. Winther-Jensen, K. West, *Macromolecules* **2004**, *37*, 4538.

[244] T. Park, C. Park, B. Kim, H. Shin, E. Kim, *Energy Environ. Sci.* **2013**, *6*, 788.

[245] D. K. Taggart, Y. Yang, S.-C. Kung, T. M. McIntire, R. M. Penner, *Nano Lett.* **2010**, *11*, 125.

[246] K.-C. Chang, M.-S. Jeng, C.-C. Yang, Y.-W. Chou, S.-K. Wu, M. Thomas, Y.-C. Peng, *J. Electron. Mater.* **2009**, *38*, 1182.

[247] K. Fang-Fang, L. Cong-Cong, X. Jing-Kun, J. Feng-Xing, L. Bao-Yang, Y. Rui-Rui, L. Guo-Dong, W. Jian-Min, *Chinese Phys. Lett*. **2011**, *28*, 037201.

[248] K. C. See, J. P. Feser, C. E. Chen, A. Majumdar, J. J. Urban, R. A. Segalman, *Nano Lett*. **2010**, *10*, 4664.

[249] C. Yu, L. Shi, Z. Yao, D. Li, A. Majumdar, *Nano Lett.* **2005**, *5*, 1842.

[250] J. Hone, I. Ellwood, M. Muno, A. Mizel, M. L. Cohen, A. Zettl, A. G. Rinzler, R. E. Smalley, *Phys. Rev. Lett.* **1998**, *80*, 1042.

[251] Z. Han, A. Fina, *Prog. Polym. Sci.* **2011**, *36*, 914.

[252] C. T'Joen, Y. Park, Q. Wang, A. Sommers, X. Han, A. Jocobi, *Int. J. Refrig.* **2009**, *32*, 763.

[253] M. Hu, D. Yu, J. Wei, *Polym. Test* **2007**, *26*, 333.

[254] J. G. Speight. *Lange's Handbook of Chemistry*, 16th ed., McGraw-Hill, New York **2005**, p. 2.794.

[255] P. Kim, L. Shi, A. Majumdar, P. L. McEuen, *Phys. Rev. Lett.* **2001**, *87*, 215502.

[256] Y. Xu, G. Ray, B. Abdel-Magid, *Composites A* **2006**, *37*, 114.

[257] P. C. Ma, B. Z. Tang, J. K. Kim, *Carbon* **2008**, *46*, 1497.

[258] J. Hong, J. Lee, C. K. Hong, S. E. Shim, *Curr. Appl. Phys.* **2010**, *10*, 359.

[259] W. T. Hong, N. H. Tai, *Diam. Relat. Mater.* **2008**, *17*, 1577.

[260] Y. S. Song, J. R. Youn, *Carbon* **2005**, *43*, 1378.

[261] S. Wang, R. Liang, B. Wang, C. Zhang, *Carbon* **2009**, *47*, 53.

[262] S. Ghose, K. A. Watson, D. C. Working, J. W. Connel, J. G. Smith, Y. P. Sun, *Compos. Sci. Technol.* **2008**, *68*, 1843.

[263] C. Guthy, F. Du, S. Brand, K. I. Winey, J. E. Fischer, *J. Heat Transfer* **2007**, *129*, 1096.

[264] J. A. King, D. L. Gaxiola, B. A. Johnson, J. M. Keith, *J. Compos. Mater.* **2010**, *44*, 839.

[265] F. H. Gojny, M. H. G. Wichmann, B. Fielder, I. A. Kinloch, W. Bauhofer, A. H. Windle, K. Schulte, *Polymer* **2006**, *47*, 2036.

[266] A. Das, K. W. Stockelhuber, R. Jurk, M. Saphiannikova, J. Fritzsche, H. Lorenz, M. Kluppel, G. Heinrich, *Polymer* **2008**, *49*, 5276.

[267] S. Shenogin, L. Xue, R. Ozisik, P. Keblinski, *J. Appl. Phys.* **2004**, *95*, 8136.

[268] S. T. Huxtable, D. G. Cahill, S. Shenogin, L. Xue, R. Ozisik, P. Barone, M. Ursey, M. S. Strano, G. Siddons, M. Shim, P. Keblinski, *Nat. Mater.* **2003**, *2*, 731.

[269] C. W. Nan, G. Liu, Y. Lin, M. Li, *Appl. Phys. Lett.* **2004**, *85*, 3549.

[270] C. W. Nan, R. Birringer, D. R. Clarke, H. Gleiter, *J. Appl. Phys.* **1997**, *10*, 6692.

[271] N. Shenogina, S. Shenogin, L. Xue, P. Keblinski, *Appl. Phys. Lett.* **2005**, *87*, 133106.

[272] H. Wang, L. Yin, X. Pu, C. Yu, *Polymer* **2013**, *54*, 1136.

[273] K. Zhang, M. Davis, J. Qiu, L. Hope-Weeks, S. Wang, *Nanotechnology* **2012**, *23*, 385701.

[274] J. Xiang, L. T. Drzal, *Polymer* **2012**, *53*, 4202.

[275] L. Wang, D. Wang, G. Zhu, J. Li, F. Pan, *Mater. Lett.* **2011**, *65*, 1086.

[276] Q. Yao, L. Chen, W. Zhang, S. Liufu, X. Chen, *ACS Nano* **2010**, *4*, 2445.

[277] K. T. Kim, S. Y. Choi, E. H. Shin, K. S. Moon, H. Y. Koo, G. G. Lee, G. H. Ha, *Carbon* **2013**, *52*, 541.

[278] D. D. Freeman, K. Choi, C. Yu, *PLoS One* **2012**, *7*, e47822.

[279] P. G. Collins, K. Bradley, M. Ishigami, A. Zettl, *Science* **2000**, *287*, 1801.

[280] M. Stanford, H. Wang, I. Ivanov, B. Hu, *Appl. Phys. Lett.* **2012**, *101*, 173304.

[281] M. He, J. Ge, Z. Lin, X. Feng, X. Wang, Y. Yang, F. Qiu, *Energy Environ. Sci.* **2012**, *5*, 8351.

[282] Y. Wang, K. F. Cai, X. Yao, *J. Nanoparticle Research* **2012**, *14*, 0848.

[283] J. N. Coleman, M. Lotya, A. O'Neill, S. D. Bergin, P. J. King, U. Khan, K. Young, A. Gaucher, S. De, R. J. Smith, I. V. Shvets, S. K. Arora, G. Stanton, H.-Y. Kim, K. Lee, G. T. Kim, G. S. Duesberg, T. Hallam, J. J. Boland, J. J. Wang, J. F. Donegan, J. C. Grunlan, G. P. Moriarty, A. Shmeliov, R. J. Nicholls, J. M. Perkins, E. M. Grieveson, K. Theuwissen, D. W. McComb, P.D. Nellist, V. Nicolosi, *Science*, **2011**, *331*, 568.

[284] R. J. Smith, P. J. King, M. Lotya, C. Wirtz, U. Khan, S. De, A. O'Neill, G. S. Duesberg, J. C. Grunlan, G. P. Moriarty, J. Chen, J. Wang, A. I. Minett, V. Nicolosi, J. N. Coleman, *Adv. Mater.* **2011**, *23*, 3944.

[285] C. Hewitt, D. Carroll, M. Craps, R. Czerw, A. Kaiser, S. Roth, *Nano Lett.* **2012**, *12*, 1307.

[286] G. P. Moriarty, S. De, P. J. King, U. Khan, M. Via, J. A. King, J. N. Coleman, J. C. Grunlan, *J. Polym. Sci. B* **2013**, *51*, 119.

[287] G. P. Moriarty, B. Stevens, K. Briggs, C. Yu, J. C. Grunlan, *Energy Technology* **2013**, *1*, 265.

[288] G. P. Moriarty, H. Harrity, C. Yu, J. C. Grunlan, *Adv. Mater.*, in revision.

[289] H. P. Li, B. Zhou, Y. Lin, L. R. Gu, W. Wang, K. A. S. Fernando, S. Kumar, L. F. Allard, Y. P. Sun, *J. Am. Chem. Soc.* **2004**, *126*, 1014.

[290] W. Wenseleers, I. I. Vlasov, E. Goovaerts, E. D. Obraztsova, A. S. Lobach, A. Bouwen, *Adv. Funct. Mater*. **2004**, *14*, 1105.

[291] R. Haggenmueller, S. S. Rahatekar, J. A. Fagan, J. H. Chun, M. L. Becker, R. R. Naik, T. Krauss, L. Carlson, J. F. Kadla, P. C. Trulove, D. F. Fox, H. C. DeLong, Z. C. Fang, S. O. Kelley, J. W Gilman, *Langmuir* **2008**, *24*, 5070.

[292] J. A. Fagan, J. Y. Huh, J. R. Simpson, J. L. Blackburn, J. M. Holt, B. A. Larsen, A. R. Walker, *ACS Nano* **2011**, *24*, 3943.

[293] J. Y. Chen, C. P. Collier, *J. Phys. Chem. B* **2005**, *109*, 7605.

[294] T. Hasobe, S. Hattori, P. V. Kamat, S. Fukuzumi, *Tetrahedron* **2006**, *62*, 1937.

[295] M. Alvaro, P. Atienzar, P. la Cruz, J. L. Delgado, V. Troiani, H. Garcia, F. Langa, A. Palkar, L. Echeqoyen, *J. Am. Chem. Soc*. **2006**, *128*, 6626.

[296] G. Chen, M. S. Dresselhaus, G. Dresselhaus, J. P. Fleurial, T. Caillat, *Int. Mater. Rev*. **2003**, *48*, 45.

[297] W. K. Asbeck, M. Vanloo, *Ind. Eng. Chem*. **1949**, *41*, 1470.

[298] M. Lei, L. F. Francis, L. E. Scriven, *J. Coating Technol*. **2003**, *75*, 95.

[299] J. C. Weaver, *J. Coating Technol*. **1992**, *64*, 45.

[300] J. C. Grunlan, Y. S. Kim, S. Ziaee, X. Wei, B. Abdel-Magid, K. Tao, *Macromol. Mater. Eng.* **2006**, *291*, 1035.

[301] Y. C. Ou, Z. Z. Yu, A. Vidal, J. B. Donnet, *J. Appl. Polym. Sci*. **1996**, *59*, 1321.

[302] F. W. Starr, T. B. Schroder, S. C. Glotzer, *Macromolecules* **2002**, *35*, 4481.

[303] O. Borodin, G. D. Smith, R. Bandyopadhyaya, E. Byutner, *Macromolecules* **2003**, *36*, 7873.

[304] J. C. Grunlan, A. Grigorian, C. B. Hamilton, A. R. Mehrabi, *J. Appl. Polym. Sci*. **2004**, *93*, 1102.

[305] J. M. Benoit, B. Corraze, S. Lefrant, W. J. Blau, P. Bernier, O. Chauvet, *Synthetic Met.* **2001**, *121*, 1215.

[306] R. Prasher, *Phys. Rev. B* **2008**, *77*, 1.

[307] A. Kasuya, Y. Saito, Y. Sasaki, M. Fukushima, T. Maeda, C. Horie, Y. Nishina, *Mater. Sci. Eng. A* **1996**, *217-218*, 46.

[308] Y. T. Park, A. Y. Ham, J. C. Grunlan, *J. Phys. Chem. C* **2010**, *114*, 6325.

[309] Y. Ryu, D. Freeman, C. Yu, *Carbon* **2011**, *49*, 4745.

[310] B. Zhang, J. Sun, H. E. Katz, F. Fang, R. L. Opila, *ACS Appl. Mater. Interfaces* **2010**, *11*, 3170.

[311] Y. Chalopin, S. Volz, N. Mingo, *J. Appl. Phys.* **2009**, *105*, 084301.

[312] J. M. Keith, C. D. Hingst, M. G. Miller, J. A. King, R. A. Hauser, *Poly. Comp.* **2006**, *27*, 1.

[313] P. N. D'yachkov, D. V. Makaev, *Phys. Rev. B* **2006**, *74*, 155442.

[314] L. A. Girifalco, M. Hodak, R. S. Lee, *Phys. Rev. B* **2000**, *62*, 13104.

[315] S. De, P. E. Lyons, S. Sorel, E. M. Doherty, P. J. King, W. J. Blau, P. N. Nirmalraj, J. J. Boland, V. Scardaci, J. Joimel, J. N. Coleman, *ACS Nano* **2009**, *3*, 714.

[316] G. Decher, *Science* **1997**, *277*, 1232.

[317] M. A. Priolo, D. Gamboa, K. M. Holder, J. C. Grunlan, *Nano Lett.* **2010**, *10*, 4970.

APPENDIX A

INFLUENCE OF POLYMER PARTICLE SIZE ON THE PERCOLATION THRESHOLD OF ELECTRICALLY CONDUCTIVE LATEX-BASED COMPOSITES*

A.1 Introduction

Electrically conductive polymer composites, comprised of an electrically conductive filler added to a polymer matrix, have been widely used in recent years for applications that include electromagnetic shielding, actuation, sensing (chemical, temperature, and pressure), and electrostatic charge dissipation. As more conductive filler is added to the matrix, a network begins to form that will allow the composite to transition from insulator to conductor. This transition occurs when an interconnected network is formed at a critical concentration of conductive filler, which is known as the percolation threshold. Composite electrical conductivity generally obeys the percolation power law as a function of electrically conductive filler concentration:

$$\sigma = \sigma_0 (V - V_c)^s \tag{A.1}$$

where σ_0 is a proportionality constant related to the intrinsic conductivity of the filler, V is the volume fraction of conductive filler, V_c is the critical volume fraction of filler

*Reprinted with permission from G. P. Moriarty, J. H. Whittemore, K. A. Sun, J. W. Rawlins, J. C. Grunlan. Influence of Polymer Particle Size on the Percolation Threshold of Electrically Conductive Latex-Based Composites. *J. Polym. Sci. B* **2012**, *49*, 1547-1554.

associated with the percolation threshold, and *s* is the power law exponent (typically 1.6 – 2.0 for three-dimensional cases).

Classical percolation theory predicts a percolation threshold of approximately 16 vol% filler when there is no interaction between the matrix and filler, (and the filler is assumed to be spherical). Unfortunately, this concentration of filler can cause a reduction in desirable mechanical properties (e.g. flexibility). Lowering the percolation threshold of these composites will help to retain the desired mechanical behavior of the polymer matrix, while simultanously increasing the electrical conductivity at a given filler loading. The percolation threshold can be reduced by utilizing a segregated network approach in which relatively large polymer domains create excluded volume that forces conductive filler to form networks at low concentration. First coined by Kusy while using electrically conductive mixtures of polymer and metal powders, segregated networks have been extensively studied in recent years. These networks are typically achieved with a polymer blend, or a particulate polymer (e.g. polymer powder or emulsion), as the composite matrix. Immisicible polymer blends segregate conductive filler due to its preference to be in one polymer relative to the other, or by causing the filler to occupy the interstitial space between the two polymers. Percolation thresholds of these blend-based composites can be as low as 1 vol%, although conductivity is also low. A similarly low threshold can be achieved with higher electrical conductivity through the use of a polymer emulsion.

Polymer emulsions (also known as latex) are composed of suspended microscopic solid polymer particles in water. Emulsion-based segregated networks have

been used to create electrically conductive polymer composites with antimony-doped tin oxide, carbon black, and carbon nanotubes. Electrical conductivities of these filled emulsions can achieve values greater than 1000 S cm^{-1} and percolation thresholds below 0.1 vol%. This low percolation threshold is attributed to the solid polymer particles excluding volume and forcing the smaller electrically conductive nanoparticles (nanotubes, carbon black, etc.) into the interstitial space between them during drying. The polymer particles assume a close-packed configuration as water evaporates out of the system and ultimately coalesce into a coherent film if the minimum film formation temperature of the polymer is exceeded. This restricted organization of the conductive filler leads to the creation of a three-dimensional segregated network, as shown schematically in **Figure A.1**.

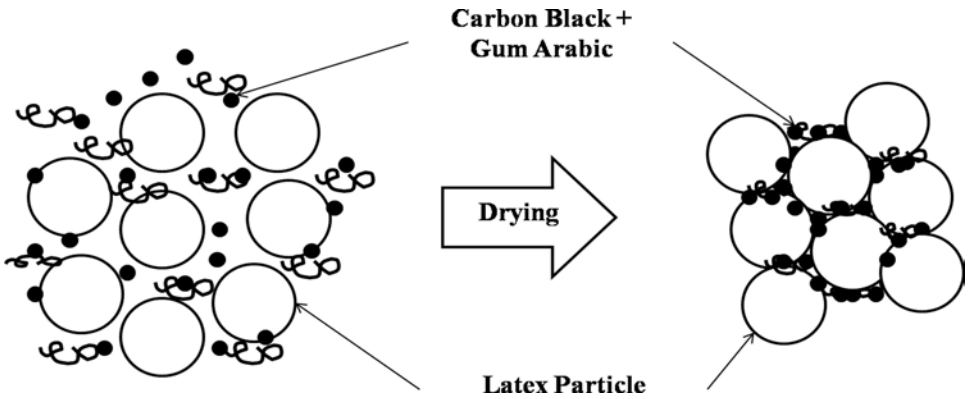

Figure A.1. Carbon black, stabilized by gum arabic in water, exists as a homogeneous aqueous suspension with latex particles. Upon drying, a segregated network of CB forms in the interstitial space between these polymer particles.

In theory, latex particle size can be used to tailor percolation threshold. For a compacted mixture of polymer and conductive particles, the percolation threshold should decrease as the ratio of polymer to conductive particle size increases according to:

$$V_c = 50A\left[1 + B\left(\frac{R_p}{R_m}\right)\right]^{-1} \quad \text{(A.2)}$$

where V_c is the critical volume fraction of conductive filler necessary to impart macroscopic composite electrical conductivity (i.e., the percolation threshold), A and B are constants related to the distribution and packing of conductive filler, R_p is the radius of the polymer particle and R_m is the radius of the conductive particle (~7.5 nm). While the above relationship qualitatively holds for powder-based composites, composites using latex as the polymer matrix starting material have never been studied experimentally. Although the general relationship between particle size and percolation threshold holds, latex is able to create much lower than expected thresholds.

In the present work, carbon black (CB)-filled latex-based polymer composites, made with varying polymer particle diameters, were examined. Monodispersed acrylic latexes were synthesized with four different particle sizes, ranging from 83 – 771 nm. It is shown that the percolation threshold is reduced from 2.7 to 1.1 vol% CB as the polymer particle size increases. These segregated network composites also exhibit an increase in storage modulus with increasing CB concentration, although there is no discernable influence of polymer particle size. Glass transition temperatures of the different composite series did not show any affect as the CB concentration increased, which suggests little interaction between matrix and filler. This is an ideal situation for producing the highest conductivity composites due to intimate contact amongst

conductive particles. The ability to decrease percolation threshold, with increasing latex particle size, is an important tool in creating electrically conductive polymer composites with minimal added filler.

A.2 Experimental

A.2.1 Latex Synthesis

The polymer emulsions used as the composite matrix starting material for this study were synthesized with four different number average particle diameters (83, 128, 527 and 771 nm), from methyl methacrylate (MMA) (Fisher Scientific, Houston, TX) and butyl acrylate (BA) (Acros Organics, Geel, Belgium) monomers. Latex diameter (nm) is referred to as particle size throughout this study. **Table A.1** shows the weight of each ingredient used to prepare each size of latex. The MMA and BA monomers were added to a flask and magnetically stirred for 10 minutes. In a separate flask, sodium dodecyl sulfate (SDS) (Sigma-Aldrich Inc., Saint Louis, MO) surfactant, ammonium persulfate (APS) (Acros Organics, Geel, Belgium) initiator, and sodium hydrogen carbonate ($NaHCO_3$) (Sigma-Aldrich Inc., Saint Louis, MO) buffer were mixed together while magnetically stirring for 10 minutes. The monomer and aqueous solutions were then mixed together at 1800 RPM for 30 minutes to form a pre-emulsion. A round bottom, three-necked flask was then equipped with a nitrogen inlet, thermocouple, condenser, mechanical stirrer, pre-emulsion injection tube, and filled with 100 g of deionized water. The flask was then purged with nitrogen for 30 minutes, while heating the water to 70°C. After mixing, a seed was formed by adding the specified weight of

pre-emulsion, while mechanically agitating at 70°C with a nitrogen flow. After one hour of heating at this temperature, the rest of the pre-emulsion was fed into the solution at 1.5 mL min^{-1} until finished. Once completely fed, the reaction was continued for another three hours to finish the synthesis. The final emulsions were all 23 wt% solids, with each having an approximate glass transition temperature of 19°C.

Table A.1. Weights of ingredients used to make polymer emulsions with varying particle size.

Pre-Emulsion (g)	**MMA/BA 83**	**MMA/BA 128**	**MMA/BA 527**	**MMA/BA 771**
MMA	72	72	72	72
BA	60	60	60	60
SDS	2.64	1.32	0.132	0
APS	0.99	0.99	0.99	0.66
$NaHCO_3$	0.66	0.66	0.66	0.66
H_2O	300	300	300	300
Seed (g)				
Pre-Emulsion	105.8	9.74	6.49	6.49
H_2O	100	100	100	100
Post Synthesis (g)				
SDS	0	0	1.188	1.32

A.2.2 Composite Preparation

Carbon black (VULCAN XC72R provided by Cabot Corporation, Billerica, MA), with an average primary particle size (diameter) diameter between 10 – 15 nm, was used as the model electrically conductive filler. The BET surface area was estimated to be 230 m^2 g^{-1} while intraparticle porosity was assumed to be 2 g cm^{-3}. Gum Arabic (GA) (Sigma-Aldrich Inc., Saint Louis, MO) was used to stabilize the CB in

water during composite preparation. The glass transition temperature (T_g) of GA is reported to be 62°C at a relative humidity of 33%. CB:GA with a dry weight ratio of 2:1 was prepared using an aqueous solution of 3 wt% GA. This ratio was chosen based on a stabilization study showing this weight ratio as the lowest mass of GA to sufficiently stabilize CB. The aqueous suspensions were then sonicated with a VirTis Virsonic 100 ultrasonic cell disrupter (SP Industries Inc., Warminster, PA) for 10 minutes at 50 W in a water bath. The latex system, with a given polymer particle diameter, and deionized water were added to the 2:1 CB:GA aqueous suspension and sonicated again for another 10 minutes at 50 W. The solutions were all left at their natural pH levels. This final aqueous suspension contained 5 wt% total solids. Composites with six different CB concentrations (2, 4, 6, 8, 10, 12, 14, and 16 wt%), were prepared with each latex by drying suspensions in a 26 cm^2 plastic mold for 2 days under ambient conditions and then for 24 hours in a vacuum desiccator. The wt% of these composites were converted to vol% by assuming a polymer particle density of 1.14 g cm^{-3}, based on the densities of MMA and BA, and a carbon black density of 1.89 g cm^{-3}.

A.2.3 Characterization

The polymer particle size of each latex was determined with a light scattering particle analyzer (Microtrac UPA 250, Toronto, Canada) using the following solution parameters: 1.33 refractive index for the fluid, 1.49 refractive index for the polymer particle, polymer particle density of 1.14 g cm^{-3}, and a viscosity between 0.797 – 1.002 mPa s. Each analysis was run for three, 30-second periods, with the average polymer

particle size reported in Table A.1. The sheet resistance (Ω) of CB-filled composites was measured with a four-point probe system (Signatone S-301 series, Gilroy, CA). Resistance was converted to electrical conductivity (S cm^{-1}) by taking the product of the inverse of both sheet resistance (S) and film thickness (cm^{-1}). Five measurements were taken on the top and bottom surfaces of the composites to ensure that a given sample was isotropic. Storage moduli and glass transition temperatures were measured with a Q800 Dynamic Mechanical Analyzer (DMA) from TA Instruments (New Castle, DE). The composites were cut into strips (~25 mm in length and 3 mm in width) and measured in tensile mode, with the amplitude of oscillation maintained at 10 μm. Temperature was ramped at a rate of 5°C min^{-1}, from -60 to 60°C, during testing. The scanning electron micrographs (SEMs) of composite cross-sections were taken with an FEI Quanta 600 FE-SEM (Hillsboro, OR). Samples were soaked in liquid nitrogen and freeze-fractured by hand, then sputter coated with 4 nm of platinum prior to imaging. During imaging, the accelerating voltage was 10 kV, with a spot size of 3.0 nm and a working distance of approximately 10 nm.

A.3 Results and Discussion

Figure A.2 shows SEM cross-sectional micrographs of CB-filled latex-based composites containing 2.56 vol% CB. The composite made with MMA/BA 83 (i.e., 83 nm particle size latex) does not clearly show the expected segregated network. This lack of apparent structure may be due to the sample being too close to the percolation threshold, meaning there is not sufficient CB (bright spots) to create long pathways

around the many small latex particles (dark regions). At this concentration, the electrical conductivity is not measurable for this composite, as will be discussed in the next section. Figure A.2b is a composite with MMA/BA 128 that better shows the segregated CB network throughout the cross-section. The extensive CB pathways suggest that the percolation threshold has been exceeded with 2.56 vol% CB. Both latex systems (83 and 128 nm) coalesced well, enveloping the CB pathways and reducing the porosity that accompanies incomplete coalescence. Figures A.2c and d show composites made with MMA/BA 527 and MMA/BA 771, respectively. These two composites exhibit incomplete coalescence, with spherical polymer particles easily discerned. Poor coalescence creates microvoids that make it difficult to see the much smaller CB particles in these cross-sectional images. It is important to note that the close-packing behavior of these latex particles (schematized in Figure A.1) is observed in Figure A.2c. In all four images, the CB does not appear to significantly interact with the latex-based matrix, which contributes to stronger networks and higher electrical conductivity.

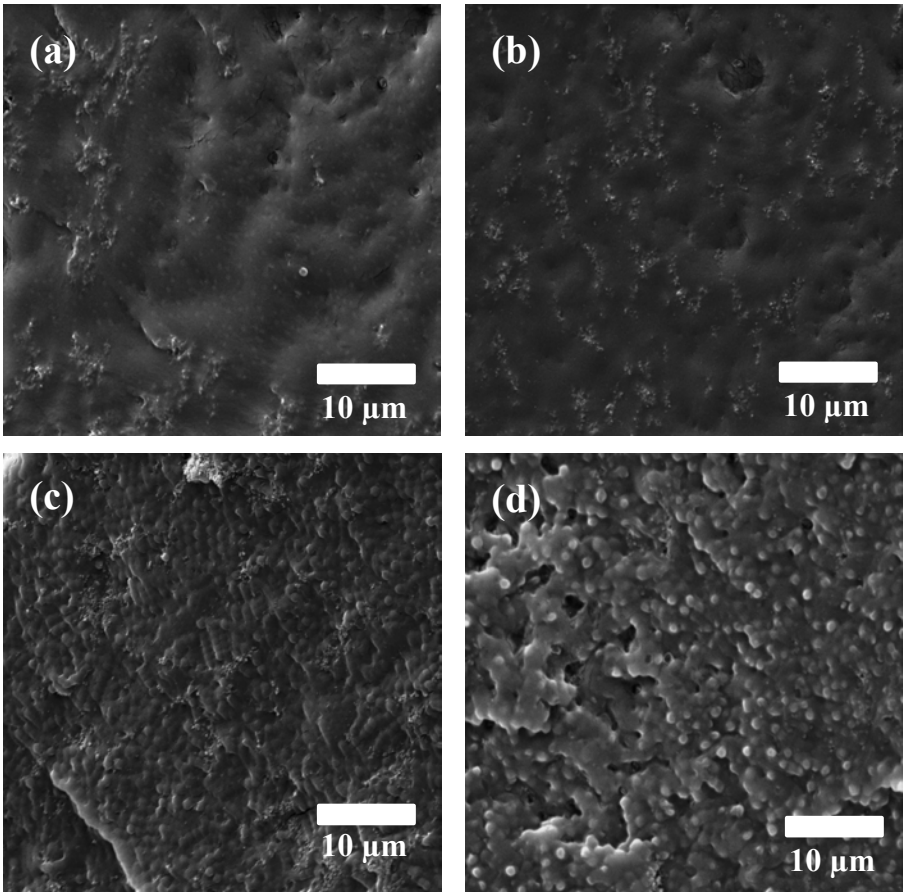

Figure A.2. SEM cross-sectional images of 2:1 CB:GA composites containing 2.56 vol % CB in MMA/BA 83 (a), MMA/BA 128 (b), MMA/BA 527 (c), and MMA/BA 771 (d).

Figure A.3 shows SEM cross-sectional micrographs of composites containing 7.88 vol% CB, made with varying latex particle sizes. The composite made with MMA/BA 83, shows an increased amount of CB aggregation and porosity relative to the same composite system with 2.56 vol% CB (Figure A.2a). Additionally, CB appears to be well dispersed throughout the cross-section, with electrically conductive pathways much more apparent. The MMA/BA 128 based composite (Figure A.3b), with its larger polymer particle size, shows a very developed segregated network, much like that with

2.56 vol%. More porosity is again observed with this higher concentration of carbon black. Both the 83 and 128 nm emulsions coalesce and envelop the filler very well at this higher CB concentration, which is consistent with the lower concentration. Although the MMA/BA 527 (Figure A.3c) and 771 (Figure A.3d) latexes fail to completely coalesce, it is interesting to note that the 527 nm latex exhibits improved coalescence with this greater CB concentration (compare Figure A.2c and A.3c). This filler induced coalescence has been observed previously, and may be due to enhanced colloidal interactions induced by the stabilized CB, which acts as a compatibilizer. The interfacial tension between the larger latex particles was reduced, which promoted better coalescence. The CB in MMA/BA 527 appears to form pathways around polymer domains where many latex particles have coalesced. Cracks in all of these composites are due to CB aggregation that creates porosity that ultimately interconnects. MMA/BA 771 (Figure A.3d) still shows significant latex particle packing, with limited coalescence between particles. Lack of sufficient coalescence makes it difficult to see the CB pathways, even at this increased CB concentration. In general, increasing CB concentration creates more porosity and microcracks that can degrade composite mechanical behavior.

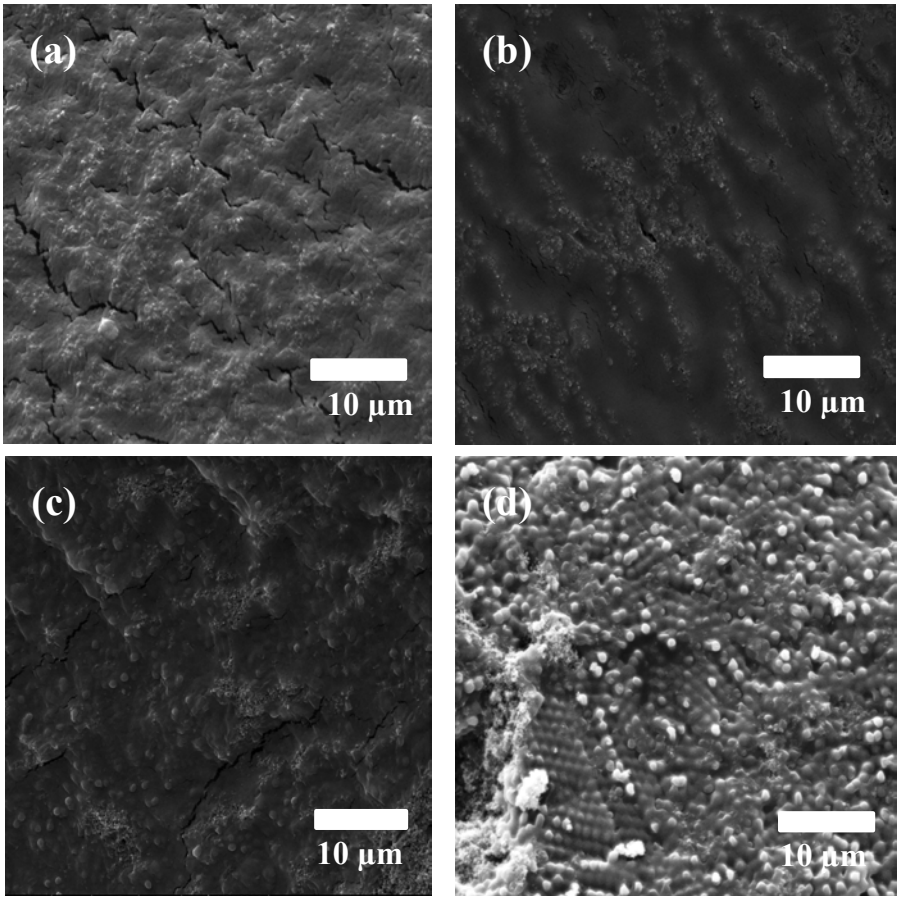

Figure A.3. SEM cross-sectional images of 2:1 CB:GA composites containing 7.88 vol % CB in MMA/BA 83 (a), MMA/BA 128 (b), MMA/BA 527 (c), and MMA/BA 771 (d).

Figure A.4 shows glass transition temperatures (T_g) for the different latex particle size composites as a function of CB concentration. T_g values were taken as the inflection point of the loss modulus curves measured with DMA. The neat latexes (0 vol% CB) exhibit the highest T_g (~33°C) with the smallest particle size, which is likely due to the greatest film coalescence. MMA/BA 527 has the lowest T_g of only 15°C. Even with this seemingly broad T_g range, each latex had a minimum film formation temperature (MFFT) near or below room temperature, which is signified by the neat

latex films being relatively transparent. If dried below the MFFT, a latex film would appear white (or opaque) air-filled voids between uncoalesced polymer particles (that causes light scattering). As the CB concentration increases, the disparity amongst T_g for all four latexes becomes negligible and very similar to the neat latex. This confirms that the CB network does not interact strongly with the polymer matrix and indirectly confirms that CB enhances coalescence. If there was a strong interaction between the filler and matrix, the T_g would increase more dramatically with increasing filler concentration due to the restriction of polymer chains. The influence of GA on the T_g of these composites is expected to be minimal due to its relatively low concentration. At the highest CB concentration, GA makes up 8 wt% of the composite, which would only produce a two degree increase in T_g (according to the Flory-Fox relationship [i.e., parallel rule of mixtures] and ignoring non-interacting CB).

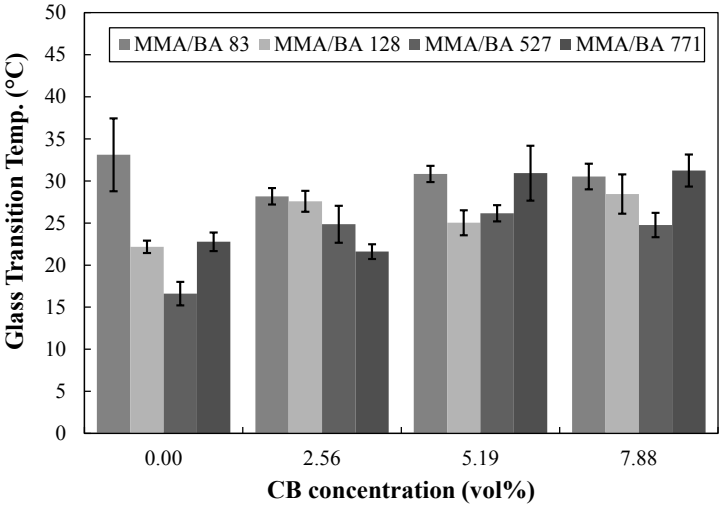

Figure A.4. Glass transition temperatures, as a function of carbon black concentration, for composites made with increasing latex particle size.

The storage moduli of these composites, measured at -40°C, are shown in **Figure A.5**. As expected, stiffness increases with increasing CB concentration. Greater coalescence of MMA/BA 83 results in the higher storage modulus shown here, relative to the other latexes, especially at low CB concentration. Additionally, the size similarity between polymer and CB particles gives this composite system a more solution-like structure that minimizes aggregation and associated porosity. Neat MMA/BA 128 exhibits the lowest storage modulus, which is why it is able to deform around the CB most effectively, creating a tighter network. This strong network explains the highest modulus (~11 GPa) exhibited with 7.88 vol% CB. Neither MMA/BA 527 or 771 show significant improvement in their moduli with increasing CB concentration. This is attributed to the porosity shown in the SEM images (Figure A.3c and d) that acts as a zero modulus filler. MMA/BA 771 exhibits a critical pigment volume concentration (CPVC) near 7.88 vol%, which is signified by a peak in modulus followed by a steady decrease with greater filler concentration. Porosity is a critical issue for segregated networks due to the inability of the polymer to effectively fill voids between particles. Beyond the CPVC, which is often below 10 vol% for most segregated networks, porosity becomes extensive and begins to degrade composite mechanical behavior. Improved CB dispersion and elevated drying conditions (to promote latex coalescence) would potentially reduce the amount of porosity and increase modulus.

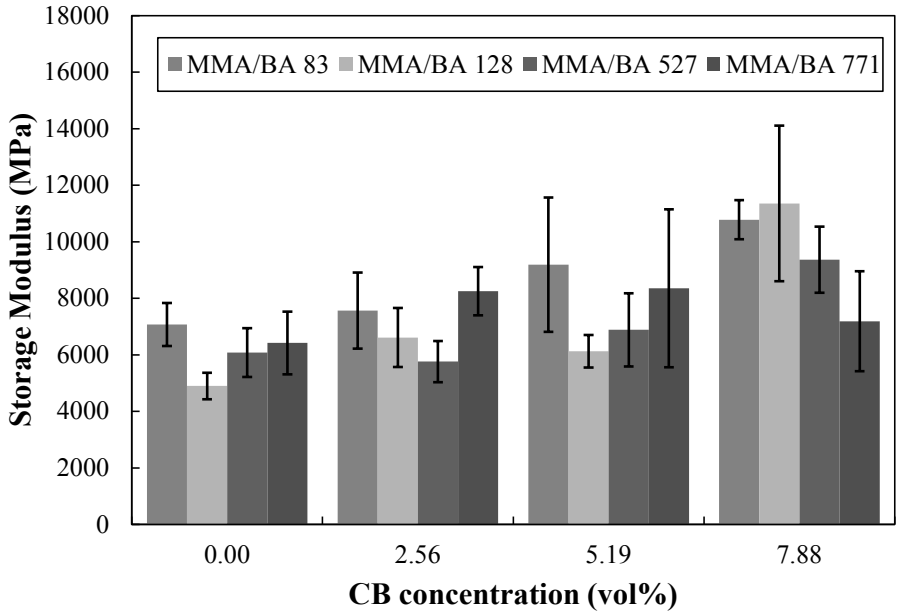

Figure A.5. Storage moduli, measured at -40°C, as a function of carbon black concentration, for composites made with different latex particle size.

Figure A.6a shows electrical conductivity as a function of carbon black concentration for the four latex particle size composite systems. All of the composites seem to obey classical percolation theory, emphasized by fitting the percolation power law (Equation A.1) to the experimental loading curves. Electrical conductivity increases exponentially with CB concentration, with all composites reaching approximately 0.7 S cm^{-1} at 6 vol% CB beyond their respective percolation threshold. It is important to note that the smaller the latex particle size, the greater amount of CB required to reach the same conductivity. This behavior can be explained by the greater amount of surface area associated with smaller latex particles, which creates a random, less segregated microstructure. In theory, a latex whose particles were the same size as the filler would

have a truly random structure. **Table A.2** summarizes latex matrix particle size, percolation power law fitting parameters, percolation threshold prediction, and quality of fit for these latex-based composites. Percolation threshold predictions for the different latex-based composites (V_p) were calculated using Equation A.2. In this case, the constants A and B are 0.33 and 0.2775, which correspond to hexagonal packing of filler particles to produce the smallest threshold values. As expected from the model, the smallest particle size latex yields the largest percolation threshold. Despite this qualitative agreement, all of the experimental data points for the latex-based composites fall well below the theoretical prediction especially for particles below 200 nm.

Table A.2. Latex matrix particle size, percolation power law fitting parameters, percolation threshold prediction, and quality of fit for latex-based composites.

Latex Matrix	**D_n (nm)**	**σ_0 (S/cm)**	**s**	**$100V_c$**	**V_p**
MMA/BA 83	83	24.6	1.73	2.70	7.49
MMA/BA 128	128	22.6	1.69	2.22	5.65
MMA/BA 527	527	26.9	1.59	1.43	1.77
MMA/BA 771	771	29.8	1.67	1.09	1.24

Figure A.6b shows how percolation threshold decreases with increasing latex particle size. MMA/BA 771 has less than half the threshold (~1.1 vol% CB) of MMA/BA 83 (~2.7 vol% CB). The solid line represents the prediction of the percolation threshold (V_p) using Equation A.2. A theoretical latex particle size of 891

nm is needed to obtain the same percolation threshold as MMA/BA 771. The discrepancy between theory and experiment gets larger as the latex particle size decreases, with a theoretical particle size of 84 nm needed to achieve the V_p exhibited by MMA/BA 83. This can be explained by the small latex particles aggregating into larger effective particle sizes due to colloidal forces. Figure A.2a provides some visual evidence of these larger, multi-particle domains. It should be noted that the stabilization of CB by GA negatively affects conductivity, resulting in an increase in the overall percolation threshold. GA is an intrinsically insulating stabilizer that deters electron transport through the CB pathways. It is possible that the thresholds could be reduced further with lower stabilizer concentration or a conductive stabilizer. Other segregated network systems that have achieved comparable percolation threshold reductions tend to attain maximum electrical conductivity plateaus closer to 0.01 S cm^{-1}. The conductivity plateau of 0.7 S cm^{-1} shown for all series here (Figure A.6a) is quite extraordinary when combined with a percolation threshold as low as 1.1 vol% CB.

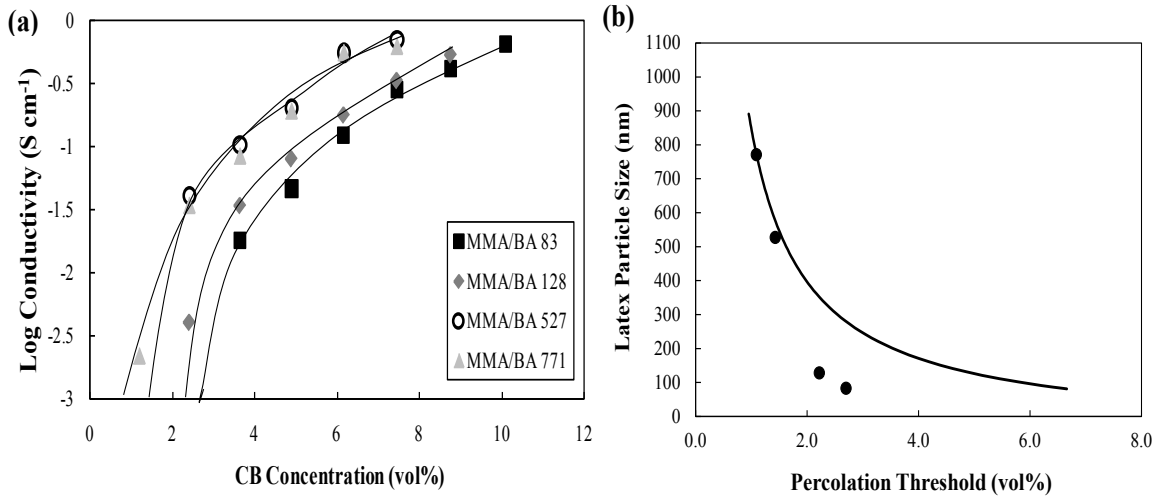

Figure A.6. Electrical conductivity is shown as a function of carbon black concentration for different latex particle sizes (a) and their respective percolation thresholds as a function of latex particle size (b). The solid lines in (a) represent sight lines for the respective composite series, while the line in (b) represents the predicted threshold using Equation A.2 and 15 nm for CB particle size.

A.4 Conclusions

Four series of latex-based carbon black-filled polymer composites were prepared with differing latex particle sizes in an effort to tailor the percolation threshold and associated properties. SEM images show characteristic differences between the microstructure of the four systems as the CB concentration is increased. The glass transition temperatures for all systems were relatively unaltered with changing CB concentration, which suggests that there was little interaction between the polymer matrix and the stabilized electrically conductive filler. Storage modulus was shown to increase for all four latex particle sizes as the CB concentration increased. The percolation threshold was reduced, from 2.7 to 1.1 vol% CB, as the latex particle size was increased, from 83 to 771 nm. These thresholds are much lower than those

predicted based upon particle size ratios due to aggregation of polymer particles during drying, which resulted in a much larger effective particle size. The reduction in percolation threshold demonstrated here could be combined with clay, higher modulus latex particles, or other dispersing aids, to further reduce the percolation threshold.

A.5. References

C. C. Ma, A. T. Hu, D. K. Chen, *Polym. Compos.* **1993**, *1*, 93.

G. Lu, X. Li, H. Jiang, X. Mao, *J. Appl. Polym. Sci.* **1996**, *62*, 2193.

B. J. Landi, R. P. Raffaelle, M. J. Heben, J. L. Alleman, W. VanDerveer, T. Gennett, *Nano Lett.* **2002**, *2*, 1329.

K. J. Albert, N. S. Lewis, C. L. Schauer, G. A. Sotzing, S. E. Stitzel, T. P. Vaid, D. R. Walt, *Chem. Rev.* **2000**, *100*, 2595.

B. Lundberg, B. Sundqvist, *J. Appl. Phys.* **1986**, *60*, 1074.

J. F. Feller, Y. Grohens, *Synth. Met.* **2005**, *154*, 193.

K. Arshak, D. Momis, A. Arshak, O. Korostynska, *Thin Solid Films* **2008**, *516*, 3298.

P. Murugaraj, D. E. Mainwaring, T. Jakubov, N. E. Mora-Huertas, N. A. Khelil, R. Siegele, *Solid State Commun.* **2006**, *137*, 422.

M. K. Tiwari, A. L. Yarin, C. M. Megaridis, *J. Appl. Phys.* **2008**, *103*, 044305.

N. A. Aal, F. El-Tantawy, A. Al-Hajry, M. Bououdina, *Polym. Compos.* **2008**, *29*, 125.

M. Narkis, G. Lidor, A. Vaxman, L. Zuri, *J. Electrostat.* **1999**, *47*, 201.

B. Voight, D. Rouxel, D. H. McQueen, R. W. Rychwalski, *Polym. Compos.* **2005**, *26*, 144.

S. Kirkpatrick, *Rev. Mod. Phys.* **1973**, *45*, 574.

G. Deutscher, A. Kapitulnik, M. Rappaport, in *Annals of the Israel Physical Society, Vol. 5: Percolation Structures and Processes* (Eds.: G. Deutscher, R. Zallen, J. Adler), American Institute of Physics, New York, USA **1983**, Ch. 10.

H. Scher, R. Zallen, *J. Chem. Phys.* **1970**, *53*, 3759.

X. S. Yi, G. Wu, D. Ma, *J. Appl. Polym. Sci.* **1998**, *67*, 131.

R. P. Kusy, *J. Appl. Phys.* **1977**, *48*, 5301.

M. Sumita, K. Sakata, S. Asai, K. Miyasaka, H. Nakagawa, *Polym. Bull.* **1991**, *25*, 265.

F. Gubbels, S. Blacher, E. Vanlathem, R. Jerome, R. Deltour, F. Brouers, P. Teyssie, *Macromolecules* **1995**, *28*, 1559.

O. Breuer, R. Tchoudakov, M. Narkis, A. Siegmann, *J. Appl. Polym. Sci.* **1997**, *64*, 1097.

S. H. Foulger, *J. Polym. Sci., Polym. Phys.* **1999**, *37*, 1899.

J. Y. Feng, C. M. Chan, J. X. Li, *Polym. Eng. Sci.* **2003**, *43*, 1058.

P. Potschke, A. R. Bhattacharyya, A. Janke, *Carbon* **2004**, *42*, 965.

D. P. Dharaiya, S. C. Jana, S. F. Lyuksyutov, *Polym. Eng. Sci.* **2006**, *46*, 19.

J. L. Keddie, *Mater. Sci. Eng., R* **1997**, *21*, 101.

Y. C. Wang, C. Anderson, *Macromolecules* **1999**, *32*, 6172.

J. Sun, W. W. Gerberich, L. F. Francis, *J. Polym. Sci. Part B: Polym. Phys.* **2003**, *41*, 1744.

J. C. Grunlan, W. W. Gerberich, L. F. Francis, *J. Polym. Sci. Part B* **2001**, *80*, 692.

J. W. Hu, M. W. Li, M. Q. Zhang, D. S. Xiao, G. S. Cheng, M. Z. Rong, *Macromol.*

Rapid Commun. **2003**, *24*, 889-893.

Y. S. Kim, J. B. Wright, J. C. Grunlan, *Polymer* **2008**, *49*, 570.

S. M. Miriyala, Y. S. Kim, L. Liu, J. C. Grunlan, *Macromol. Chem. Phys.* **2008**, *209*, 2399.

J. C. Grunlan, A. R. Mehrabi, M. V. Bannon, J. L. Bahr, *Adv. Mater.* **2004**, *16*, 150-153.

M. L. P. Ha, B. P. Grady, G. Lolli, D. E. Resasco, W. T. Ford, *Macromol. Chem. Phys.* **2007**, *208*, 446.

P. Vandervorst, C. H. Lei, Y. Lin, O. Dupont, A. B. Dalton, Y. P. Sun, J. L. Keddie, *Prog. Org. Coat.* **2006**, *57*, 91.

N. Grossiord, H. E. Miltner, J. Loos, J. Meuldijk, B. Van Mele, C. E. Koning, *Chem. Mater.* **2007**, *19*, 3787.

Y. S. Kim, D. Kim, C. Yu, J. C. Grunlan, *Nano Lett.* **2008**, *8*, 4428.

D. Kim, Y. S. Kim, K. Choi, J. C. Grunlan, C. Yu, *ACS Nano* **2010**, *4*, 513.

H. Pang, T. Chen, G. Zhang, B. Zeng, Z.-M. Li, *Mat. Lett.* **2010**, *20*, 2226.

A. Malliaris, D. T. Turner, *J. Appl. Phys.* **1971**, *45*, 614.

A. M. Righetto, F. M. Netto, *Int. J. Food Prop.* **2005**, 8, 337.

A. E. Nesterov, Y. S. Lipatov, *Polymer* **1999**, *40*, 1347.

Y. S. Lipatov, A. E. Nesterov, T. D. Ignatova, D. A. Nesterov, *Polymer* **2002**, *43*, 875.

J. C. Grunlan, Y. S. Kim, S. Ziaee, X. Wei, B. Abdel-Magid, K. Tao, *Macromol. Mater. Eng.* **2006**, *291*, 1035.

Y. C. Ou, Z. Z. Yu, A. Vidal, J. B. Donnet, *J. Appl. Polym. Sci.* **1996**, *59*, 1321.

F. W. Starr, T. B. Schroder, S. C. Glotzer, *Macromolecules* **2002**, *35*, 4481.

O. Borodin, G. D. Smith, R. Bandyopadhyaya, O. Byutner, *Macromolecules* **2003**, *36*, 7873.

A. Bansal, H. Yang, C. Li, K. Cho, B. C. Benicewicz, S. K. Kumar, L. S. Schadler, *Nat. Mater.* **2005**, *4*, 693.

J. C. Grunlan, A. Grigorian, C. B. Hamilton, A. R. Mehrabi, *J. Appl. Polym. Sci.* **2004**, *93*, 1102.

G. Chen, M. S. Dresselhaus, G. Dresselhaus, J. P. Fleurial, T. Caillat, *Int. Mater. Rev.* **2003**, *48*, 45.

W. K. Asbeck, M. Van Loo, *Ind. Eng. Chem.* **1949**, *41*, 1470.

M. Lei, L. F. Francis, L. E. Scriven, *J. Coat. Technol.* **2003**, *75*, 95.

J. C. Weaver, *J. Coat. Technol.* **1992**, *64*, 45.

A. Zhang, L. Wang, Y. Lin, X. Mi, *J. Appl. Polym. Sci.* **2006**, *101*, 1763.

C. C. Furnas, *Ind. Eng. Chem.* **1931**, *23*, 1052.

A. E. R. Westman, H. R. Hugill, *J. Am. Ceram. Soc.* **1930**, *13*, 767.

Z. Tokumitsu, *Zairyo* **1964**, *13*, 752.

J. Kawamura, E. Aoki, K. Okusawa, *Kagaku Kogaku* **1971**, *35*, 777.

J. Yacubowicz, M. Narkis, L. Benguigui, *Polym. Eng. Sci.* **1990**, *30*, 459.

M. C. Hermant, B. Klumperman, A. V. Kyryluk, P. van der Schoot, C. E. Koning, *Soft Matter.* **2006**, *99*, 084302.

J. C. Grunlan, F. L. Bloom, W. W. Gerberich, L. F. Francis, *J. Mat. Sci. Lett.* **2001**, *20*, 1523.